Probing SNARE-Induced Membrane Fusion Using Peptidic Model Fusogens

Dissertation

for the award of the degree
"Doctor rerum naturalium"
of the Georg-August-Universität Göttingen

within the doctoral program chemistry
of the Georg-August University School of Science
(GAUSS)

submitted by
Pirajeev Selvachandran
from Kassel

Göttingen 2021

Thesis Committee

Prof. Dr. Ulf Diederichsen
Institute of Organic and Biomolecular Chemistry, University of Göttingen

Prof. Dr. Claudia Steinem
Institute of Organic and Biomolecular Chemistry, University of Göttingen

Members of the Examination Board

Reviewer:
Prof. Dr. Claudia Steinem
Institute of Organic and Biomolecular Chemistry, University of Göttingen

2nd Reviewer:
Prof. Dr. Kai Tittmann
Department of Molecular Enzymology, University of Göttingen

Further Members of the Examination Board

Prof. Dr. Ulf Diederichsen
Institute of Organic and Biomolecular Chemistry, University of Göttingen

Prof. Dr. Jörg Enderlein
III. Physical Institute, University of Göttingen

Dr. Holm Frauendorf
Institute of Organic and Biomolecular Chemistry, University of Göttingen

Dr. Michael John
Institute of Inorganic Chemistry, University of Göttingen

Date of oral examination: 13. December 2021

The work described in this thesis was carried out under the supervision of Prof. Dr. Ulf Diederichsen at the Institute of Organic and Biomolecular Chemistry of the Georg-August University of Göttingen between January 2018 and September 2021. It was supported by the Deutsche Forschungsgemeinschaft within the Collaborative Research Center 803 (SFB 803) "Functionally controlled by organization in and between membranes".

Declaration of Authorship

Hereby, I declare that this doctoral thesis with the title "Probing SNARE-Induced Membrane Fusion Using Peptidic Model Fusogens" is written all by myself with no other sources and aids than mentioned.

Göttingen, September 30, 2021

Pirajeev Selvachandran

Contents

1 Introduction

Membrane proteins are critical components of cellular processes such as signal transduction, transport of molecules across the membrane and molecular sensing. Due to their specific role in biological systems, related biomolecules have generated great interest in the scientific society and especially in the field of applied science (*e.g.* medical sciences)[1,2] Therefore, biologically useful molecules have been designed in order to understand these mechanisms of action with respect to medical applications.[3–5]

In the past decades, progress in solving crystal structures of membrane proteins originated more insight into the function and arrangement of such biomolecules. To provide a foundation for further membrane studies, it is essential to establish well-characterized membrane systems.[6,7] This requires membrane proteins that mimic natural environment or properties such as polarity, dipole moment and reconstitution into a lipid bilayer.[8]

Cellular processes are often supported by complex interactions driven by membrane proteins. To obtain a large number of biophysical information and a better understanding of complex membrane interaction, it is useful to reduce the complexity into well-defined compartments using model systems.[9,10]

A variety of vital processes of eukaryotic cells such as membrane trafficking, secretion of neurotransmitters and signal transduction are described as membrane fusion events.[11] These events are mediated by proteins called fusogens, which specifically interact with each other to form stable complexes, leading to lipid bilayer deformation. One set of fusogens is called SNARE (soluble *N*-ethylmaleimide-sensitive factor attachment protein receptor) proteins. SNAREs are an evolutionary conserved protein family.[12,13] They can be found in a variety of living species and have been found as the core machinery to mediate membrane fusion.[14,15] They are located on opposing membranes and are assumed to assemble via their characteristic SNARE motifs by zippering $N \rightarrow C$-terminal direction. Thereby, a stable coiled-coil bundle of four intertwined-helices

is formed. The detailed mechanism of how SNARE assembly is linked to the distinct steps of membrane fusion is not fully understood so far. Simplified SNARE model systems provide an excellent method to study membrane fusion *in vitro*. They exhibit a less complex structure allowing an easy and systematic modification of the domains of interest, thus elucidating their influence on the fusion process. Artificial SNARE model systems commonly consist of two interacting SNARE-mimicking peptides incorporated into artificial membranes (*e.g.* liposomes).

In order to gain more insight into the mechanism of membrane fusion, Diederichsen *et al.* has developed artificial SNARE analogues with recognition units made of either short coiled-coil sequences or peptide nucleic acid (PNA) oligomers attached to the native linker and transmembrane domains (TMD) of two neuronal SNAREs.[16] The native sequences of Synaptobrevin-2 (Syb) and Syntaxin-1A (Sx) were attached to several artificial recognition units. The analogues are synthesized by means of solid-phase peptide synthesis (SPPS).[17] In previous work, the fusogenicity of SNARE analogues with artificial recognition units could be successfully verified.[18–20]
By applying Förster resonance energy transfer (FRET) based liposome fusion assays, we show that the analogues are capable of membrane fusion. The extent of liposome fusion was shown to be controllable by the type of the recognition unit. By introducing different recognition motifs, we explored how further structural changes influence the liposome fusion process resulting in a more detailed insight into docking, zippering and fusion of liposomes.

In this thesis, novel coiled-coil peptide fusogens were developed, targeting different strategies to enhance the membrane fusion process. By functionalizing at a specific position of the coiled-coil heptad, the molecular recognition can be regulated. These peptides are designed following the rules of coiled-coil peptides to form heterodimer or tetrameric coiled-coil bundles. Preliminary studies using the E3/K3-TMD model system have revealed difficulties during the recognition process.[21,22] The structural change of the E3/K3 recognition unit will be facilitated by alternating the heptad sequence to reduce membrane interaction and enhance molecular recognition. Moreover, an additional recognition unit was designed, which mimics the natural tetrameric coiled-coil helix bundle. Introducing a tetrameric coiled-coil recognition unit enables a specific alignment, bringing the model system closer to the natural system.[23] In consequence, this novel recognition strategy could offer access to new insights in membrane fusion. Using FRET based liposome fusion assays, the novel coiled-coil peptide fusogens were

tested in terms of fusion efficiency.

In a second project, caged-PNA/peptide hybrids were developed. Therefore, PNA recognition comprising photolabile protecting groups were used.[24] The caging groups attached to the native transmembrane domains inhibit the hybridization of two complementary PNA strands by sterically blocking the respective hydrogen bonding sites.[25] After applying UV-light, the photolabile protecting groups can be cleaved, and liposome fusion should be restored. Within this project, the assumed SNARE zippering process would be investigated by removal of caging groups. To test whether these photocleavable protecting groups based model systems have the ability to fuse vesicles and mimic the zippering process, caged-PNA/peptide hybrids have been examined via FRET based liposome fusion assays and DLS measurements.

2 Membranes and Membrane Fusion

2.1 Biological Membranes

Biological membranes are essential structural elements of the cell, for whose functions they play a crucial role. One function is the ability to enclose vacuoles inside the cell, protecting them from the outer environment and controlling the molecule transportation.[26] Essential cell organelles surrounded by membranes are, *e.g.* mitochondria, chloroplasts and dictyosomes.[27]

Membranes, in general, are commonly described using the fluid mosaic model (Figure 2.1).[26] The fluid mosaic model by SINGER and NICOLSON was the first approach to evaluate biological membranes as functional units. Therefore, biological membranes are defined as two-dimensional fluid structures containing peripheral and integral proteins diffusing through lipids and forming functional complexes.[28] However, this concept does not consider sufficient the complex interactions between membrane components with cytosolic structures (*e.g.* cytoskeleton), extracellular receptor-ligand interactions and the interaction between membrane components like lipid-lipid, lipid-protein and protein-protein interactions.[29]

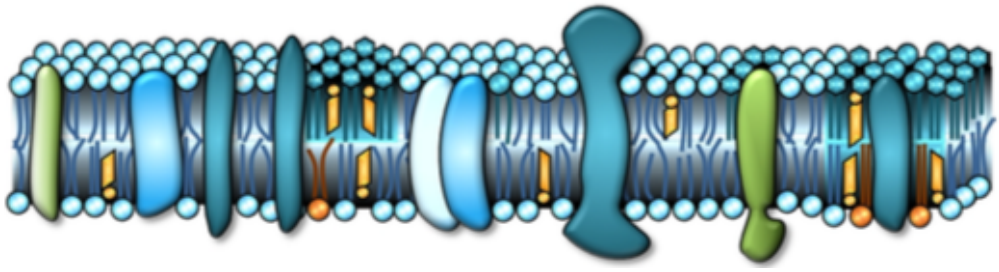

Figure 2.1: Schematic representation of the fluid mosaic model introduced by SINGER and NICOLSON. It illustrates the cell membrane consisting different membrane proteins embedded into the lipid bilayer. The two-dimensional structures containing peripheral and integral proteins diffusing through the lipid membrane representing the complex functional structure. Based on ref.[26].

Nevertheless, biological membranes are mainly composed of lipids. Especially for the function and stability of membrane proteins, lipids are indispensable. Due to their hydrophobic acyl side chains and polar headgroups, lipids tend to form bilayers.[30–32]

Although membranes separate cell compartments from each other, allowing specific transport of substances between the compartments. Due to their structural motif, membranes are always selectively permeable and allow specific entry and exit of molecules.[26,33] Biological membranes, consequently, are critical in controlling the permeation of small molecules. They can also mediate the lateral diffusion of small molecules. Therefore, biological membranes in the field of pharmacokinetics, bioavailability, and drugs are gaining importance.[34–36]

Also, specific processes for cell compartmentalization and cell protection are truly critical features of membranes. One vital role is also the control of substance transportation, *e.g.* during the exocytosis or signal transduction.[29,37,38] These compartments allow separating different reaction centres from each other. In general, these specific compartments are located in different regions of the living organism (*e.g.* endoplasmatic reticulum (ER), golgi apparatus, endosome and lysosome).

The transport process runs according to two different ways. On the one hand, the transportation of proteins occurs directly through the membrane and only when a specific protein translocator is present. In addition, only the unfolded proteins can surpass the membrane.[39] On the other hand, vesicles are used to transport substances from one compartment to another. This specific movement of vesicles and substances within the cell is referred as an intracellular transport process.[40] Therefore, exocytosis can be taken as an example to describe the active process in the synaptic gap, where the vesicles fuse with the cell membrane to transport neurotransmitters from one location to another. The vesicle cavities are filled with neurotransmitters which are then released after fusion with the plasma membrane.

Besides the remarkable complex structure and its functionality, membranes are highly dependent on the organization of their components. Either way, biological membranes can embed different set of small molecules and proteins. The proteins are located in different positions on the membrane. Peripheral membrane proteins are, for instance, located outside the membrane and integral proteins are located inside the membrane surface. Therefore, these proteins have to fulfill a specific requirement to be able to

surpass the lipid water interface.[41,42] Additionally, the processes like ion transportation via channel formation due to specific proteins has also been essential as one of the key roles of membranes.[43,44]

2.2 Model Membrane Systems

Model membrane systems allow studying the interaction with other molecules. Therefore, highly complex systems have been represented using membrane lipids. Model membrane systems can be reproduced easier, especially for the most abundant lipids found in the biological membrane. The reduced complexity allows systematically investigating the influence of small molecules (*e.g.* proteins, sugars) in different environments. In addition, model systems can also be used to investigate particular effects, *e.g.* lipid composition, pH, ionic strength. The best-studied model systems are the pure lipid bilayers, *e.g.* those of phosphatidylcholines. They form the basic structure of biological membranes and already provide important information about the properties of natural membranes.[45]

In order to get a better insight of model membrane systems, membrane lipids will be on closer examination (Figure 2.2). Membrane lipids are amphipathic molecules consisting of a polar head group and a hydrophobic acyl tail chain. Due to the unique construction of the membrane lipids, lipid bilayers are formed preferentially. Based on physicochemical properties which are needed or should be reproduced, the properties of the lipids have to be adapted in order to obtain either micelles, liposomes or lipid bilayers.[46]

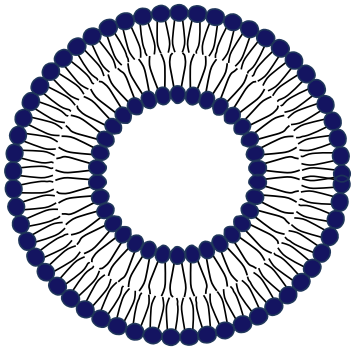

Figure 2.2: Schematic representation of a liposome. Liposomes are formed due to the amphipathic character of membrane lipids. Each lipid consists of a hydrophobilic head (blue) and a hydrophobic tail (black).

Lipid membranes can be represented through the diversity of membrane composition depending on which lipids are used. For instance, mammalian plasma membranes are built up of three zwitterionic phospholipids (DOPC, DPPC, POPC).[47] However, other membranes, for example, erythrocytes are built up with over 100 different lipid molecules.[48,49] In general, the most common lipids to be found in biological membranes are phospholipids. The hydrophobic acyl side chain can be between 14 to 24 carbon atoms and differ in the saturation level.[45] The basic structure of extracelluar vesicle consisting of different lipids is illustrated in Figure 2.3.

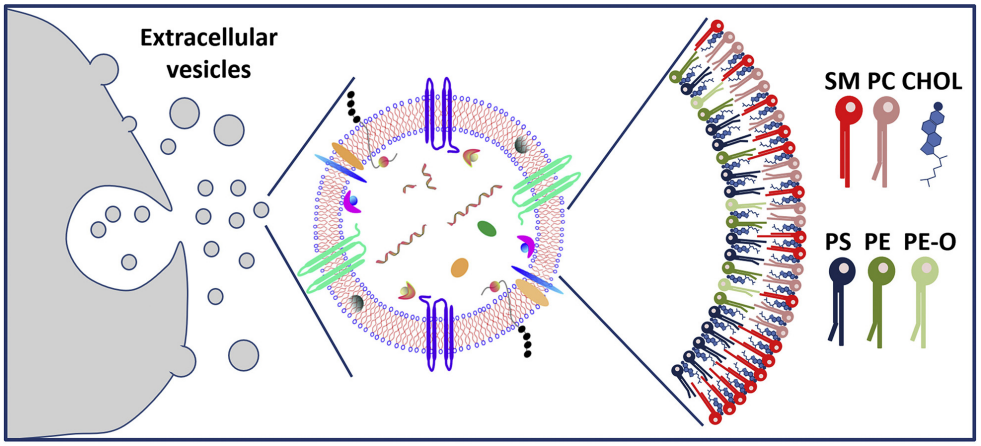

Figure 2.3: Extracelluar vesicles are lipid bound vesicles, which consists of different lipids. The represented vesicle contains, *e.g.* sphingomyelin (SM), phosphatidylcholines (PC), cholesterol (CHOL), phosphatidylserin (PS), phosphatidylethanolamine (PE) and phosphatidylethanolamines (PE-O). Based on ref.[50].

The classification of biological lipids can be divided into three significant groups. These are glycerophospholipids, sphingolipids and sterols.[46] The chemical diversity of lipids is enormous depending on the type and particular mixture of different lipids, a change in several properties can be achieved. However, membrane thickness and flexibility, even changing polar headgroups, can influence the curvature of membranes.[51] Therefore, lipids offer a variety of application opportunities when the interaction between the lipids and proteins influences flexibility and fluidity.[52–54]

2.3 Fusion Proteins

2.3.1 SNARE-Proteins

Soluble *N*-ethylmaleimide-sensitive-factor attachment receptor (SNARE) proteins are a prominent family of eukaryotic proteins. These proteins are characteristic for their specific SNARE motif, which contains an evolutionary conserved fragment of approximately 60 amino acids in a repeating manner of seven amino acids.[55] Since 1980s, the interest in SNARE proteins have drawn attention, after their role to mediate synaptic vesicle fusion has been characterized.[56] Currently, 25 SNARE proteins were discovered in yeast (*saccharomyces cerevisiae*), 36 in the human body, and 54 in plants (*arabidopsis thaliana*).[57]

Synaptobrevin-2, Syntaxin-1A and SNAP-25 (25-kDa synaptosome-associated protein) be part to these specific set of proteins. Synaptobrevin-2 is a vesicle-bound membrane protein, which was purified from synaptic vesicles.[56] On the contrary, Syntaxin-1A and SNAP-25 were located in the plasma membrane.[58–60] Particularly, the essential characteristics of these proteins is their structure. The individual SNARE structure consists of the SNARE motif and, in some cases, a transmembrane domain. The role of the transmembrane domain is to anchor the protein into the hydrophobic surface of the membrane.

In the beginning SNARE proteins were distinguished between *v*-SNAREs (vesicle membrane SNAREs) and *t*-SNAREs (target membrane SNAREs). This classification was categorized based on the location of the SNARE proteins.[61] The classification based on the location have been adjusted after showing that membranes of the same nature are also able to fuse. Fasshauer *et al.* proposed a new classification based on X-ray structure analysis.[62] The new classification differentiate the SNARE proteins based on their structural properties in Q- SNAREs and R-SNAREs. In general, a SNARE complex is constructed by containing 16 levels of four interacting amino acids. These level are mainly hydrophobic, except for the '0'-level. The specific '0'-level can be classified into three glutamine (Q) and one arginine (R) residue, leading to Qa-, Qb-, Qc-SNAREs and also in R-SNARE. In Figure 2.4, Qa-, Qb-, Qc-SNARE and also R-SNARE-Proteins are illustrated.

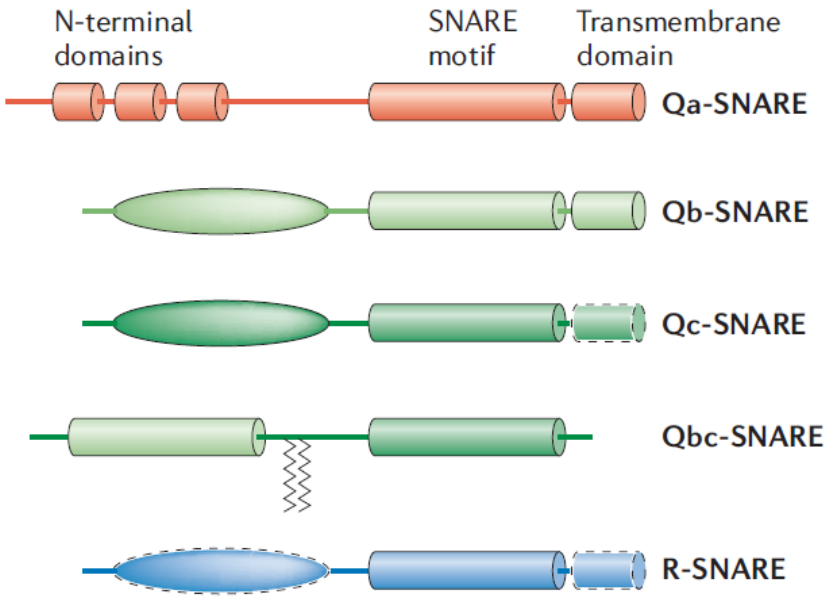

Figure 2.4: Schematic representation of SNARE proteins. Depending on different *N*-terminal domains distinction between Qa-, Qb-, Qc-SNARE and also in R-SNARE-Proteins can be made. Based on ref.[63].

Exocytosis ends in the release of neurotransmitters into the synaptic gap after membrane fusion. Key player in membrane fusion are as follows, Synaptobrevin-2 (VAMP), Syntaxin-1A and SNAP-25. Syntaxin-1A and Synaptobrevin-2 consists of transmembrane domain and a their characteristic SNARE motif. In general, it can be assumed that a stable SNARE complex can be formed if one Qa-, Qb- or Qc-SNARE finds an R-SNARE motif. The secondary structure of Syntaxin-1A was observed in physiological salt solutions to form an α-helix. In comparison to that, the secondary structure of SNAP-25 (Qb- und Qc-SNARE) and Synaptobrevin-2 (R-SNARE) were also observed but only in very small abundance.[64]

2.3.2 SNARE-Induced Membrane Fusion

Membrane fusion mediated by SNARE proteins have been generating great interest in the past decades. Their role and a mechanistic scheme of this characteristic cylcle has been presented by JAHN *et al.*[57] In general, two membranes will not merge with each other without a driving force, which helps to surpass the energy barrier of these membranes. SNARE proteins fill these specific role by interacting with each other. It has been assumed that the interaction between the SNARE motifs starts by zippering

$N \rightarrow C$-terminally. The SNARE proteins are located in opposing membranes and start to interact in a parallel orientation. The X-ray structure analysis confirmed the parallel orientation.[62] The function of the SNARE proteins and their properties was studied based on neuronal exocytosis.[60,65–67]

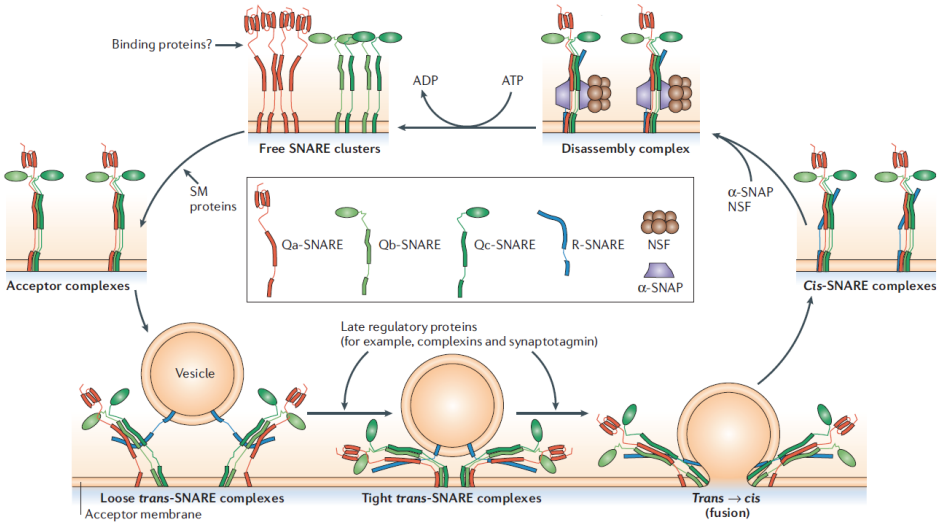

Figure 2.5: Schematic representation of the SNARE cycle introduced by Jahn *et al.*, describes the mechanistic steps during membrane fusion. The neuronal SNAREs Syntaxin-1A and SNAP-25 are positioned on the plasma membrane. The process is initiated by forming the acceptor complex with Syntaxin-1A and SNAP-25. The loose-*trans*-SNARE complex is formed by interacting with Synaptobrevin-2, which is located on the vesicle membrane. The zippering from $N \rightarrow C$-terminus can be proceed, forming the *cis*-complex. SNARE proteins can be restored with ATP, NSF and a cofactor (α-SNAP). Based on ref.[55].

In Figure 2.5, a schematic representation of the characteristic SNARE cylce is displayed. The membrane fusion mediated by SNARE proteins can be described in a simplified manner. The process is initiates when SNAP-25 and Syntaxin-1A forming the acceptor complex, followed by the interaction with Synaptobrevin-2. The interaction with the vesicle-bound SNARE protein leads to the formation of a loose *trans*-complex. In this stage, the interactions are strongly reduced, where the protein complex is bound loosely. Regulatory proteins can initiate the next step, which leads to zippering from $N \rightarrow C$-terminus, forming the tight *trans*-SNARE complex. The tight *trans*-complex switch then to the *cis*-complex during the membrane fusion stage. After merging the vesicle membrane to the plasma membrane, the *cis*-SNARE complex is located on the plasma membrane. The final step is the disassembly of the *cis*-complex and recycling of the SNARE proteins. This can be achieved with the help of ATP, NSF (*N-ethylmaleimide-sensitive factor*) and a cofactor (α-SNAP).

2.4 Concepts of Membrane Fusion

The mechanistic principles of membrane fusion mediated by SNARE proteins has not been fully understood. However, the zippering has been proposed to play a key role in membrane fusion. As mentioned in Section 2.3.2, the formation of the parallel SNARE *trans*-complex initating the membrane fusion between the plasma membrane and a vesicle membrane, by bringing them into close proximity, the zippering the $N \rightarrow C$-terminal assumed to be started.[68–70]

In biological studies, the first signs of zippering were observed after testing Syntaxin-1A and Synaptobrevin-2 binding with each other. A ordered binding of these SNARE proteins could be observed.[71,72] Liu *et al.* investigated the specific interactions during the disassembly process of the SNARE complex. The SNARE complex is formed by binding Synaptobrevin-2 to Syntaxin-1 and SNAP-25.[73] This specific SNARE complex reported to be present in parallel or anti-parallel orientation. However, the anti-parallel SNARE complex have been stated to be less stable. The enthalpies of the parallel and antiparallel SNARE complexes were determined (42.1 k_BT and 39.8 k_BT) and the difference of 2.3 k_BT shows that the parallel orientated SNARE complex is more stable than the antiparallel one.[74]

An approach to get more insight of the zippering mechanism were made by Hua *et al.* Therefore, clostridial toxins and antibodies were injected to the SNARE motifs, in order to mutate the hydrophobic core of the SNARE complex.[75] The experiments were performed with two different botulinum toxins to cleave Synaptobrevin-2 either $N \rightarrow C$-terminally. Botulinum D toxin has been reported to cleave the SNARE protein N-terminally, while Botulinum B cleaves the C-terminal side. However, a cleavage of the SNARE proteins was not possible once the stable SNARE complex was formed.[76]

The importance of the zippering during the SNARE complex have been intensively studied. On the one hand, the SNARE complex catalyzes membrane fusion by bringing the membranes into close proximity.[28,77–79] On the other hand, SNARE proteins have been stated to form a fusion pore. In Figure 2.6, two assumed fusion pathways have been presented. The first pathway illustrates two lipid bilayers forming a hemifusion-diaphragm and leading to the fusion pore (Figure 2.6a). The second pathway illustrates the formation of a protein pore after protein interaction (Figure 2.6b). At the end, the bilayers can fuse, which completes the membrane fusion process.[80]

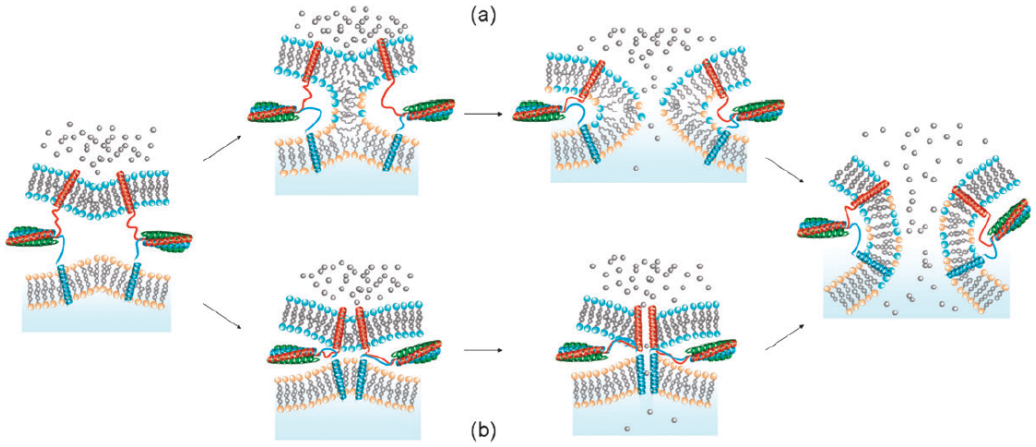

Figure 2.6: Mechanistic representation of the key steps during membrane fusion. Two lipid bilayers interact with each other forming the lipid *stalk*. (a) Then, the lipid *stalk* is expanded by forming the hemifusion-diaphragm, followed by a fusion pore formation. (b) Alternative a protein pore can be formed and the membrane fusion of two lipid bilayers can be reached. Based on ref.[26].

Chernomordik *et al.* proposed opening steps of membrane fusion.[81] Similar to the previous described pathways, membrane fusion starts by the formation of the lipid *stalk*. In this stage, a few lipid molecules come in close contact and interact with each other. The next stage was proposed to be the formation of the hemifusion-diaphragm, followed by membrane fusion. In general, these steps are not energetically favourable.[68–70] The presence of the *stalk* intermediate could be successfully verified via X-ray experiments.[82] Also, the hemifusion stage has been reported to be mediated by the synaptic vesicles.[65,83,84]

As mentioned above, there are two stages during membrane fusion. The specific curvature of membranes plays a important role. Depending on the specific curvature the presence or absence of these two stages could be observed.[85] The membrane curvature is depending on lipid composition. In general, lipids can form either negative, neutral or positive curvature.[86] The curvature is efficient enough to determine if fusion is favored or not. A positive membran curvature have been reported to inhibit the *stalk* intermediate formation.[87]

Several groups have analyzed the importance of the transmembrane domain in membrane fusion. Therefore, Jahn *et al.* discovered that the cytosolic domain of Synaptobrevin is not structured enough and suggested that Synaptobrevin-2 have to be rather

rigid.[88] Gao *et al.* have investigated the specific interaction between Syntaxin-1A and Synaptobrevin-2.[89] They have stated relatively small affinity of Syntaxin-1A to Synaptobrevin-2. The group of sansom *et al.* proposed a zippering in three stages due to the flexible the linker region, while the group of pincet *et al.* suggested that the zippering is a two step mechanism.[90,91]

2.5 Model Systems for SNARE-Induced Membrane Fusion

In general, model systems offer the advantage to selectively adapt environmental conditions precisely to native ones allowing to study only specific regions of interest. Therefore, mimic synaptic vesicles and membranes can easily be reproduced by choosing various liposomes that differ in sizes and compositions. Membrane fusion is highly regulated by SNARE proteins. Thus, to study the mechanistic features of membrane fusion, model systems have been developed to simplify the complex processes. Therefore, the complex system was reduced to a minimum and specific compartments were modified and adjusted to mimic membrane model systems. The function of the highly specialized SNARE proteins with their characteristic SNARE motif of four helices is simplified to model system of a heterodimer forming artificial model peptides.

Struck *et al.* introduced a model system to study membrane fusion.[92] The liposome fusion assays were designed to detect Förster resonance energy transfer (FRET) due to membrane size changes. FRET-based liposome fusion assays are commonly used to study membrane fusion. Therefore, fusion between two lipid bilayers can be monitored using total lipid mixing or content mixing. Total lipid mixing can be monitored by preparing two liposome populations with respective model peptides. For FRET-based liposome fusion assays can be prepared either in the dequenching setup or quenching setup (see more detail in Section 4.2). Content mixing can be applied to distinguish between complete and hemifusion. Therefore, the outer leaflets were quenched, leaving only the inner leaflets labeled.[93,94] Nevertheless, leakage or burst of vesicles has been a significant issue of content mixing assays leading to false results. Alternative studies that distinguish between leakage or vesicle bursting were monitored using planar pore-spanning membranes. Content release during the fusion process shows that two lipid bilayers' fusion pore formation continues within 40 ms.[95]

Membrane fusion can be analyzed in various approaches. Therefore, artificial model systems mimicking the native sequence of SNARE proteins can be used to synthetically modify and systematically control and improve the fusion process in general. Therefore, artificial SNARE analogues are prepared consisting of a recognition unit, linker region and transmembrane domain. These model peptides can easily be modified and adapted to each condition for detailed studies. The systematical variation and modification provide opportunities in terms of membrane fusion studies. Some model systems using artificial SNARE proteins to promote membrane fusion will be listed hereafter.

Model systems allow studying the fusion machinery of SNARE proteins in many ways. For instance, Stengel *et al.* developed a model system consists of DNA-base pairing. Therefore, dioctadecyl-glycerol anchored DNA strands were synthesized. The DNA recognition unit were designed to form stable DNA duplexes using complementary or partially complementary DNA sequences attached to cholesterol anchors (Figure 2.7).[96]

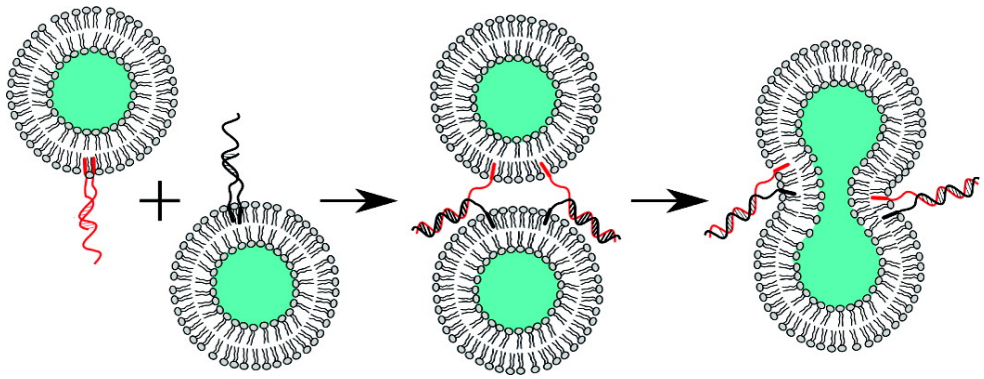

Figure 2.7: Lipid mixing assay consists of DNA-anchored liposomes with complementary DNA recognition motifs. The DNA model peptides have been cholesterol anchored containing a PEG4-linker. Presenting the membrane fusion process after successful DNA base pairing. Based on ref.[96].

Lipid mixing with the DNA model system could be monitored only up to 30 %. Additionally, studies varying the length between recognition units were achieved by introducing mono- or double cholesterol anchor containing PEG4-linker. An increase of distance due to the long DNA spacer enhances membrane docking and reduce full fusion. The role of distances has a significant impact on enhancing membrane fusion.[96–99] Chan *et al.* also developed an artificial model system using DNA-base pairing. However, the duplex formation of complementary DNA sequences is sufficient for membrane

fusion.[99] The recognition unit shows enhanced membrane fusion character when established 5- and 3-end DNA attached to separate liposomes.

Vacuolar SNARE transmembrane domains have been reported as a non-specific membrane anchor, prone to self-aggregation or interaction.[100] However, identical transmembrane domain attached to complementary peptide nucleic acid (PNA) recognition units showed a valuable decrease in fusion efficiency compared to different transmembrane domains. Lygina *et al.* established a different model system using PNA as a recognition unit. As PNA building blocks, two complementary aeg-PNA-decamer were chosen, which already were probed by Wittung *et al.* in several experiments.[101] PNA recognition units reported to be able to form stable duplexes in parallel and antiparallel orientation. This model systems differ from others due to the specific design of model fusogens. Therefore, the linker and transmembrane domain sequence of the native SNAREs Syntaxin-1A and Synaptobrevin-2 is attached to an artificial recognition unit. In particular, PNA enables characteristic features in similarity to DNA. Additionally, they are also thermally stable and allow a variety of possibilities in developing PNA/peptide hybrids. PNA/peptide hybrids with a decameric PNA recognition unit show maximized fusion efficiency when duplex assembly was achieved in parallel orientation (Figure 2.8).[102]

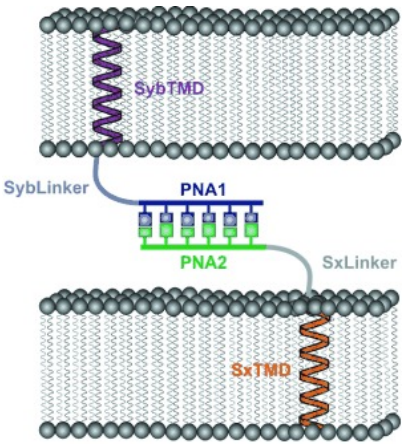

Figure 2.8: SNARE-mimicking model system consisting of a transmembrane domain with artificial PNA recognition motifs. The PNA recognition motifs were designed to form stable duplexes in parallel or antiparallel orientation. Here, the antiparallel recognition of two complementary PNAs are presented. The native transmembrane domain sequences of Syntaxin-1A and Synaptobrevin-2 were used as lipid anchor. Based on ref.[102].

Furthermore, Wehland *et al.* could observe a significant increase in fusion efficiency when exchanging the net charge of SNARE model peptides. Indicating that a neutral net charge leads to an enhanced fusogenicity, and two-fold negatively charged model peptides lead to a decrease in fusogenicity.[103] Hubrich *et al.* was showing that the PNA/peptide hybrids containing pentameric PNA as recognition unit are also sufficient to mediate membrane fusion. In Addition, fluorescence cross-correlation spectroscopy (FCCS) measurement gave insight and allowed to distinguish between complete fusion and hemifusion of the pentameric PNA/peptide hybrids.[104]

Mardsen *et al.* demonstrated a wide range of model systems. One model system was introduced using coiled-coils as molecular recognition units.[105] Therefore, a lipid anchor was elongated by a flexible PEG linker attached to EIAALEK (E) or KIAALKE (K) (Figure 2.9). These peptides recognition motifs are composed of three repeating heptad units of E or K, which allow them to assembly by forming a heterodimeric coiled-coil structure. Previous studies showed that fusogens containing lipid anchors are insufficient for membrane fusion, leading only to docking.[106,107] The reduced curvature stress induced by a lipid anchor leading to reduced fusion efficiency. Nevertheless, sufficient membrane fusion via lipid mixing and content mixing could be observed using these specific fusogens.

Recent studies of Kros *et al.* reported the crucial role of K3 and E3 in the SNARE model system process. The role of K3 during the fusion process has been illustrated in recent studies. However, the strong interaction of K3 with the lipid membrane and also forming homodimer has been investigated extensively. However, the specific role of K3 interacting with the membrane and disruption of lipid membrane has been proposed as an essential step to induce membrane fusion. One key effect from that specific membrane interaction result in dropping the energy barrier and facilitate the membrane fusion process.[21,22] Nevertheless, the developed model fusogens have generated great interest in applied science (*e.g.* drug delivery). Kong *et al.* designed lipopeptides containing photosensitive protecting groups, which allow controlling membrane fusion temporarily.[108]

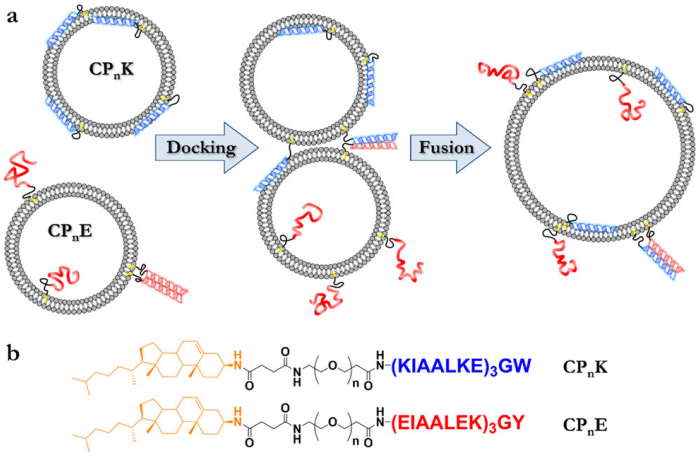

Figure 2.9: Coiled-coil model system using a lipid anchor attached to a flexible PEG linker and E3 or K3 in order to form stable heterodimers. (a) The schematic view of the designed model system during membrane fusion is shown.(b) Specific designed model systems with either E3 or K3 attached to PEG linker are displayed. Based on ref.[22].

The presented model system of Mardsen *et al.* was further modified by Meyenberg *et al.* Therefore, the peptides E3 and K3 were used as recognition units to replace the native SNARE motif. Additionally, the recognition units were connected with a linker and the neuronal transmembrane domain of Synaptobrevin-2 and Syntaxin-1A, respectively. The fusion between the membranes was successfully probed using lipid-mixing and content mixing assays.[81] The fusogenic construct has shown some disadvantages for attaching the recognition, which does not allow the recognition process compared to the native systems. These specific differences can limit and influence fusion efficiency.[109] In this thesis, SNARE analogues will be designed and employed to investigate the membrane fusion process further. Additionally, caged-PNA/peptide hybrids will be applied to investigate if control over membrane fusion can be observed.

3 Liposome Fusion Analysis

Liposome fusion assays can be monitored in many different ways. One commonly applied technique to study membrane fusion is the use of FRET-based fluorescence measurement, which occurs in various assays (*e.g* quenching and dequenching assays). In this chapter, specific fusion assays which were used in this work will be presented.

The analysis of artificial fusogens in combination with LUVs has been effective to verify sufficient membrane fusion. Also, pore-spanning assays, as well as fluorescence microscopy, are established techniques to study membrane fusion.[95,105] Liposome fusion assays can be described as a process where lipid membranes merge with each other. Thus, the driving force of the membrane mixing process can be mediated by a specific set of SNARE proteins. To study this specific behavior, total lipid mixing- and inner lipid mixing assays can be applied. Either way, the FRET-based fluorescence measurement was designed to monitor the specific membrane fusion process initiated by artificial fusogens.

The different approaches to study membrane fusion rely on the FRET effect. Therefore, specific, fluorescent FRET pairs were used. Incorporation into the lipid bilayer enables monitoring of successful conversion by artificial SNARE model peptides. The use of total lipid mixing assay can be chosen between the dequenching or quenching assays. These assays have a similar approach to study membrane fusion. However, depending on the applied assay, preparation and monitoring of measurements differ slightly. A detailed description will be presented in Section 4.2. In general, an increase or decrease in fluorescence intensity can be detected when the distance of FRET pair has been change during membrane fusion. The progression can be observed in the fluorescence spectra and will explained hereafter.

3.1 Förster Resonance Energy Transfer (FRET)

As one of the critical achievements of lipid mixing assays, STRUCK *et al.* provided in 1981 an assay that demonstrated lipid mixing via FÖRSTER resonance energy transfer (FRET).[92] FRET is a measurable nonradiative transfer of energy between a donor and acceptor dye. The energy transfer is a physical process, which illustrates the occurrence of donor- and acceptor dye nearby within 10 nm.[110] Consequently, in order to observe FRET specific criteria has to be fulfilled. In general, donor dye can be excited, transmits energy to the acceptor dye, whose emission can be detected. Thus, the emission spectrum of the donor dye has to overlap with the excitation spectrum of the acceptor (see Figure 3.1).

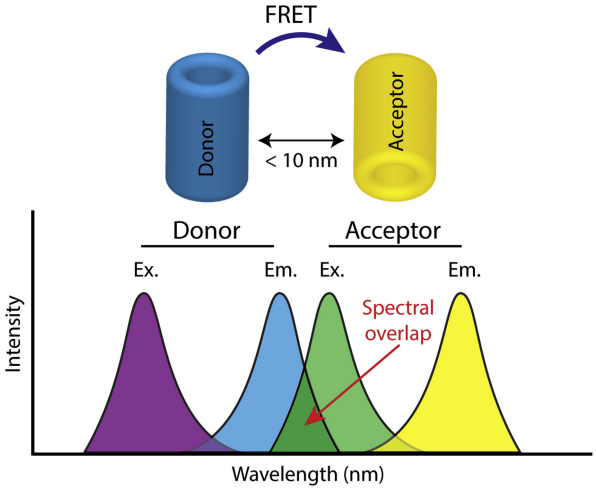

Figure 3.1: Specific criteria for FRET are illustrated. The donor emission spectrum (Em.) and acceptor excitation spectrum (Ex.) have to overlap in order to observe FRET. The minimum distance between donor and acceptor dye has to be within 10 nm. Based on ref.[111].

FRET allows a wide range of application possibilities and enables the extensive analysis of biological processes. Especially in the field of nanomedicine, FRET could enable new perspectives as a effective tool to show specific changes and interaction of small molecules after transportation. Additionally, plenty of other biological processes like Protein-protein interactions, membrane fusion and membrane mapping can be investigated by application of the FRET-technique.[112]

As stated by FÖRSTER in 1981, the FRET efficiency of the energy transfer is dependent on the radius of the applied donor- and acceptor dyes. The following equation (3.1) describes the FRET dependence η_{FRET} energy transfer which is related to the distance r between the applied donor- and acceptor dyes.

$$\eta_{\mathrm{FRET}} = \frac{1}{1 + \left(\frac{r}{r_0}\right)^6} \tag{3.1}$$

Here, r is the distance between donor- and acceptor dye and r_0 the FÖRSTER radius. The FÖRSTER radius describes the distance between the FRET pair which results in 50 % FRET efficiency. In general, an overlap of 30 % of the energy transfer from donor to acceptor has to occur for reliable FRET detection.[113]

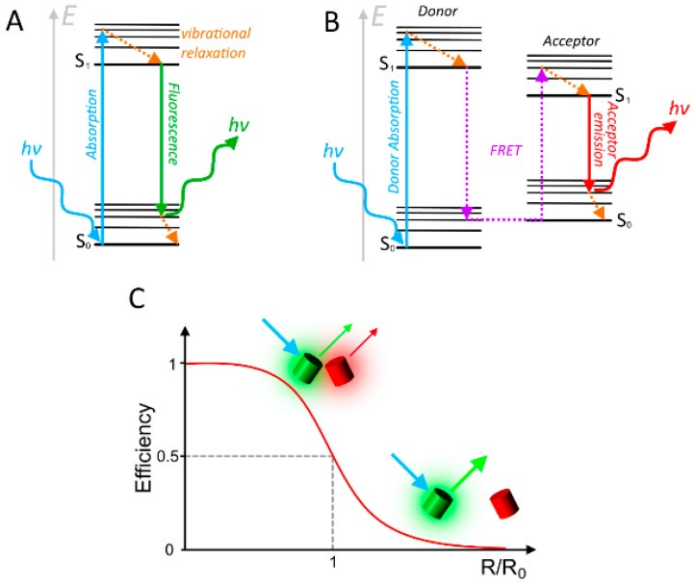

Figure 3.2: Sketch of the FRET effect through the JABLONSKI-diagram. The donor dye is irradiated with its characteristic wavelength, where the energy is absorbed by electrons in the ground state (S_0). After excitation the state S_1, either the electron relaxe to the ground state, or the excitation transfer to the acceptor dye. Based on ref.[110].

The phenomenon of FRET can be visualized using the JABLONSKI-diagram which can be found in Figure 3.2.2. The JABLONSKI-diagram shows the specific electronic states and transitions during energy transfer. For FRET the donor dye is irradiated with its characteristic wavelength, where the energy is absorbed by electrons in the ground state (S_0). After excitation the state S_1, two occasions can occur. Either the electron

relaxe to the ground state, or the excitation leads to the acceptor dye. The energy transfer to the acceptor dye can be explained due to dipole-dipole interaction.[114] Thus, the electrons of the acceptor will be excited into the S_1 level, thereby fluorescence at emission wavelength will be detected, when electron relaxe back to S_0.

3.2 Total Lipid Mixing Assays

Lipid mixing assays belong to the most common methods to study membrane fusion. This method is based on the physical process of the distance-dependent FRET effect. Total lipid mixing assays can be differentiated between quenching- and dequenching assays.

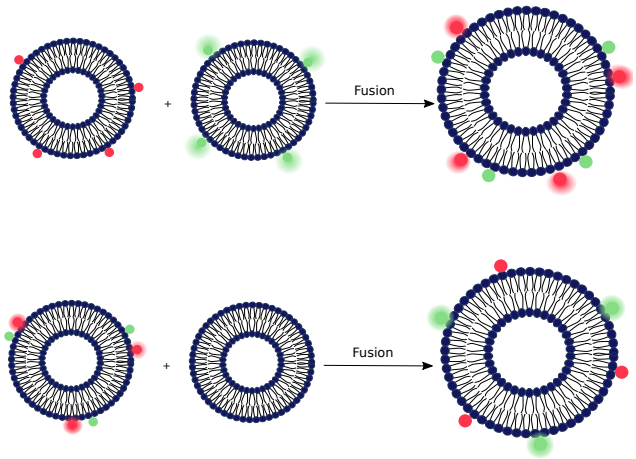

Figure 3.3: A schematic view of the two different total lipid mixing assays. In the fluorescence dequenching assay an increase of the donor emission could be detected when two membranes had to be merge together. While in the fluorescence quenching assay a decrease of the donor emission could be detected when membrane fusion occured.

In Figure 3.3, the two different total lipid mixing assays are presented. In the fluorescence dequenching assay, both dyes are located in the same liposome population. Furthermore, acceptor and donor dye are already in close proximity, which allows energy transfer to occur. Regarding the fluorescence measurement setup, in the dequenching assay, the donor emission is reduced prior to fusion. While the membrane fusion proceeds, the average distance between the dyes is extended. The change in distance leads to no further FRET, which results in a donor emission increase. The quenching assay differs in setup with two different liposomes populated with either a

donor or an acceptor dye, respectively. In terms of fusion measurements, due to the increased distance between donor and acceptor dye the donor emission is increased prior to fusion. During liposome merging, distance between the FRET pair is increasing when fusion occur. Therefore, positive membrane fusion results in a decrease of the donor emission.

3.3 Dynamic Light Scattering (DLS)

Dynamic light scattering (DLS) can be provided as a complementary method to study membrane fusion between liposomes. According to this technique, reliable information about size and aggregation of liposomes can be gained. Especially in lipid mixing assays, the change in liposome size can provide useful information about effective fusion.[115–117]

In a DLS instrument, when monocromatic light encouters macromoleclues or particles (*e.g.* liposomes), the incident light will be scattered, which can be detected. However, the detector of a DLS instrument can be employed in regard to the incident light. In this work, a Zetasizer Nano S from *Malvern* was utilizied with a detector angle of 173°.[118] The instrument allows to measure highly concentrated samples by avoiding multiple scattering phenomena.[118]

As long as individual particles of dispersion can move independently in the surrounding medium, the Brownian motion of the particles provides accurate information about the particle size. The Stokes-Einstein formula provides the relationship between the diffusion coefficient D and the particle size d. The temperature T and the viscosity η of the medium were measured or known.

$$D \sim \frac{T}{\eta d} \text{ (Stokes-Einstein)}$$

The diffusion coefficient D can be established by DLS experiments. Therefore, the motion of the particles is connected with the measured intensity fluctuation. The evaluation takes place via the autocorrelation analysis of the fluctuations.[119]

In equation 3.2, the analyzed relationship according to the Stokes-Einstein formula is shown. This equation represents analyzed fluctuations of the scattered light. Additionally, the hydrodynamic diameter d_h can provide information on the size by the following equation.

$$d_{\mathrm{h}} = \frac{k_B T}{3\pi\eta D} \tag{3.2}$$

Here, k_{B} is the BOLTZMANN constant, T is the absolute temperature, η is the viscosity of the medium, and D is the diffusion coefficient. The equation 3.2 relies only on calculating spherical particles. Therefore, the equation applies only to spherical particles, making it difficult for other particle studies. DLS measurements are very sensitive to certain parameters (*e.g.* temperature, solvent viscosity). However, the resolution in DLS cannot separate related molecules bound to the surface (*e.g.* ions and hydration sphere).[118] Therefore, variation in size may occur.

4 Fusion Assays

Different working groups have extensively studied membrane fusion using artificial model peptides.[22,102] Depending on the used model peptides, different outcomes in fusion activity could be detected. In previous studies, substantial loss on fusogenicity has been a significant problem leading to various adjustments in applied lipid mixing assays.[18,20] Primarily, the preparation procedure and the applied fusion will be described and explained in detail in the first sections (Sections 4.1 and 4.2). Followed by the uncaging experiments of caged-PNA/peptide hybrids (Section 4.3). In addition, dynamic light scattering (Section 4.4) was utilized to confirm the size change after membrane fusion.

4.1 Liposome Preparation

The standard procedure of liposome preparation will be explained in more detail. For the dequenching and the quenching assay, the preparation is very similar. The main difference of these two assays is the preparation setup. Depending on the applied assay, FRET fluorophores were located in the same or different liposome population.

The reconstitution of artificial peptide fusogens in LUVs was performed by adding a certain amount of peptide and lipid stock solutions in a test tube. The model peptides were dissolved in trifluoroethanol (TFE). Lipid stock solutions were prepared by dissolving different lipids in chloroform. During the preparation, attention has to be paid to potential solvent evaporation, which can falsify the measurement. Therefore, the preparation of the proteoliposomes was carried out under cooling at 0 °C . However, the used solvents TFE and chloroform have been revealed to be inhomogenous at 0 °C. After reaching room temperature, the test tubes were vortexed for 30 s. Subsequently, solvents were removed from the test tubes under a nitrogen stream. Finally, the test tubes were stored in the vacuum oven at 50 °C overnight to obtain dry lipid films.

On the following day, the lipid films were rehydrated in buffer and in order to obtain

homogeneous suspension of multilamellar vesicles (MLVs). Then, the samples were incubated at 40 °C for 1.5 h in a thermoshaker. The samples were placed at 40 °C for 30 min in a water bath. The formation of MLVs was completed by sonicating the samples for a less than 10 s. After sonication, the MLVs were directly extruded through a polycarbonate membrane (100 nm pore size) to acquire LUVs. Lipid loss during the extrusion process was determined via phosphate test or fluorescence measurement depending on the used fusion assay.

During the liposome preparation, especially in films of model peptides containing SxTMD, aggregates were formed, and higher lipid loss could be observed. A reasonable explanation for this variation could be the strong interaction of SxTMD with lipids. Also, other factors could have an influence during the preparation process. Adding glass beads into the test tubes of SxTMD based model peptides did improve liposome quality significantly. For fusion measurements, low peptide concentration was sufficient to observe membrane fusion. To obtain a precise value, UV/Vis measurements were applied to determine peptide concentrations. The absorption of each model peptide was measured and the concentration was calculated via Beer-Lambert law by the sum of the extinction coefficient for PNA and aromatic amino acids.

4.2 Total Lipid Mixing Assays

Lipid mixing experiments were performed by applying either the quenching assay or the dequenching assay. In the particular case of the quenching assay, some adaptation to the standard preparation had to be made. In general, fusion assays were performed using a HEPES (4-(2-hydroxyethyl)-1-piperazineethanesulfonic acid) buffer.[102,120] The HEPES buffer was prepared with ethylenediaminetetraacetic acid (EDTA) as a chelating agent to trap divalent ions. Additionally, dithiothreitol (DTT) was added to prevent the oxidation of cysteine moieties and thus from forming disulfide bridges.

In previous studies, the dequenching assay was more frequently used in our working group. However, in this thesis, the quenching assay was also a major part of studying membrane fusion and have been used intensively. The basic description of both assays has been presented in Section 3.2. In general, for the quenching assay, liposomes were prepared by incorporating SxTMD based peptides and SybTMD based peptides. The different sets of liposomes were prepared to contain a donor and a acceptor fluo-

rophores, respectively.

In the dequenching assay, the liposome populations were prepared to contain SybTMD based peptides while unlabeled liposomes were prepared with SxTMD based peptides. Significant differences between both fusion assays could not be detected. Nevertheless, specific liposomes had to be prepared differently depending on the type of model peptide used. In general, SxTMD based peptides tend to have liposome stability issues during preparation. Therefore, SybTMD based peptides were prepared first. SxTMD based peptides were prepared afterwards and measured subsequently. The SxTMD based peptides turned out to be challenging. Therefore, the preparation had to be performed in a particular preparation procedure. If not, highly cloudy precipitate in liposome containing SxTMD based peptide was observed after few hours. The occurrence of this phenomenon can be caused by strong interaction of the SxTMD based peptides with each other forming aggregates. For that reason, liposomes had to be prepared more precisely in order to be comparable with former fusion event measurements. Additionally, a decrease in fusion efficiency could be observed if fusion measurements were not performed immediately. A possible explanation for liposome instability, which Hubrich and Groth also observed, is that a kind of ageing process of the liposomes or interaction between the peptides could lead to liposome bursting.

The standard setup for the dequenching assay will be introduced hereafter. The liposome ratio of labelled to unlabeled liposomes was set to 1:4.[18–20,102] This specific ratio was determined as the optimal ratio for effective membrane fusion. For the quenching assay, the ratio was set to 1:1. This setup has been chosen in order to ensure the exact same amount of both liposome populations. In the particular case of the quenching assay, the exact liposome concentration was determined via fluorescent spectroscopy. Before every fusion measurement, the fluorescent spectrum of the donor and acceptor fluorophore was recorded. The resulting spectra facilitated the proper stoichiometry of liposomes. After that, the donor fluorophore containing liposomes were filled first, and the emission spectrum was detected. As soon as a clear spectrum was recorded, the acceptor fluorophore containing liposome was added to the cuvette to start the fusion process. Based on the applied fusion assay, different measurements were recorded to observe membrane fusion. For the quenching assay, the fluorescence emission of the acceptor fluorophore and for the dequenching assay, the emission of the donor fluorophore was monitored over time. In the case of the quenching assay, it was not possible to reach constant progression over time. Instead, a slight and continuous decrease in

donor emission was recorded, likely due to photobleaching or liposomes sticking to the cuvette wall.

Commonly, the FRET pair of the donor fluorophore N-(7-nitro-2-1,3-benzoxadiazol-4-yl) (NBD) and the acceptor fluorophore lissamine rhodamine B (Rh) was used to monitor membrane fusion. For the quenching assay, a different set of FRET pairs was used. The FRET-based experiments for the quenching assay were performed with Oregon Green (OG) and Texas Red (TR). In the case of practical fusion observation, these quenching setups could be used to do fluorescence cross-correlation spectroscopy (FCCS) measurements in order to distinguish between hemifusion and fullfusion.[20]

As already mentioned before, the properties of fluorophores can have an impact due to environmental circumstances. Therefore, FRET-based measurements were performed with liposomes containing 1.5 mol % of labeled lipids.[121] In the specific case of PNA/peptide hybrids, OG was not deployed as a FRET donor fluorophore. It was assumed that the present π-delocalized electron system could interact with nucleobases to falsify signals. Therefore, for caged-PNA/peptide hybrids, fluorophores were exchanged by the smaller NBD molecule with a less extended π-system.

Finally, after each measurement, but only for the dequenching assay, the bursting of the liposome had to be performed to normalize each measurement. Therefore, the detergent Triton X-100 (TX-100) was added to the lipid solution after each measurement. TX-100 as a detergent was used to destroy the mixed liposomes in the way that the highest fluorescent intensity could be detected. For the quenching assay, no detergent was added. Nevertheless, each fusion measurement was corrected according to Yu *et al.*[122] Basically, due to the different normalization a comparability between dequenching and quenching assay was not possible.

4.3 Caged-PNA/Peptide Hybrids Uncaging Experiments

The caged-PNA/peptide hybrids were made of a decameric PNA attached to the TMD sequence of either Syntaxin-1A (Sx) or Synaptobrevin-2 (Syb). Additionally, the NPP caging groups were introduced at a specific position in the recognition motifs to prevent Watson-Crick-base pairing. Therefore, caged monomers of Fmoc-adenine(NPP)-OH and Fmoc-cytosine(NPP)-OH were synthesized and introduced according to Guha *et al.*[25] Then, liposomes reconstituted with caged PNA/peptide hybrids containing either adenine(NPP)-aeg-OH or cytosine(NPP)-aeg-OH had to be prepared. The fusion capability was tested in two different ways. This method was applied to investigate if the caged group could be sufficiently removed. Consequently, liposomes containing caged-PNA/peptide hybrids were prepared without any fluorophores. This specific setup was chosen to monitor effective membrane fusion while cleaving the photosensitive protecting group. The change of procedure was necessary due to photobleaching of FRET pairs while irradiation. Dynamic light scattering (DLS) measurements were applied for each sample of reconstituted liposome before and after laser irradiation. Fusion events were observed after series of different irradiation duration.

Additionally, FRET-based measurements were applied for those model peptides with particular fluorophores. The liposome preparation was applied following the dequenching procedure (Section 4.1 and 4.2). The proteoliposomes were prepared in a specific manner. Therefore, SxTMD containing caged peptides were prepared without fluorophore, and the SybTMD containing peptides were prepared with donor and acceptor fluorophore. Then, the fluorescent measurement had to be prepared by changing the fluorescent spectrometer lid. Therefore, a lid incorporated with a 365 nm laser was constructed. This setups provided the possibility to continue the measurement after uncaging without removing the cuvette. At first, the labeled proteoliposome was added to the cuvette, and the measurement was initiated. Next, the second proteoliposome was added, and the measurement was continued for 30 s. The release of the caging groups was started by irradiation of the sample for 15 min. The duration of 15 min turned out to be the minimum irradiation time to release the photolabile protecting group. During the irradiation process, the measurements were stopped to reduce the false signals produced from the 365 nm laser. Subsequently, the measurement was continued. In the end, samples for DLS measurements were taken from the cuvette, and the remaining sample was destroyed by adding TX-100.

4.4 DLS Measurements

DLS measurements were applied for every fusion measurements (quenching, dequenching and uncaging experiments). In order to examine membrane fusion, DLS has been a beneficial method to verify the size of liposomes before and after each measurement. Therefore, the standard procedure for fusion measurement was to check the liposome sizes to assure comparability. The liposomes were measured few minutes after extrusion. Additionally, mixed liposomes were measured after each time course measurement. Therefore, a small amount of liposome suspension was taken and diluted with buffer. Dilution of the sample had the advantage that on the one hand, cuvette sizes were quite large, and a high amount of samples would be needed. On the other hand, diluting the sample would also prevent false signals caused by highly concentrated samples. An advantage was to measure DLS and fusion measurements simultaneously to prevent time-dependent variations.

In general, model peptides containing liposomes can significantly differ in size. Depending on the applied assay, the calculation of fused liposomes could be determined according to the formula of spherical volume. Therefore, in Equation 4.1, the volume of spherical volume will be presented:

$$d = \sqrt[3]{\frac{d \cdot 6}{4\pi}} \tag{4.1}$$

The increase in liposome size after extrusion for SybTMD and SxTMD based peptides was more significant than expected. Especially, liposome size distribution of SxTMD containing liposomes was significantly larger in size than SybTMD containing liposomes. This phenomena had been observed during liposome preparation when working with SxTMD based peptides. A plausible explanation of this phenomenon could not be provided. As already described in Section 4.1, aggregation formation and lipids' ageing was observed during time, which forced to measure lipsome containing SxTMD right after extrusion. The average diameter of liposomes varied between 110 nm and 145 nm after extrusion. In Figure 4.1, the size distribution of liposomes containing E3Ts-SybTMD (**44**) in a peptide to lipid ratio of 1:200 is illustrated.

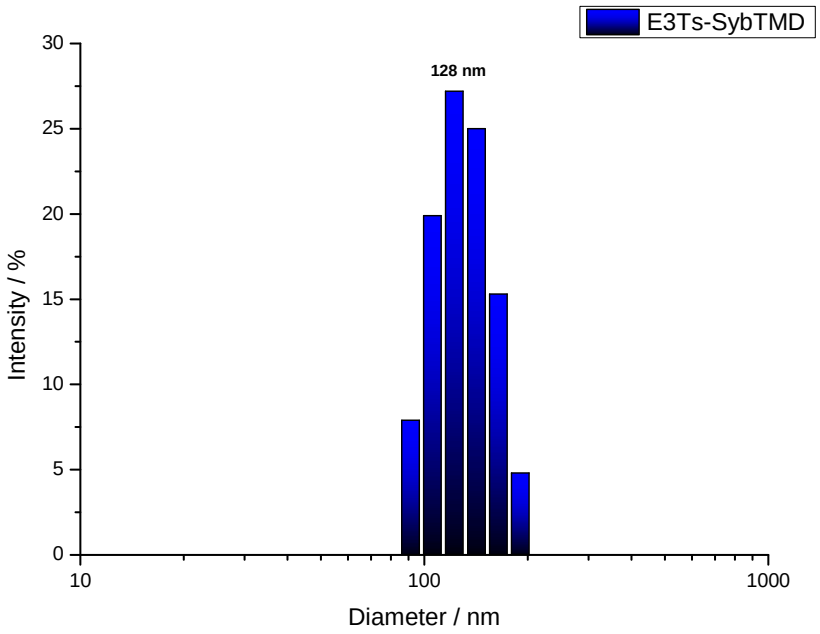

Figure 4.1: Size distribution analysis of prepared liposomes containing E3Ts-SybTMD **44**. The measurement was performed three times and the average was calculated. For the specific liposomes an average size distribution is 128 nm.

5 Design and Synthesis of Novel PNA/Peptide Hybrids

This chapter details the development and investigation of novel PNA/peptide hybrids. SNARE model peptides with different recognition units were prepared from complementary aeg-PNA strands to study membrane fusion *in vitro*. It is known from previous studies that these units can initiate membrane fusion.[18,20] To gain deeper insight into the fusion mechanism, 2-(*o*-nitrophenyl)-propyl (NPP) caging groups were incorporated into the recognition motifs. As a light-triggered steric demanding entity, it should enable the controlled stopping and reactivation of the recognition process during membrane fusion.

In Section 5.1, basic principles of solid-phase peptide and PNA synthesis will be explained. The motivation and design for the artificial model fusogens will be presented in Section 5.2. In particular, the structure of the PNA recognition motifs is discussed here. Afterwards, the synthetic strategy of the caged building blocks will be demonstrated (Section 5.3). Section 5.4 deals with the synthesis of the PNA/peptide hybrids as artificial model fusogens with different recognition motifs. The synthesis strategies for hybrids with and without caging groups is explained here. Additionally, in Section 5.5, the purification process of PNA/peptide hybrids will be illustrated. Finally, in Section 5.6, the successfully synthesized PNA/peptide hybrids have been investigated via FRET based measurements in terms of membrane fusion capability.

5.1 Basic Principles of Solid-Phase Peptide Synthesis

In biomolecular chemistry, the synthesis of defined peptides was greatly facilitated through solid-phase peptide synthesis (SPPS). Merrifield introduced the formation of peptide bonds on a solid support, which can be cleaved in a single step after successful peptide synthesis.[123] Initially, the synthesis strategy was implemented using *tert*-butyloxycarbonyl (Boc)- and benzyl-based (Z) protecting groups. The α-amino acid was *N*-terminally protected with Boc and the side chain was benzyloxycarbonyl (Z) protected. This protecting group strategy (Boc/Z) was invented to increase the deprotection yield under milder conditions. Experiments have revealed that Boc deprotection is almost always quantitative.[124] Boc protecting group is still used in the field of SPPS frequently. For peptide synthesis or even PNA synthesis, Boc has been used with different protecting groups (*e.g.* Boc/Z or Boc/Fmoc).

Currently, orthogonal protecting group strategy (*e.g.* Fmoc/^{t}Bu) are more commonly used for SPPS.[125] These strategies are better applicable for peptide or PNA/peptide hybrids synthesis.[126,127] Especially manual synthesis of PNA oligomers can be easier introduced applying these protection group strategies. For this, the α-amino acids is Fmoc-protected, while the potentially reactive side chains is protected with ^{t}Bu. The main advantage of the orthogonal protecting group strategy is the possibility of selective cleavage by using either acidic or basic conditions. New methods have been introduced employing microwave techniques and coupling reagents.[128] Coupling efficiency and duration has been constantly improved due to microwave assistance and new types of resins. The progress in SPPS allows the synthesis of high-quality peptides in a short period of time. In terms of PNA, SPPS is fully compatible with introducing PNA building blocks in peptide sequences, making it more attractive for the design and synthesis of complex model peptides (*e.g.* PNA/peptide hybrids).

The reaction on resin is highly effective due to speed and efficiency through avoidance of unnecessary loss of product during the coupling process. Under these specific conditions, complex peptides with up to 60 amino acids chain lengths can be realized. The general procedure in SPPS starts with resin preparation. Commonly used resins are shown in Figure 5.1.

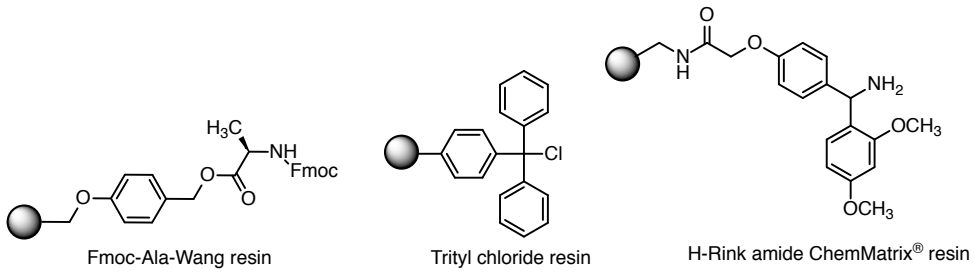

Figure 5.1: Fmoc-Wang resin is typically a resin that is preloaded with the first amino acid. Depending on the resin type, the first amino acid can be purchased preloaded. Trityl chloride resin and H-Rink amide ChemMatrix resin can be utilized if *C*-terminal modification is needed.

The SPPS or solid-phase PNA synthesis are similarly structured, except some minor differences for the PNA synthesis has to be considered. In this case, the solid-phase PNA synthesis will serve as an example to describe the applied procedure. The synthesis procedure can generally be divided into three segments: *N*-terminal deprotection, coupling reaction and cleavage.

First, the resin was left to swell for 2 h in NMP. Subsequently, the synthesis is initiated by removing the Fmoc protecting group using a solution of 20 % piperidine in DMF as a weak base. However, before the peptide bond can be formed, preactivation of the functional groups is necessary. For peptide synthesis, the commonly used activator pair of Oxyma and *N*,*N*-diisopropylcarbodiimid (DIC) was chosen. A solution of Oxyma in DMF is utilized as an activator base while DIC acts as an activating reagent by increasing the reactivity of the carboxyl group by forming an active ester. Compared to the conventional triazoles HOBt/HBTU, it is possible to increase the reaction temperature without enhancing the formation of side products. This is particularly advantageous in the application of microwave-assisted synthesis.

For solid-phase PNA synthesis, the manual coupling has been applied more frequently. According to the PNA synthesis protocol of Casale *et al.*, the activator pair of HOAt/HATU facilitate the highest conversion.[129] Therefore, HOAt/HATU and solution of DIPEA/2,6-lutidine were added to the PNA monomer prior to use. After mixing the activated solution with the on-resin peptide, the dipeptide can be formed by nucleophilic attack of the amino group of the first PNA. The solid-phase PNA synthesis cycle can be repeated until the desired PNA/peptide hybrid is obtained. The final step is the cleavage of the target PNA/peptide hybrid from the resin under acid conditions. The orthogonal protecting group strategy has proven to be advantageous,

allowing the simultaneous removal from the resin as well as the cleavage of the side-chain protecting groups. For PNA/peptide hybrids cleavage only, the resin is treated with a mixture of trifluoroacetic acid (TFA), *m*-cresol, thioanisole, 1,2-ethandithiol (EDT) and triisopropylsilane (TIS). The cleavage cocktail has to be adapted for peptides depending on specific amino acids. The detailed manual synthesis of Fmoc-PNA will be illustrated in Figure 5.2.

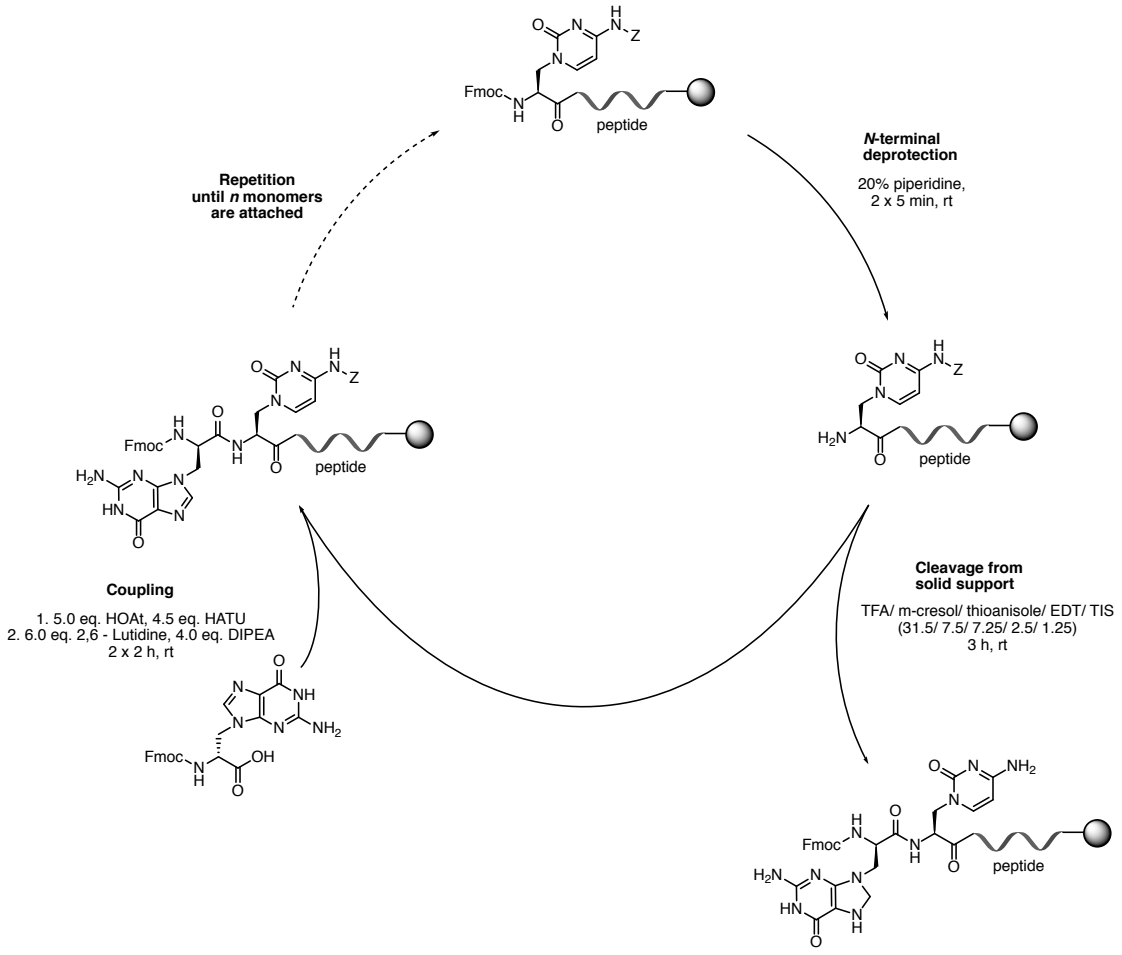

Figure 5.2: Aeg-PNA attached to peptide on-resin was treated with 20 % piperidine solution. After removing the Fmoc-protecting group, the α-amino group is activated by adding a solution of HOAt/HATU. Next, the coupling process is initiated after a solution of 2,6-Lutidine/DIPEA has been added. After that, the process can be repeated multiple times until the target PNA/peptide hybrid is achieved. The final step is the cleavage from the resin in order to obtain the product.

5.2 Design of Novel PNA/Peptide Hybrids

The natural SNARE mechanism has attracted great interest for decades. As a convenient approach to study this mechanism, artificial model systems were invented in a simplified and reduced complexity. Inspired by the tertiary SNARE complex formed during the neuronal exocytosis, a SNARE mimicking model systems were developed.[17,102] As a template, the SNARE proteins Syntaxin-1A, Synaptobrevin-2, SNAP-25 were used. However, the initial recognition motif of four units was replaced with a two recognition motifs system that could form stable dimers.

Here, the SNARE model system was designed based on the native transmembrane domain and linker region, originally discovered in *rattus norvegicus*, of Syntaxin-1A and Synaptobrevin-2.[130] The transmembrane domain and linker region will be abbreviated as only "transmebrane domain" (TMD) to make it less complicated and better understandable for this thesis. Also, abbreviations for the specific neuronal SNARE peptides have been introduced. Therefore, the transmembrane and linker region of either Synaptobrevin-2 or Syntaxin-1A are abbreviated as "SybTMD" and "SxTMD". The concept of the model peptides was established based on the native sequences due to their ability to form stable membrane anchors. Also, going for two different TMDs has been known from literature to enhance the fusion activity. Groth showed that an optimal recognition could be realized adapting the native sequence of Syntaxin-1A, elongating the sequence by two additional amino acids in order to adjust the length and its recognition.[19] This change in sequences improves the recognition process enabling more insight into the native system (Figure 5.3).

Figure 5.3: The native transmembrane sequences of Syntaxin-1A (85-116) and Synaptobrevin-2 (256-288) are presented. The sequences are divided in linker region (grey) and transmembrane anchor (light grey).

With the intention of elucidating the zipper-like fusion mechanism in more detail, various PNA/peptide hybrids were prepared in this work. The focus has been on novel PNA/peptide hybrids with photosensitive NPP caging groups in the recognition motif. The synthesis and the objective regarding the protected building blocks are explained

in the following chapters.

In general, model fusogens have the great advantage of allowing the study of the complex processes of docking and membrane fusion of SNARE proteins in a variety of ways. Here, we introduced a SNARE model system that allows modifying the recognition units as well as the linker region to monitor these processes. In the following, a schematic overview (Figure 5.4) of current model systems will be presented for better understanding.

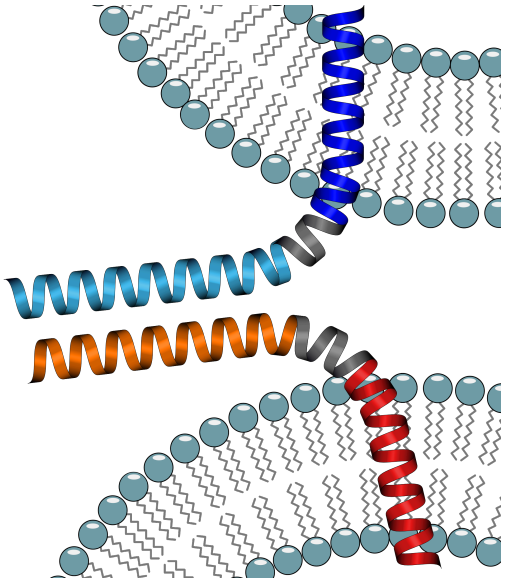

Figure 5.4: Artificial model peptide incorporated into the lipid membrane. The recognition motifs have been highlighted (blue or orange) and been presented outside the membrane. The linker region (grey) and the TMDs of Sx and Syb have been also highlighted (blue and red) and been incorporated inside the membrane. In this word, PNA-oligomers and coiled coils were used as recognition motifs.

5.3 PNA Recognition motif

To these adapted TMDs, artificial recognition units were added. From a variety of different recognition units (see Section 2.5), two were chosen for this work: *N*-(2-aminoethyl)-glycine (aeg)-PNA oligomers and coiled-coils. Similar model fusogens have already been thoroughly studied in our group. As a result, their function to mediate membrane fusion has been successfully verified.[17–20,102] While this chapter deals with novel PNA/peptide hybrids, the study of coiled-coil peptides as recognition units is described in Section 6.2.

5.3.1 *N*-(2-aminoethyl)-glycine (aeg)-PNA

PNAs were firstly reported by Nielsen *et al.* in 1991.[101] Since then, PNAs have been capturing the interest of the scientific community. The opportunity to implement new application as a molecular biology tool have generated the greatest attention recently. The initial approach was to develop a DNA analogous. Therefore, PNAs were introduced by replacing the deoxyribose backbone with a pseudo-peptide backbone. The different nucleobases are shown in Figure 5.5. The functional groups of these aeg-PNA monomers, except for Thymine, are illustrated with a benzylhydroxylcarbonyl (bhoc) protecting group.

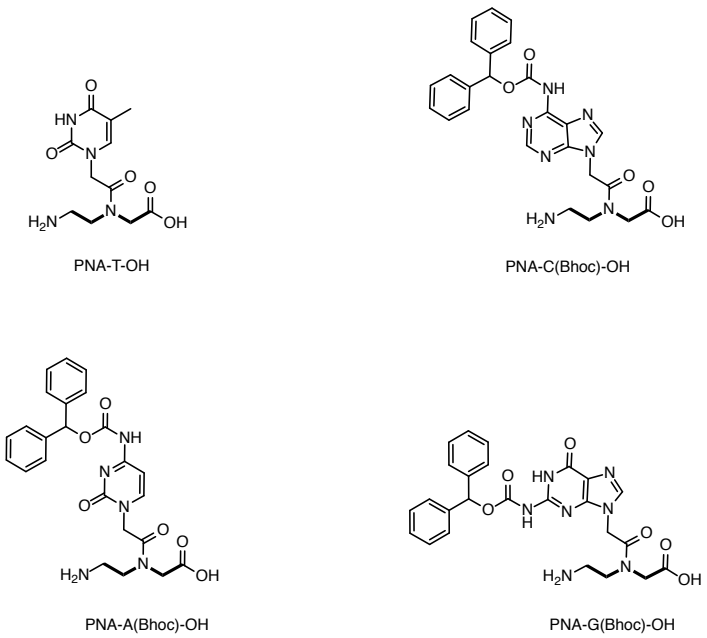

Figure 5.5: Structures of aeg-PNA monomers and highlighted structures of aeg-backbone. PNA-t-OH, PNA-c(Bhoc)-OH, PNA-a(Bhoc)-OH and PNA-g(Bhoc)-Oh are used to synthesized PNA recognition motifs. The amino group of c, a and g was bhoc protected to prevent side reactions.

The intramolecular spacing between two complementary PNA base pairs has been proven to greatly match with DNA or RNA helix.[131,132] This makes PNAs well suitable as DNA analogues. The strong resemblance reveals that PNA can form a hydrogen bond even with a DNA or RNA strand. When compared to DNA/DNA strands, PNA/DNA strands present a stronger binding affinity due to the achiral and neutral properties of the PNA backbone.[133] Also, the resistance towards hydrolytic cleavage and their extraordinary thermal stability make PNAs in many respects interesting and facilitate many application opportunities in the field of diagnostics and

pharmaceuticals.[134–137] Compared with DNA and RNA, PNAs can form more stable duplex structures.[138,139] Furthermore, strong duplex formation between DNA/DNA strands can be disturbed by adding PNA. However, a triplex or double duplex is formed instead of a denaturation, making PNAs highly desirable as antigen agents.[140,141]

The structure and high thermal stability of PNAs is of great advantage for various synthesis approaches. For example, the highly complex PNA/peptide hybrids can be adapted for Fmoc or Boc solid phase PNA synthesis.[142–144] Also, stereo-selective modifications of PNA monomers (*e.g.* nucleobase modification or photosensitive protecting groups) can be introduced. Especially, these synthesized PNAs have been showing unique physiochemical properties, which makes them attractive in further studies.[25] The synthesis of nucleobase caging of adenine and cytosine is presented in the following section.

5.3.2 Synthesis of Nucleobase Caging Groups

The caging group strategy has already been utilized for various biomolecules (*e.g.* amino acids, lipids, nucleic acids).[145–152] The 2-(*o*-nitrophenyl)-propyl (NPP) caging group has been proven to be stable under peptide and PNA oligomer synthesis conditions, thereby serving as permanent protection until photochemical cleavage. The synthesis of nucleobase caging of PNAs was introduced and extensively tested by Guha *et al.*[25] A number of studies on the different caged-decamer-PNAs were performed for this purpose. It has shown to be suitable as light-triggered recognition units to study the zipper-like recognition during membrane fusion. NPP has been chosen as a caging group due to its compatibility with the solid-phase peptide synthesis conditions.

The fundamental task of this thesis was to successfully synthesize caged-PNA building blocks and then further synthesize the PNA/peptide hybrids via SPPS to obtain the caged-PNA model peptides. To obtain the 2-(*o*-nitrophenyl)-propyl caging group, a multi-step synthesis had to be performed for this purpose. The synthesis was prepared following the protocol by Rodrigues-Correia *et al.*[153]

The desired compound could be obtained functionalizing the hydroxyl group of 2-(2-nitrophenyl)propane-1-ol to an amine group in a multiple step synthesis. The first step was to transfer the hydroxyl group into a more suitable leaving group. Therefore, 2-(2-nitrophenyl)propane-1-ol was added to *p*-toluenesulfonyl chloride to form toluene-

4-sulfonic-acid-2-(2-nitrophenyl)propyl ester (**1**). The next step was to convert the tosylate moiety to 1-azido-2-(2-nitrophenyl)propane (**2**) in a nucleophilic substitution. The last reaction step was performed via a STAUDINGER reaction. Therefore, (**2**) was treated with triphenylphosphine. This step led to the formation of triphenylphosphine phenylimide intermediate, followed by adding water and ammonium to convert the azide into a primary amine. This final step leads to the formation of the target compound 2-(2-Nitrophenyl)propylamine (NPP) (**3**).

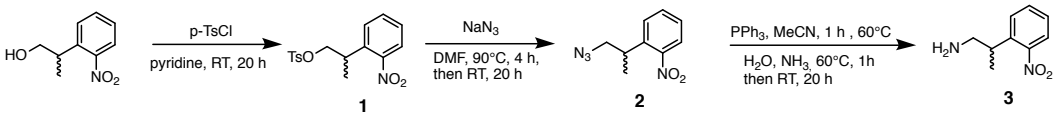

Figure 5.6: Reaction schemata of the multiple step synthesis of NPP.

After the successful synthesis of 2-(2-nitrophenyl)propylamine (**3**), the nucleo amino acid coupling to obtain Fmoc-a^{NPP}-aeg-OH and Fmoc-c^{NPP}-aeg-OH could be performed. The multiple step synthesis with different starting material for both building blocks will be presented in the following. Synthesis of Fmoc-a^{NPP}-aeg-OH (**8**) (Figure 5.7) was carried out by NPP protection with 6-chloropurine-9-*tert*-butylacetate (**4**). Therefore, 6-chloropurine-9-*tert*-butylacetate (**4**) had to be prepared by nucleophilic substitution beginning from 6-chloropurine with *tert*-butylbromoacetate. The caging of the nucelobase was completed by introducing NPP by nucleophilic substitution, followed by the secondary amine coupling of the Fmoc-aeg-*tert*-butylester using PyBOP as activating reagent. Finally, removal of *tert*-butyl protecting group was performed with TFA, providing the NPP-caged Fmoc-a^{NPP}-aeg-OH.

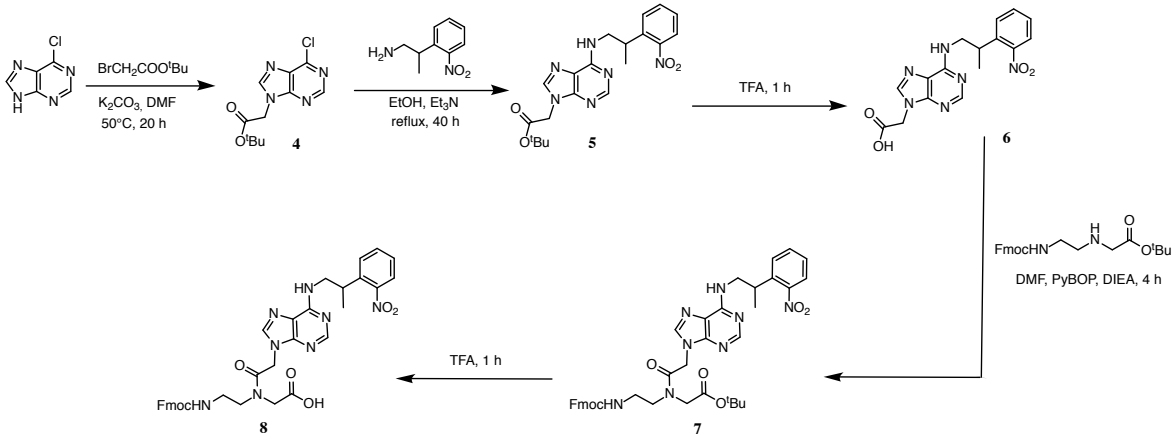

Figure 5.7: Reaction schemata of Fmoc-a^{NPP}-aeg-OH.

The overview of the second synthesis of caged-cytosine nucleo amino acid can be observed in Figure 5.8. Similar to Fmoc-a^{NPP}-aeg-OH synthesis, the NPP protection was provided by nucleophilic substitution of *tert*-butyl-uracil-1-yl-acetate (**9**) which had to be prepared beforehand. For this purpose, uracil derivate **9** had to be activated by mesitylene sulfonate in order to introduce the NPP protection group. After obtaining the NPP-protected nucleobase, the peptide backbone had to be introduced using PyBOP activation followed by ester hydrolysis. The peptide backbone insertion was performed according to the first Fmoc-a^{NPP}-aeg-OH synthesis providing the NPP caged Fmoc-c^{NPP}-aeg-OH (**13**). The monomeric building blocks were further used for solid-phase PNA synthesis to obtain caged-PNA/peptide hybrids. The design and synthesis of the caged-PNA/peptide hybrids will be explained in the next section.

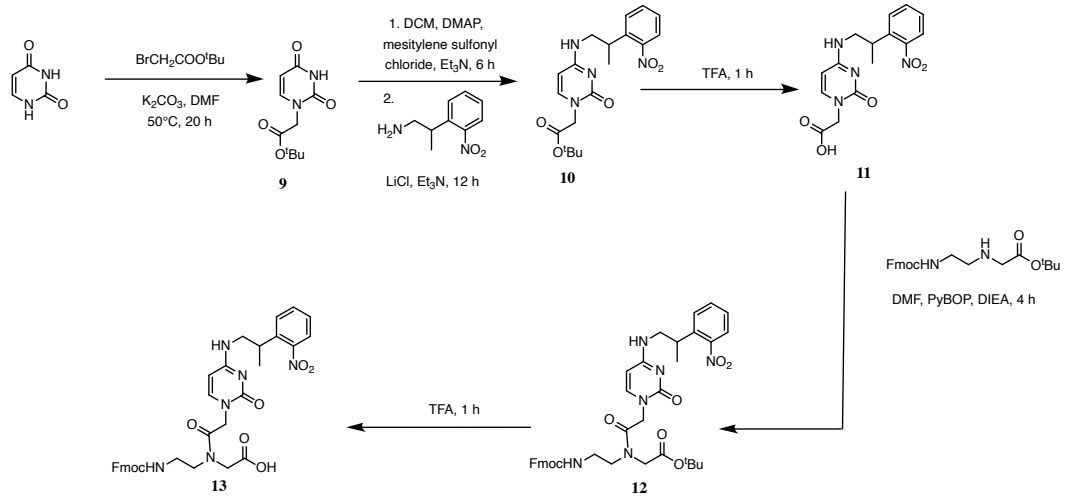

Figure 5.8: Reaction schemata of Fmoc-c^{NPP}-aeg-OH.

5.4 PNA/Peptide Hybrids

5.4.1 Synthesis of PNA/Peptide Hybrids

Artificial SNARE model peptides were designed with complementary recognition strands of PNA attached to TMDs. Various sets of complementary PNA/peptide hybrids have been intensively studied by Lygina and Hubrich.[20,102] Especially, the complementary strands of the decameric PNAs (PNA1 and PNA2) are known to form parallel or antiparallel stable duplexes. The parallel orientation have been known to provide the highest fusion efficiency.[102] Therefore, these PNA/peptide hybrids were used as reference for the PNA/peptide hybrid studies in this thesis. Also, pentameric PNA/peptide hybrids were synthesized due to the fact that these PNA recognition have also been known to be sufficient for membrane fusion.[20] These peptides will be used to evaluate the studies on light-triggered membrane fusion and its applicability. The successfully synthesized compounds are listed in Table 5.1.

Table 5.1: Sequences of decameric and pentameric PNA/peptide hybrids.

	Pentamer-PNA/Peptide Hybrid	Entry
PNA1s-SybTMD	tcact-SybTMD	**14**
PNA2s-SxTMD	agtga-SxTMD-OH	**15**
	Decamer-PNA/Peptide Hybrid	
PNA1-SybTMD	gtagatcact-SybTMD	**16**
PNA2-SxTMD	catctagtga-SxTMD	**17**

PNA/peptide hybrids were synthesized following the rules of SPPS and solid phase PNA synthesis. First, the TMD had to be synthesized by automated microwave-assisted SPPS. Therefore, preloaded Wang-resin was used as the supporting material. The peptide synthesis was performed according to SOP1. Nevertheless, after successful peptide synthesis, PNA monomers had to be attached manually to the peptide sequence. This process was performed according to SOP2. The specific synthesis procedure was adapted from Lygina *et al.*[102] The attachment of the transmembrane domain with the PNA building blocks had to be prepared by letting the resin preloaded with TMD swell at least for 2 h. Hereafter, the resin was treated with a piperidine solution (20 % in NMP) in order to cleave the Fmoc-protecting group.

Several reaction steps are required for the attachment of the PNA monomers (see Section 5.1). Between each of these steps, a washing step (NMP, DCM, NMP) was per-

formed to remove impurities. For activation, a mixture of HATU/HOAt was combined with the PNA monomer and sonicated until complete dissolution. Then, the bases 2,6-Lutidine and DIPEA were added to the dissolved components. Within a short period of time, the solution of activator and PNA building block was added quickly. The reaction for each coupling was performed twice, 1 h respectively. Furthermore, a capping step was also performed after the second coupling process in order to acetylate the amino function of abortive sequences.

5.4.2 Synthesis of Caged-PNA/Peptide Hybrids

Not only the membrane fusion process but also the the zipper-like recognition process has been of major interest. Until now, specific peptides especially fusogens had not be reported for their light-controlled release by laser irradiation. The idea of developing fusogens which are controllable by UV-light release is of major interest in the field of controllable drug-release processes.[154] For this reason, the caged-PNA/peptide hybrids were designed and synthesizied. Therefore, the PNA monomers mentioned in Section 5.4.1 have been modified by introducing photolabile-caging groups at specific positions. Pfleiderer *et al.* intensively studied the use of 2-(*o*-nitrophenyl)-propyl (NPP) as a caging group.[155]

NPP as caging group was selected due to its high compatibility to solid-phase PNA synthesis. This means that the cleavage under basic conditions does not interfere with the NPP protecting group. An additional benefit in NPP is the photocleavage at 365 nm releasing α-methyl nitrosytrene as by-product. In comparison to other similar photolabile protecting groups it has been reported as less harmful.[156–158]

The specific nucleotide modification was firstly introduced by Heckel *et al.* Modifying nucleotides at the $N6$-position of adenine and the $N4$-position in cytosine by introducing NPP as caging group lead to the presented caged-PNA building blocks.[159,160] The destabilization of nucleobase pairing was realized by introducing the caging group at specific amino group position. The amino groups are the most promising position in order to destabilize nucleobase pairing. However, complete inhibition is not achieved, the formation of Watson-Crick base pairing via hydrogen bonding can still be formed. The low extinction coefficient of NPP for quick realease makes it less efficient as a caging group. Nevertheless, compared to other similar groups it fits the most to the condition of SPPS.[153]

Before manual PNA coupling could be applied to obtain the caged-PNA/peptide hybrids, a multiple step synthesis had to be performed. The detailed reaction scheme of NPP and also the synthesis of the caged-PNA monomers have been presented in Section 5.3.2. After successful synthesis of caged-PNA monomers, the caged-PNA/peptide hybrid synthesis was continued. The synthesis was performed according to SOP2. The detailed procedure has been presented in Section 5.4.1. The sequence of the synthesized caged-PNA/peptide hybrids will be presented in Table 5.2. In Figure 5.9 the exact position of the NPP caging group is illustrated.

Table 5.2: Sequences of caged-PNA/peptide hybrids. *N*-terminal caging of PNA/peptide hybrids.

	Caged-PNA/Peptide Hybrid	Entry
NPP-PNA1-SybTMD	gta^{NPP}ga^{NPP}tcact-SybTMD	**18**
NPP-PNA2-SxTMD	c^{NPP}atc^{NPP}tagtga-SxTMD	**19**

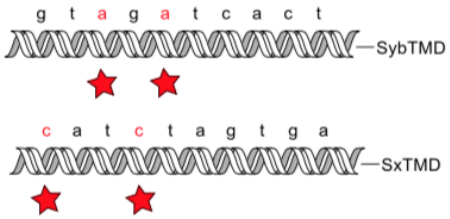

Figure 5.9: *N*-terminal caged-PNA/peptide hybrids linked to the native TMDs of Sx and Syb.

5.5 Purification PNA/Peptide Hybrids

The purification of model fusogens is of crucial importance in order to obtain reliable data on fusion activity. In previous studies, purification has already been challenging. Especially, due to the hydrophobic transmembrane domain core, artificial SNARE model peptides are harder to dissolve in terms of HPLC solvent conditions.[17,18,20,102] A decisive part of this work was to purify SNARE mimicking model peptides with artificial recognition units (*e.g.* PNA and coiled-coil). By changing the preparation, the purity was significantly improved. The purification process will be presented in the following.

In this thesis, artificial model peptides containing either PNA or coiled-coil as recognition unit will be presented. Depending on the used model peptide, additional modifications had to be made. In the work of Groth, a purified E3/K3-TMD system was tested in order to optimize vesicle stability. The purified model peptides provided less fusogenicity than expected.[19] Nevertheless, for reliable data in research purification of model peptides is critical. In previous studies, the PNA/peptide hybrid purification was not effective.[102] However, the purification procedure will be described in the following (detailed description, Section 8.3). The successful purification of the model peptides was performed by solving the sample in hexafluoro-2-isopropanol (HFIP) and water prior to use. The significant change in preparation procedure improved peptide purity.

After successful synthesis completion, the PNA/peptide hybrids have to be purified. A common purification method for peptide or PNA purification is HPLC. In case of TMD based peptides, the application turned out to be more challenging than expected. Purification procedures for similar peptides were considered for the PNA/peptide hybrids. After testing various reverse phase (RP)-C18 and RP-C8 columns with different sizes at the HPLC instrument, an ACE semi-preparative C-18 column was chosen. Due to the highly hydrophobic property of transmembrane petides dissolving using standard solvents was the biggest challenge. The most promising separation was realized when the hydrophobic peptide was dissolved in hexafluoro-2-propanol (HFIP). In combination with methanol (MeOH) as polar solvent good purification results could be achieved. Applying these conditions resulted in one separable sharp peak in the chromatogram. Even though the purification was difficult, good results were obtained. Similar conditions could be applied to coiled-coil peptide fusogens which also resulted

in good separation.

The change in purification quality had a major impact in the fusion activity. The precise effects will be discussed in the FRET-based measurements (Sections 5.6 and 6.5)

5.6 PNA/Peptide Hybrid based Fusion Assay

PNA/peptide hybrids as well as caged-PNA/peptide hybrids were examined via FRET based liposome fusion assays. The dequenching assay was chosen as method of choice in order to be keep comparability with former studies.[17,18,20,102] In general, the model peptides were incoporated in labeled liposomes and unlabeled liposomes (more detail, see Section 8.6.4). When labeled and unlabeled liposomes were mixed, the change of fluorescence intensity was recorded over time. Effective membrane fusion resulted in an increase of the donor emission.

As mentioned above, PNA/peptide hybrids were tested after purification. Purified model peptides led to less fusion efficiency compared to crude model peptides. This kind of phenomena was already reported in the work of Groth, showing less fusion efficiency after successful purification.[19] Pure model peptides resulted in more precise concentration determination but a decrease in overall fusion activity was observed. In this thesis, the pentameric purified PNA/peptide hybrids (Table 5.1) have been tested in order to determine the influence of purified model peptides on fusion measurements. Remarkably, the same effect of less fusion activity was observed in experiments. Therefore, Figure 5.10 will represent course of the purified model peptides of the pentameric-PNA/peptide hybrids (**14** + **15**).

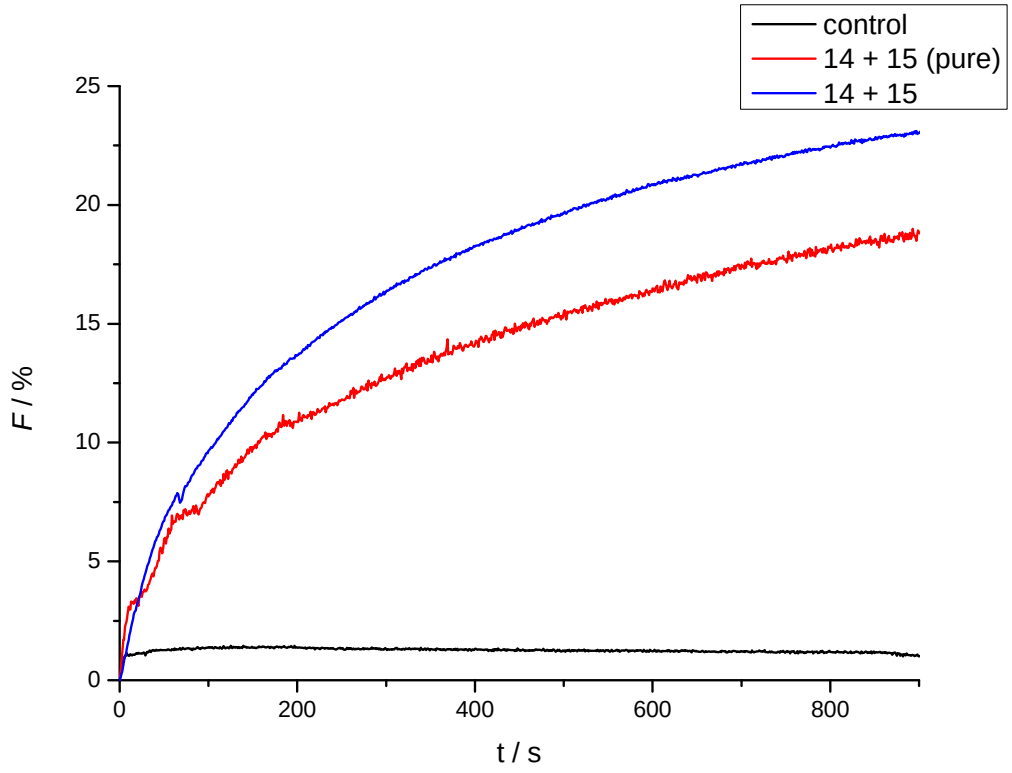

Figure 5.10: Fusion curves of purified and crude PNA/peptide hybrids of **14** + **15**. The course of fusion curves shows the decrease in fusion efficiency after purification. Additionally, a control measurement was performed mixing a liposome with PNA/peptide hybrid and liposome without any peptide.

The absolute signal intensity discrepancy between both measurements is about 6 %, confirming the reduced fusogenicity of purified model peptides. Additionally, in the early period of the measurement after initiating the fusion process a different kinetical behavior was observed. A steeper increase in donor emission could be observed in the first 200 s for the unpurified PNA/peptide hybrids. This indicates that the liposome population with unpurified model peptides (blue trace) tend to fuse more quicker, directing to an overall higher fusion intensity. An plausible explanation for this specific enhancing behavior could be resulting from fragmentary peptide sequences leading to disruption of the lipid membranes. This results has to be viewed with caution, vesicle burst or liposome docking could be also an plausible cause for the increase of the donor emission.

In addition to each measurement, model peptides incorporated in liposome were applied via DLS measurements to verify effective membrane fusion. In general, the liposome

population with SxTMD model peptides were showing a increased average size distribution compared to liposome of SybTMD model peptides. This phenomena has been noticed in several experiments in this thesis and former studies.[19] SxTMD model peptides has been prepared directly before the measurement. An increase in liposome size as well as an increase in donor emission was observed after liposome mixing, showing the mediating character of these model peptides.

As important part in this work, light-triggered membrane fusion experiments using caged-PNA/peptide hybrids were investigated. Therefore, the caged model peptides were prepared and incorporated into liposomes as previously described (see Section 5.4.2). The main difference to the earlier mentioned measurements is the sample irradiation during the FRET measurement. Labeled lipids and irradiation during FRET measurements turned out to be more challenging than expected. An approach to this challenging task was to construct a UV-laser incorporated into spectrometer lid, allowing the irradiation with UV-light and fluorescence measurement without removing the cuvette. The investigation of the fusion behavior of the caged-PNA/peptide hybrids NPP-PNA1-SybTMD (**18**) and NPP-PNA2-SxTMD (**19**) was provided according to SOP2. The emission spectrum of the experiment before and after irradiation is shown in Figure 5.11 (red and black trace).

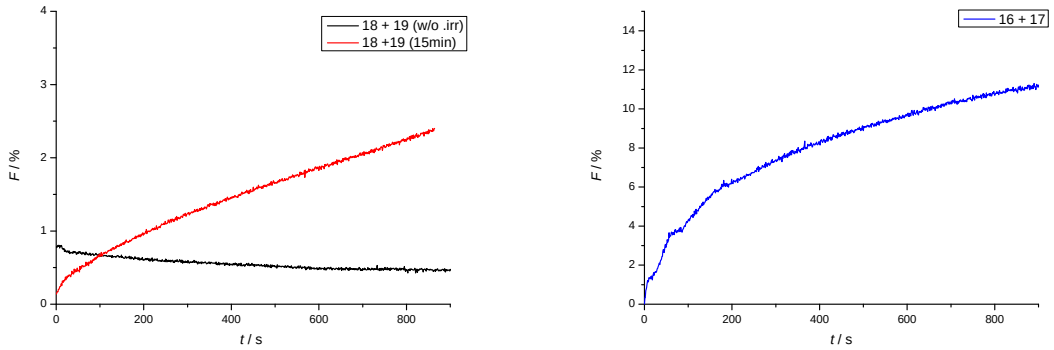

Figure 5.11: Fusion curves resulting from caged PNA/peptide hybrids before and after UV-light irradiation. The ratio of labeled and unlabeled liposomes is 4:1. The black curve describes the lipid mixing of the caged PNA/peptide hybrid without irradiation. The red curve represent the lipid mixing after 15 min irradiation.

18 and the complementary PNA strand **19** were prepared containing two photosensitive NPP-caging groups, respectively (see Figure 5.9). It was necessary to occupy the decamer PNA with more than two caging groups in order to block the nucleobase

recognition sufficiently.[25,161] Therefore, the specific order of the caging groups has been chosen to be placed *N*-terminally. Also to test if an step-wise recognition is possible in later studies.

In the control experiment, the labeled vesicles incorporated with **18** and the unlabeled vesicles with **19** were tested without UV-light irradiation. A very low fluorescence intensity of up to 0.81 % was measured, which decreased over time, indicating that the recognition process was inhibited. Consequently, it can be assumed that the introduction of NPP-caging groups into both complementary PNA strands causes a suppression of molecular recognition of PNA/peptide hybrids and thus the inhibition of a fused complex. The recovery of the recognition function of the PNA strands should be achieved by irradiation with UV-light. Employing UV-light removes the NPP-caging groups and resulting in the recovery of the initial membrane fusion.

Therefore, the light-triggered membrane fusion was investigated applying different irradiation duration. The irradiation time has been thoroughly tested by increased duration up to 60 min. 15 minutes of laser irradiation was the minimum time duration to observe an increase in donor emission.

After 15 min irradiation using a 365 nm laser as light source, a marginally increase in fusion intensity can be detected. However, increase in fluorescence has been significantly reduced due to some limitation caused due to photobleaching while irradiating with UV-light. Additionally, the increased irradiation duration have a big influence in the overall fluorescence intensity, leading to an overall increase of only 2 %. Therefore, presented fusion curves has to be viewed with caution, vesicle burst or liposome docking could be also an plausible cause for the increase of the donor emission. Figure 5.11 represents the reference PNA/peptide hybrids (blue trace) showing the progression of uncaged-PNA/peptide hybrids (**16** + **17**).

5.7 Conclusion

In this chapter, caged-PNA/peptide hybrids were investigated for their suitability to perform light-triggered membrane fusion. In order to do that, PNA/peptide hybrids as well as caged PNA/peptide hybrids have been synthesized. The PNA/peptide hybrids introduced by Lygina and Hubrich served as reference.

From previous studies, NPP uncaging was reported to proceed relative slowly, but due to their good suitability to SPPS conditions, the caged model peptides were synthesized. The rehybridization of the PNA/PNA recognition after NPP deprotection could be successfully verified by Guha *et al.*[25] Nevertheless, the fusion efficiency and the applicability of these specific SNARE model peptides had to be tested by FRET-based liposome fusion assays. Different caged PNA/peptide hybrids of *N*- or *C*-terminally caged were designed to mimic the assumed zippering-like recognition. In this thesis, the *C*-terminally caged PNA/peptide hybrids **18** and **19** were prepared and incorporated into liposomes in order to check their applicability with our FRET dequenching assay.

In conclusion, caged PNA/peptide hybrids indeed show the ability in completely blocking the recognition process of PNA strands. It is clearly demonstrated that the recognition process between two artificial model peptides is a important step without membrane fusion cannot happen. Nevertheless, it was thoroughly tested by apply lipid mixing assays and showing that four caging groups are sufficient to completely block liposome fusion (black trace in Figure 5.11).

According to Fasshauer *et al.*, it was assumed that the zippering direction of native SNAREs will proceed *N*- to *C*-terminally.[162] Therefore, the *N*-terminally caged PNA/peptide was expected to represent valuable insight into the zipper-like recognition. Surprisingly, the obtained results after irradiation showed no precise and reliable data for specifically addressing the directed zippering process.

The presented uncaging fusion assays indicate a kinetic progression of the liposome fusion similar to former studies as Lygina or Hubrich. However, due to the slow release of the NPP protecting group it cannot be clearly assumed whether full fusion or only hemifusion occurred. The overall fusion intensity was to low in order to show that stepwise recognition was achievable. It was even lower than for the non-caged-PNA/peptide hybrids (blue trace in Figure 5.11).

Caged-PNA/peptide hybrids should be considered as application tool to achieve more insight in the zippering-like recognition process. However, in combination with the dequenching assay, replacement of the NPP caging group might be useful to achieve a quicker release and recovery of recognition after irradiation.

6 Design and Synthesis of Novel Coiled-Coil Peptide Fusogens

In this chapter, the novel coiled-coil recognition units and their function as model fusogens will be presented. Therefore, the previously reported artificial SNARE E3/K3 TMD model system introduced by Meyenberg *et al.* has been selected as a reference. In recent studies, the strong membrane interaction of K3 during the fusion process has been reported to have a major impact on membrane fusion.[21] Thus, alternative coiled-coil peptide fusogens have been developed by modifying the E3/K3-TMD model system.[163] By alternating the heptade register of K3 and E3, a novel coiled-coil design could be obtained. In Section 6.1, design and motivation of the new coiled-coil will be described in detail. Additionally, the synthesized novel coiled-coil recognition units as well as their respective coiled-coil peptide fusogens will be presented. Before that, recognition units have been tested to make sure that all criteria will be fulfilled to be suitable as E3/K3 substitute. Therefore, CD-spectroscopy measurement have been applied to examine the secondary structure and stability. In Section 6.2, alternating coiled-coil recognition units will be illustrated, followed by their applied FRET based measurements. In Section 6.3, a second novel coiled-coil recognition and its respective model peptides will be presented and tested via FRET based measurements.

6.1 Design of Coiled-Coil Recognition Units

The detailed description of the transmembrane domain has already been illustrated in Section 5.2. In this chapter, the design and a new approach of coiled-coil peptide fusogens will be presented. Preliminary work in understanding the fusion behavior of artificial coiled-coil peptide fusogens, the E3/K3-TMD model system of Meyenberg has been introduced. This model system has been reported to be sufficient for mediating membrane fusion.

The design of the E3/K3-TMD model system was inspired from HODGES heterodimeric E3/K3 coiled-coils. HODGES initially introduced these coiled-coil as a biological tool in order to capture and deliver applications in purification methods.[16] However, the specific interaction behavior has been demonstrated to be suitable as a recognition unit in membrane fusion studies. The model system has been developed using the heterodimeric coiled-coil recognition motif combined with either SxTMD or SybTMD.[163] Due to the absence of a chromophore in the K3-SxTMD model peptide, modification to the HODGES K3 coil were made by introducing Tryptophan (Trp) *N*-terminally (Table 6.1).

Table 6.1: E3 (blue) and K3 (red) recognition unit by MEYENBERG *et al.*

Name	*N*-term.	gabcdef	gabcdef	gabcdef	Entry
E3	G	EIAALEK	EIAALEK	EIAALEK	**20**
K3	WWG	KIAALKE	KIAALKE	KIAALKE	**21**

In recent studies, new insights using heterodimeric E3 and K3 coiled-coils attached to a lipid anchor were gained in the field of membrane fusion studies. The ability to mediate membrane fusion has been reported to act in a two-stage recognition process. In the first stage, K3 was initiated by liposome docking, followed by E3 trying to form the coiled-coil (Figure 6.1). In the second step, E3 was proposed to act as a "handle" by grabbing K3.[21] Indeed, the described mechanism cannot be fully applied to the K3/E3-TMD model system, however, due to the similarities this specific behavior can be considered to be present in our model system. Additionally, aggregate formation during extrusion in SxTMD-based peptides was repeatedly observed in membrane fusion studies. Based on these described difficulties, an approach to optimize the artificial SNARE model peptides was established. Therefore, novel coiled-coil recognition motifs have been developed.

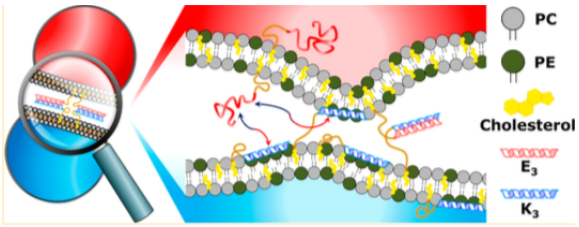

Figure 6.1: E/K-model system introduced by KROS *et al.* describes the model system consisting of E3/K3 attached to a lipid anchor in order to study membrane fusion. Additionally, the two-stage recognition process has been illustrated in this scheme. Based on ref.[21].

The aim of this research was to develop an alternative coiled-coil peptide fusogen in order to achieve higher fusion efficiency in membrane fusion studies. Therefore, a novel set of artificial recognition units was designed following the rules of coiled-coils. The specific rules will be described in the following.

The principles of coiled-coils are developed in the heptad repeating pattern, denoted as the letter sequence abcdefg.[164,165] The helical-wheel diagram (Figure 6.2) represents the recognition behavior between an E and a K coil. In general, coiled-coil designs are arranged by occupying the heptade position a and d with a hydrophobic amino acids. The specific hydrophobic interaction has been noted to be critical in the coiled coil formation process. The type of hydrophobic amino acid at these positions can determine which oligomer is preferably formed.[166] Additionally, interactions due to polar or charged amino acids introduced at positions e and g can significantly increase overall stability and support the heterodimer formation.[167]

In case of E3/K3, these positions were occupied with the charged amino acids of either Lys or Glu. The remaining positions can be occupied with any amino acids but does not have a significant influence in the recognition process, since these positions are not actively involved in the coiled-coil formation. Furthermore, Woolfson *et al.* have introduced a novel coiled-coil design occupying asparagine in the hydrophobic core to increase the heterodimer formation due to hydrogen bond formation (Figure 6.2).[168]

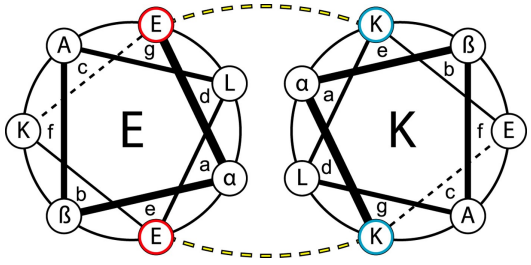

Figure 6.2: Helical wheel diagram of E and K coil representing the specific interaction during the coiled-coil formation. It shows the specific interaction related to the specific position in the heptade. Based on ref.[167].

According to these specific rules in coiled-coil design, novel coiled-coils were developed. In order to obtain a suitable recognition motif various approaches were attempted. In the next section the most promising design attempts will be illustrated.

6.2 Alternating Coiled-Coil Model Peptides

6.2.1 Alternating Coiled-Coil Recognition Unit

As already mentioned, the novel artificial recognition units were designed following the rules of coiled coil. As alternative coiled-coil recognition different coiled-coil designs were tested and had to be examined for their suitability. However, only the most promising recognition units following the alternating design will be illustrated. The motivation in designing the alternating coiled-coil was to develop a motif which will have less membrane interacting properties. Therefore, one heptad in the K3 or E3 register was exchanged by the complementary one, introducing the alternating coiled coil design. This model system design will be defined as EKE and KEK depending on the presence of either a K- or E- containing heptad. Additionally, Trp was introduced into the heptade at position f in order to prevent additional Trp *N*-terminal implementation. The change in design was performed due to the specific properties of Trp. Trp is located preferentially near the lipid-water interface and is known to play a significant role in membrane anchoring.[169] Therefore, it was assumed that the additional Trp units in the K3 sequence could limit molecular recognition when positioning *N*-terminally.

The first pair of coiled coils EKE V1 **22** and KEK V1 **23** have been designed by introducing an asparagine (Asn) in the hydrophobic core. These polar side chain modifications at the hydrophobic interfaces were proposed to support the heterodimer formation via intramolecular hydrogen bond interaction. Further coiled coil designs (**24** - **29**) were established by removing Asn from the alternating recognition motif. Additionally, Gln was incorporated in different heptad sequences. This leads to different net charge configurations which assumed to have an influence in secondary structure formation and stability. In order to investigate the secondary structure, CD-measurement was performed. The specific peptides are illustrated in Table 6.2.

Table 6.2: Coiled-coil recognition units by alternating pattern. Therefore,the heptad pattern of K3/E3 was exchanged with E-heptad or K-heptad. Additionally, minor modifications by changing specific amino acids were made.

Name	*N*-term.	gabcdef	gabcdef	gabcdef	Entry
EKE V1	G	EIAALEK	KNAALKW	EIAALEK	**22**
KEK V1	G	KIAALKW	EIAALEK	KIAALKE	**23**
EKE V2	G	EIAALEK	KIAALKW	EIAALEK	**24**
KEK V2	G	KIAALKW	EIAALEK	KIAALKE	**25**
EKE V3	G	EIAALEQ	KIAALKW	EIAALEK	**26**
KEK V3	G	KIAALKW	EIAALEQ	KIAALKE	**27**
EKE V4	G	EIAALEW	KIAALKE	EIAALEK	**28**
KEK V4	G	KIAALKW	EIAALEK	KIAALKE	**29**

The novel artificial recognition units were synthesized by means of automated SPPS (more detail, see Section 8.5.1) and purified via HPLC prior to secondary structure analysis. In order to evaluate their eligibility as coiled-coil recognition unit, these peptides had to be checked in regard of their secondary structure formation. Therefore, circular dichroism (CD)-measurements were performed on each coiled coil pair and will be presented in the following.

6.2.2 CD-Measurements

The novel coiled-coil designs have been analyzed by applying CD-spectroscopy. CD-spectroscopy is an excellent method to determine the secondary structure of peptides, which is commonly used to analyze coiled-coils. Each peptide was purified via HPLC prior to use. The characteristic CD-spectra for α-helix formation can be distinguished when two negative bands at 208 nm and 222 nm, and a positive band at 192 nm are observed.[170,171] Additionally, the melting temperature of coiled-coils can also be determined via CD-spectroscopy by temperature-dependent measurements. In terms of the Hodges coiled coils, K3 and E3 have been reported to be able to form stable α-helices when combined. Also, the melting temperature T_M = 57 °C is known from literature.[172]

The first set of coiled-coil EKE V1 **22** and KEK V1 **23** differs the most in design with an Asn in the hydrophobic core. The first version of the alternating peptide fulfills, indeed, the requirements of coiled-coil but in the combination with the concept of the conformation dynamics introduced by Woolfson *et al.* no defined secondary structure could be observed.[168] Nevertheless, the remaining coiled-coil pairs were tested

and have been successful in forming α-helices. Figure 6.3, shows the obtained CD spectra of different coiled-coils forming peptides. Additionally, melting curves of each all peptides were recorded at 222 nm (between 5 °C - 95 °C).

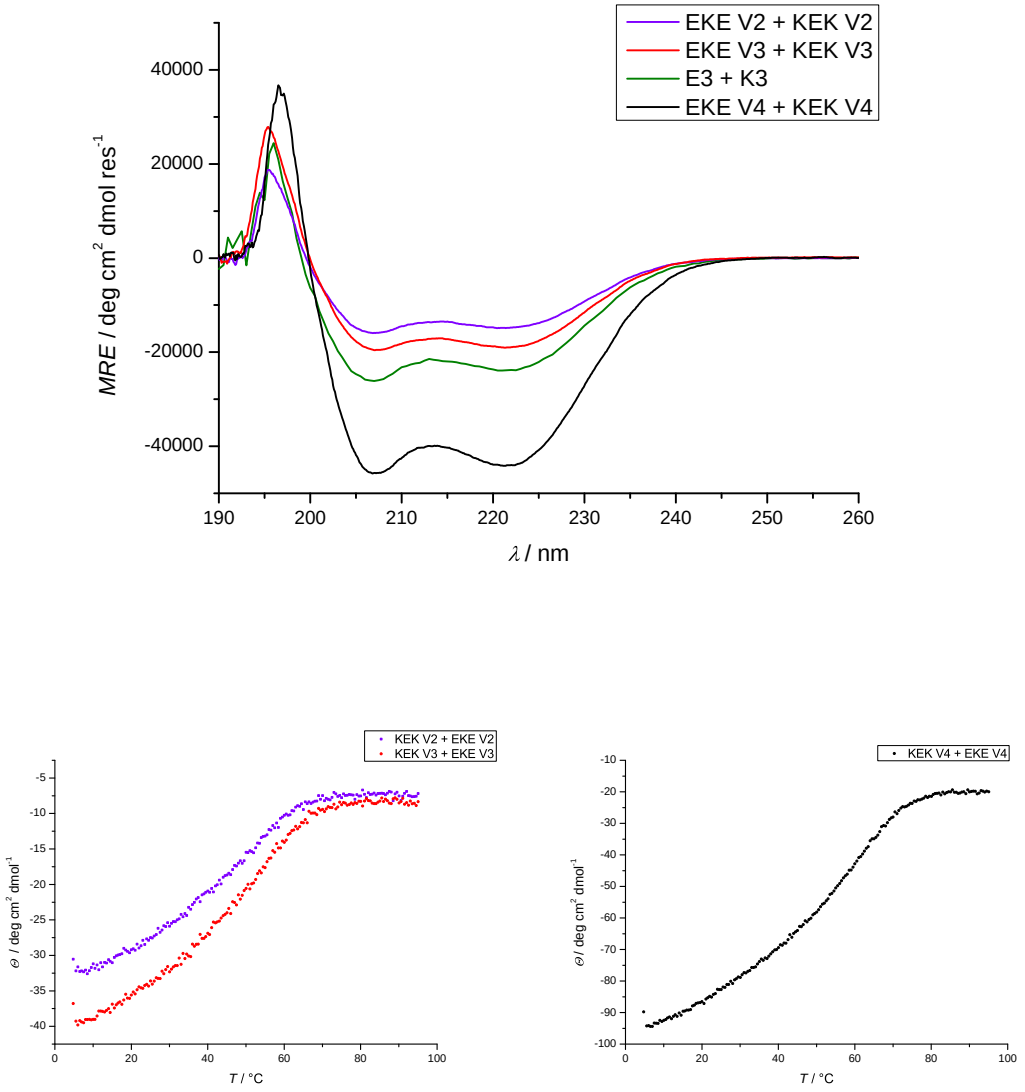

Figure 6.3: CD-spectra of alternating recognition units after combining different coils with each other. The combination of EKE V4 + KEK V4 showing the highest α-helical character. Peptide concentration was set to 40 µM. Additionally, melting curves of the alternating recognition units were obtained.

The course of the ellipticity is in good agreement with comparable α-helices. All CD spectra shows the characteristic maxima and minima of an α-helix. In comparison to the reference CD-spectra of E3/K3 major differences in intensity can be observed. Nevertheless, the unfolding of the coiled-coils of (**24** + **25** and **26** + **27**) resulted to be less stable than the reference E3/K3. Finally, the peptide pair of **28** and **29** shows the most α-helical character in comparison to the other coiled-coil pairs and also in comparison to the reference E3/K3 system. Also, the melting temperature of (**28** + **29**) was recorded and a $T_M = 65$ °C was obtained, making these coiled-coil pair highly attractive as a recognition motif.

From each coiled coil pair, CD-spectra of the monomers were recorded. For a matter of clarity, the recorded CD-spectra will not be illustrated in this section (see appendix). From the recorded CD-spectra the combination of both monomers lead to the formation of an α-helix. Nevertheless, the secondary structure of the novel coiled-coils could be successfully verified and have been used to synthesize coiled-coil peptide fusogens.

6.2.3 FRET based Fusion Measurements

After testing the different sets of coiled-coil recognition units and comparing them to the E3/K3 coiled-coil pair, coiled-coil pair (**28**+**29**) was found to be the most suitable system. Due to the promising secondary structure performance, these coiled-coil forming peptides were chosen as excellent alternatives for the artificial SNARE model system. The new designed peptides had to be linked with the TMD of Syntaxin-1A or Synaptobrevin-2 for subsequent experiments (Figure 6.4). Therefore, coiled-coil peptide model fusogens were synthesized by means of automated microwave assisted SPPS. Additionally, the coiled-coil pair (**26**+**27**) has also been prepared in order to test its fusion efficiency. The model peptides are also illustrated in Table 6.3.

Table 6.3: Alternating coiled-coil peptide fusogens.

	Coiled-coil peptide fusogen	Entry
EKE V3-SybTMD	EKE-KRKYWWKNLKMMIILGVICAIILIIIIVYFST	**30**
KEK V3-SxTMD	KEK-KYQSKARRKKIMIIICCVILGIIIASTIGGIFG	**31**
EKE V4-SybTMD	EKE-KRKYWWKNLKMMIILGVICAIILIIIIVYFST	**32**
KEK V4-SxTMD	KEK-KYQSKARRKKIMIIICCVILGIIIASTIGGIFG	**33**

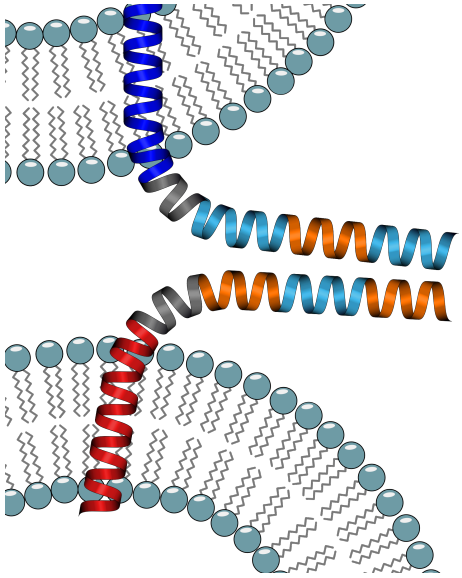

Figure 6.4: Alternating coiled-coil peptide fusogens incorporated into the lipid membrane. The recognition motifs have been highlighted (blue and orange) and been presented outside the membrane. The linker region (grey) and the TMDs of Sx and Syb have been highlighted (blue and red) and been incoporated inside the membrane.

Subsequently, the artificial model peptides have been incorporated into liposomes to analyze them via FRET based fluorescence measurements. In order to specify between docking, hemifusion or full fusion, fluorescence cross-correlation spectroscopy (FCCS) can be applied. Though its recommend to use Oregon Green and Texas Red as dyes. In this part of this work, the total lipid mixing quenching assay was applied as method of choice. Therefore, two liposome populations with either donor and acceptor fluorophore were prepared and monitored via fluorescence measurement (See Section 8.6.3 for more details). The used dyes of NBD and Rh were changed to the Texas Red and Oregon Green.

In order to maintain comparability of the fusion activity between the coiled-coild peptide fusogens and the artificial standard model system, it had to be ensured that the liposome concentrations were equal when mixing them in a ratio of 1:1. Especially, for the quenching assay, fluorescence measurement were executed to quantify the lipid concentration. Due to different labeled liposome populations, it was possible to determine the lipid concentration by comparing the emission of the fluorophores before and after extrusion. Therefore, a small amount of the liposome suspension before and after extrusion was used. The labeled samples were excited at their respective maximum excitation wavelength and on the basis of the relation of decreased intensity the lipide

concentration could be determined. In Figure 6.5, exemplarily shows a fluorescence measurement of both dyes (Oregon Green and Texas Red) before and after extrusion.

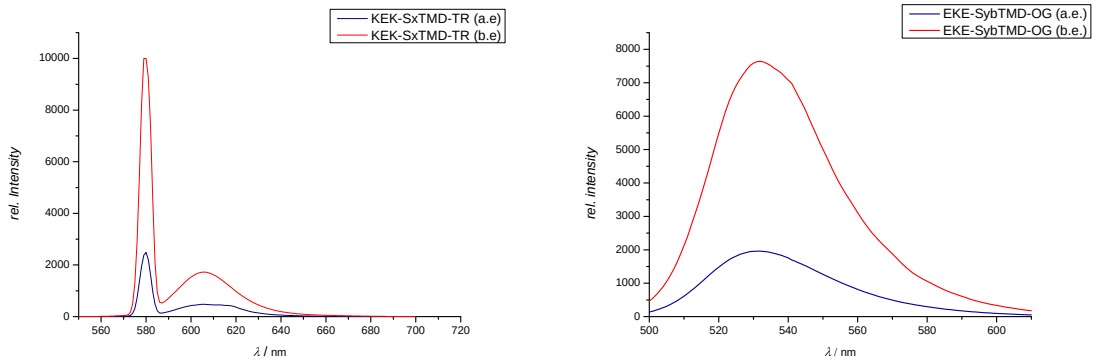

Figure 6.5: Fluorescence measurement of labeled TMD based peptides before (b.e) and after extrusion (a.e). The used fluorophores are Texas-Red and Oregon Green, abbreviated as TR and OG.

For further fusion experiments, the alternating coiled-coil peptide fusogens were anchored to the liposomes comprising Oregon Green (OG) as the donor fluorophore. In addition, the second liposome was prepared by incorporating the model peptide with Texas Red (TR) as acceptor fluorophore. By adding the second labeled liposome into the cuvette the recognition process is allowed to take place and the distance between the two liposome population is decreased and fusion can occur. If effective membrane fusion between these liposomes occurs, an increase in acceptor emission will be detected (Figure 6.6).[173,174]

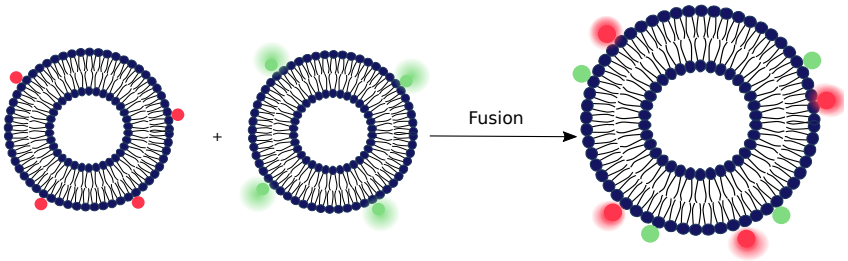

Figure 6.6: Quenching assay representing two liposomes with reconstituted TMD based peptides. Lipsomes were prepared with the fluorophore pair of Texas-Red and Oregon Green, abbreviated as TR and OG.[20]

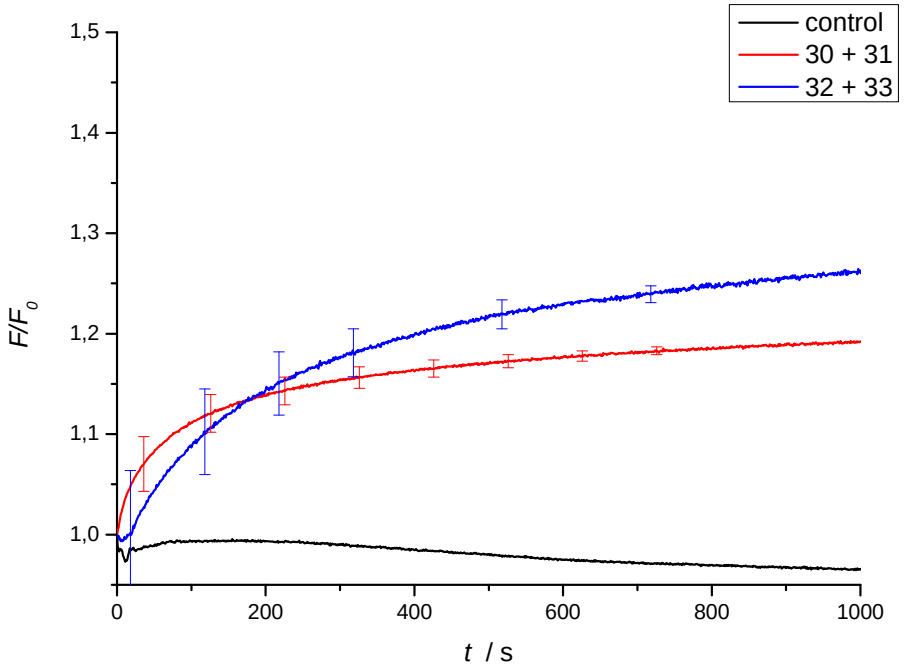

Figure 6.7: Fusion measurement of EKE-SybTMD and KEK-SxTMD. The control measurement was performed KEK-SxTMD and non-peptide containing OG-vesicles. The used fluorophores are Texas-Red and Oregon Green, abbreviated as TR and OG. P/L ratio was 1:200.

In Figure 6.7, the the extent of the quenching assay was investigated for liposomes containing EKE V3-SybTMD (**30**), KEK V3-SxTMD (**31**), EKE V4-SybTMD (**32**), KEK V3-SxTMD (**33**). Additionally, a control experiment was also performed by adding **30** or **32** to the labeled liposomes without any peptides. For the 1:1 mixtures of **30** + **31** and **32** + **33**, a significant increase in acceptor emission could be observed. Compared to the control experiment the increase in acceptor fluorescence can be clearly distinguished and shows the typical kinetical course when membranes merge with each other. Nevertheless, the characteristic fusion curves of **30** + **31** and **32** + **33** differs in their kinetical course in the beginning of each measurement when lipid membrane fusion begins. The fusion curve of **30** + **31** has an increased kinetical course compared to **32** + **33** in the beginning but the overall fusion is significant higher for the second system **30** + **31**. In later stages of the measurement, a flattening of the curves in all tested peptide systems can be observed. This course clearly differs more than former membrane fusion studies. Usually, an increasing fusion curve pattern has been observed when the dequenching assay is applied. However, for the quenching assay, a

flattening could be observed due to photobleaching.

The overall fusion intensity of 15-20 % is showing promising approaches which indicates a membrane mediating character of the novel coiled-coil peptide fusogens. The change of the peptide to lipid ratio to 1/500 and 1/1000 lead to the absence of fusion. Only the peptide to lipid ratio 1:200 showed a increase in acceptor emission. However, these measurements can not distinguish between hemi-fusion or full fusion. A comparison to former measurements was not possible due to the different plotting. In addition, the time between extrusion and measurement was observed to have a significant influence on the fusion activity. By mixing the liposomes directly after extrusion, the most prominent increase in fusion activity was observed. Therefore, and to keep all measurements comparable, all samples were used directly after extrusion. Subsequently, for every fusion event liposome sizes were checked via DLS measurements. DLS measurements could verify the increase in liposome size after FRET-based measurements.

6.2.4 Conclusion

The newly designed coiled-coil peptide fusogens have been tested and verified as excellent alternatives for the E3/K3 model system. Nevertheless, the alternative model peptides have revealed some major difficulties. The liposome preparation and the liposome stability could not be improved by introducing the novel coiled-coil peptide fusogens. The fusion experiments showed some promising approaches but not effective to exchange the K3/E3 TMD model system. Surprisingly, the increase in fusion efficiency was lower than predicted. Possible explanations for this pattern may be related to the missing membrane interacting properties of K3. In the Diederichsen group as well as in the studies of Kros *et al.*, the importance of K3 in membrane destabilizing as part of membrane fusion process has been presented.[21] The approach in this topic to reduce this specific interaction and increase the recognition process was promising but needs additional research. Apparently, it seems that the membrane destabilizing has a bigger impact than the recognition process. Therefore, it can be assumed that the recognition of each coil is important but K3 destabilization could increase the overall fusion efficiency . In order to further investigate this phenomenon, an alternative recognition motifs were developed. An alternative model system was designed to form tetrameric coiled-coils and will be presented in the following section.

6.3 Tetrameric Coiled Coil Model Peptide

6.3.1 Novel Tetrameric Coiled Coil Recognition Unit

The second coiled-coil peptide fusogen was designed following the native SNARE complex which is known to be formed by four intertwined-helices. Therefore, the model peptides were specifically designed in order to achieve a tetrameric coiled-coil recognition. Additionally, due to the difficulties during lipsome preparation and vesicle aging of SxTMD based model peptides in previous studies, minor changes in fusion assay setup will be introduced in Section 6.3.3.

In order to obtain a tetrameric coiled-coil, substitution of the non-polar amino acids have to be performed. The E3/K3 model was used as reference by exchanging isoleucine (Ile) with leucine (Leu) leading to the favoured tetrameric coiled-coil formation. Ideally, this should lead to stronger recognition and thus enhance the fusion process. By replacing polar amino acids, such as glutamate (Glu) or lysine (Lys), with a Trp unit, it was possible to generate specific net charges per coil. In Table 6.4 different variants of the tetrameric E3 or K3 analogues are illustrated.

Table 6.4: Different version of tetrameric coiled-coil recognition units. Therefore, the hydrophobic core has to be modified by changing Ile and Leu with each other. Additionally, minor modifications by changing specific amino acids were made.

Name	*N*-term.	gabcdef	gabcdef	gabcdef	Entry
E3	G	EIAALEW	EIAALEK	EIAALEK	**34**
E3T1	G	ELAAIEW	ELAAIEK	ELAAIEK	**35**
E3T2	G	ELAAIEK	ELAAIEW	ELAAIEK	**36**
E3T3	G	ELAAIEK	ELAAIEK	ELAAIEW	**37**
K3	G	KIAALKW	KIAALKE	KIAALKE	**38**
K3T1	G	KLAAIKW	KLAAIKE	KLAAIKE	**39**
K3T2	G	KLAAIKE	KLAAIKW	KLAAIKE	**40**
K3T3	G	KLAAIKE	KLAAIKE	KLAAIKW	**41**

Similar to the alternating coiled-coils the analysis via CD-spectroscopy was performed to verify the secondary structures of these newly designed coiled-coils. In the following section CD-measurements of these model peptides will be presented.

6.3.2 CD-Measurements

As already mentioned, the CD spectroscopic measurements were performed to determine the secondary structure of the newly designed model peptides. Figure 6.8 shows the CD spectra of the respective coiled-coil motifs. The measurement was performed according to the CD-measurments (See Section 8.2.4 for more detail).
The combination of E3T1 (**35**) and K3T2 (**40**) is in good agreement to the characteristic ellipticity of a α-helical structure. In the context of this work, additional recognition units were developed. Therefore, by introducing Trp in specific positions, the net charge in the recognition motif can be influenced resulting in a stronger interaction. This can be seen from the part of α-helical structure from the CD spectrum. In general, the different monomers were tested and also in different combination of K3T and E3T in order to obtain the most promising coiled-coil. In matter of clarity, the specific monomer interactions will not be presented in this chapter (see appendix).

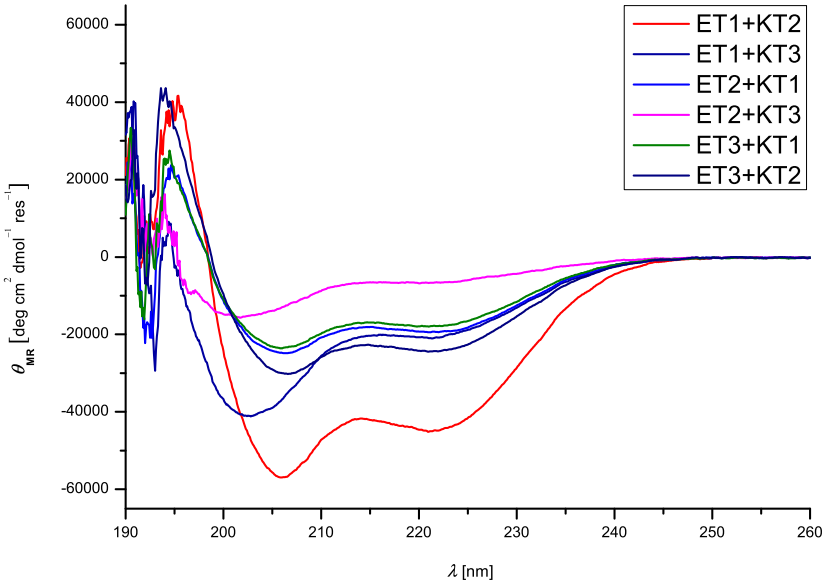

Figure 6.8: CD-spectra of different E3T/K3T-analogues. The combination of different E3T and K3T analogues with each other, showing the characteristic ellipticity of a α-helix with different helical character. The concentration was set to 40 µM.

Comparing the CD-spectra of (**35**+**40**) with **37**+**40** a significant reduced α-helical character can be observed. Some tested peptides are able to form α-helices with a few limited exceptions. The different sets of coiled coil still fulfill the requirements by

showing the characteristics of an α-helices but differs highly depending on which combination of K3T or E3T was chosen. In summary, the formation of tetrameric coiled-coil has been successfully verified, before synthesizing the respective model fusogens.

6.3.3 FRET-based Fusion Measurements

After testing the different sets of coiled-coil recognition units, a suitable coiled-coil pair (**35**+**40**) has been introduced. Due to the promising secondary structure formation, these coiled-coil forming peptides were chosen as excellent substitute for the current model system. Additionally, the fusion assay setup has been modified. Therefore, the E3T1 coil was prepared with the TMD of Syntaxin-1A and Synaptobrevin-2 for subsequent experiments. The K3T-analogue was prepared without a TMD unit. The coiled-coil peptide model fusogens were synthesized with means of automated microwave assisted SPPS and purified via HPLC. The change of fusion assay setup is illustrated in Figure 6.9. Additionally, fusion experiments were applied with the model peptides. K3T was added as additive to initiate the membrane fusion process. Unfortunately, positive fusion curves could be obtained but when checking the liposome size distribution of the mixed lipsomes an increased value of 1200-1500 nm was observed. The recognition process and the docking of the lipsomes was observed resulting in a significant increase in the fusion curve. It can be assumed that the formation of the tetrameric coiled-coil has been performed but due to less effective recognition a full fusion could not occur. Therefore, a model peptide with shorter linker length was introduced. It has been known from literature that in Sx - (KAARK) and in Syb- (WWKN) are critical because this region of the linker is actually the region which dives into the membrane. Therefore, E3T1s-SybTMD (**37**) and E3T1s-SxTMD (**38**) were developed. The synthesized model peptides are illustrated in Table 6.5.

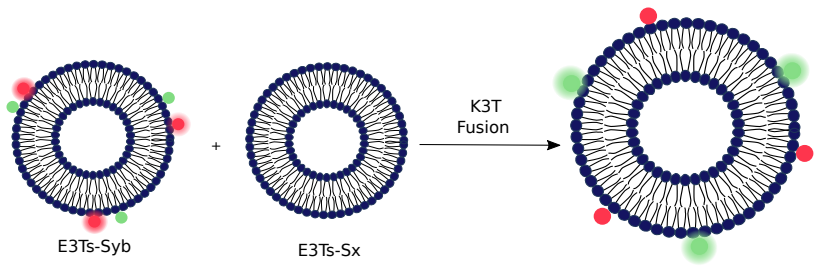

Figure 6.9: Dequenching assay representing two liposomes with reconstituted TMD based peptides. E3Ts-Syb and E3Ts-Sx are prepared as TMD based peptides and K3T was used as an additive. As Donor and acceptor fluorophores, NBD and Rh were used.

Table 6.5: Sequences of tetrameric coiled-coil peptide fusogens.

	Coiled-coil peptide fusogen	Entry
E3T1-SybTMD	E3T-SybTMD	**42**
E3T1-SxTMD	E3T-SxTMD	**43**
E3T1s-SybTMD	E3T-SybTMD	**44**
E3T1s-SxTMD	E3T-SxTMD	**45**

The reduced model peptides for E3T1-Sx and E3T1-Syb are presented in Figure 6.10

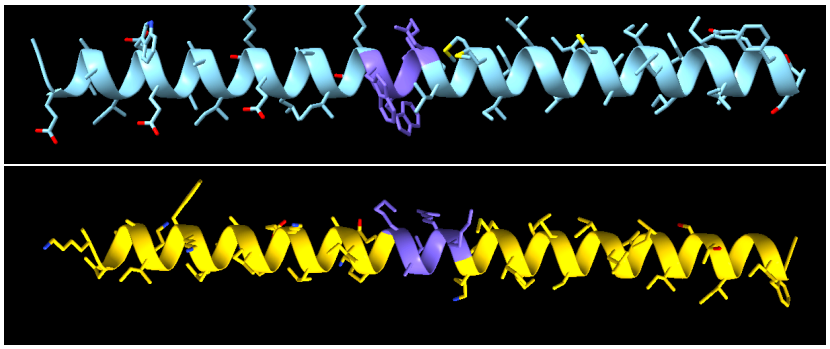

Figure 6.10: E3T1-Sx (yellow) and E3T1-Syb (cyan) with the shorter linker region (purple). The motif was created with the *UCSF Chimera* package.

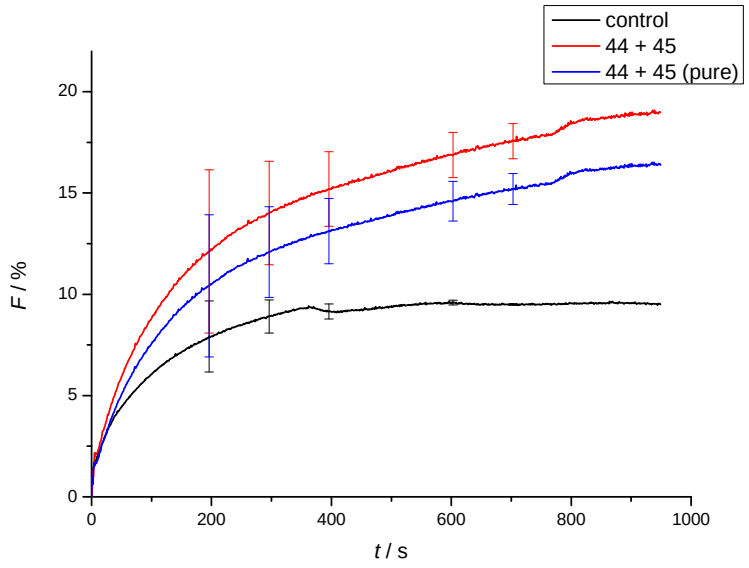

Figure 6.11: Average fusion curves of liposome mixing of **44** + **45**. Control measurement was performed with the addition of K3T. Additionally the unpurified peptides of **44** + **45** were tested.

Subsequently, the artificial model peptides has been incorporated into liposomes to perform FRET-based fluorescence measurements. In terms of the modified fusion assays, the measurement were performed according to the previous described setup (see Section 8.6.4). In Figure 6.11, two fusion curves of the lipsomes mixing of the newly designed tetrameric-coiled coil are illustrated. For the obtained control measurement an increase donor fluorescence can be observed, which may occur due to vesicle bursting or lipsome docking when **44** + **45** are interacting with each other without the presence of K3T. The fusion curves (blue and red trace) were applied under the same conditions but differs in peptide purity. Its has been noted in previous studies of Groth that purified model peptides intend to be less fusogen than expected.[19] In this specific case, the total fusion intenstiy differs about 4 % and still represent a significant increase in fusion efficiency which makes it attractive for further experiments.

6.3.4 Conclusion

The tetrameric coiled-coil approach has been thoroughly tested by applying FRET-based fusion measurements. Additionally, the increase in liposome size after mixing was verified. Fusion studies with the initial tetrameric coiled-coil peptide fusogen (**42** + **43**) were not successful. The increase in fusion efficieny could be observed when the samples were mixed with each other. Nevertheless, DLS measurements were showing an increased size distribution up to 1500 nm. This insight of fusion measurements indicates that the recognition and membrane docking occur but are not sufficient to force the membranes to merge with each other. Therefore, modifications in the linker region were performed in order to reduce the length of the linkers of the native TMDs. The idea of changing the length was to bring the membrane in more closer proximity and forcing the membrane to fuse. The newly designed coiled-coil was able to induce membrane fusion. Nevertheless, subsequent experiments have to be performed in order to distinguish between docking, hemi-fusion or full fusion.

7 Summary and Outlook

In this thesis, the main goal was to develop novel SNARE model peptides with artificial recognition units. In the first project the assumed SNARE zippering was investigated by synthesizing SNARE model peptides with artificial caged PNA recognition units. Therefore, NPP was introduced as a caging group in aeg-PNA monomers to block hybridization of the PNA recognition sites and prevent membrane fusion. First, the caged PNA build blocks were synthesized in a multiple step synthesis. Then, the TMD sequences of Sx and Syb were prepared by using Fmoc solid-phase peptide synthesis. After that, PNA monomers as well as caged-PNA building blocks were attached using manual coupling following an established protocol. Subsequently, the SNARE analogues were tested by applying FRET fusion assays. For the caged-PNA/peptide hybrids, irradiation with UV-light has been applied in order to restore the recognition of the PNA strands. The applied fusion assays revealed that NPP is indeed influencing the membrane fusion efficiency but the restored PNA recognition process was showing only a slightly increase in fusion intensity. The overall value was less than expected, leading to not reliable membrane fusion data. These results indicating that there is the possibility to influence the recognition process but additional experiments have to be made in order to study zipper-like recognition process. However, a change in caging group or a change in fusion assay setup would be recommend in order to get reliable information.

The second project was the improvement of the SNARE E3/K3-TMD model system introduced by Meyenberg *et al.*[17] This model system comprises the artificial peptides E3/K3 forming coiled-coils and the sequences of the native TMDs of Syb and Sx. During the course of this work, the system turned out to have limitation in order to achieve optimal fusion efficiency. Therefore, novel coiled-coil recognition units were introduced and tested to achieve higher yielding in fusogenicity. Following the rules of recognition motifs, various model peptides have been designed and synthesized by using Fmoc solid-phase peptide synthesis. After verifying the successful formation of the desired secondary structure, alternating dimer as well as tetrameric coiled-coils

were selected as alternative coiled-coil recognition motifs.

Therefore, model fusogens were prepared with the TMD sequence of Sx or Syb to achieve membrane anchoring. The purification which is known to be challenging was established by a new HPLC method. Furthermore, successful purification methods of PNA containing recognition units were developed.

The fusion activity of the coiled-coil peptide fusogens was examined using FRET-based liposome fusion assays. It was presented in this work that the alternating coiled-coil fusogens are sufficient to mediate membrane fusion. The alternating fusogens which were developed as part of this work showed sufficient capability of membrane fusion. The applied quenching assay allowed to get a better understanding in kinetical behavior during membrane fusion. Especially, peptide interactions can be clearly assigned to sufficient membrane fusion and not to vesicle bursting or other disturbances. The presented model peptides EKE V4 SybTMD **32** and KEK V4 SxTMD **33** were designed and developed to form the most α-helix, which was confirmed via CD-measurements. After testing different sets of alternating coiled-coil fusogens, the model peptides 32 + 33 showed promising fusion activity in membrane fusion studies.

Additionally, another coiled-coil peptide fusogens were developed following the native tetrameric SNARE complex. Before synthesizing the model fusogens using Fmoc solid-phase peptide synthesis, the recognition units were successfully tested of their secondary structure via CD-spectroscopy. A different approach was used to study membrane fusion. Therefore, the TMD sequence of either Sx or Syb were attached to E3T to get E3T-Syb and E3T-Sx. K3T was prepared without the transmembrane domain and was used as an additive to initiate the fusion process. When mixing the liposomes incorporated with model peptides together, an increase in donor emission was observed. After checking the liposome size distribution, a increased vesicle size indicating liposome docking rather than membrane fusion. According to Stengel *et al.*, variation of the linker region by PEG-units enhances mainly the docking process.[96] Therefore, the linker region was reduced to create a new type of alternative fusogens. The synthesized model peptides were tested in fusion assays in order to obtain reliable data in membrane fusion studies. The fusion efficiency of tetrameric coiled-coil peptide fusogens was also sufficient in order to mediate membrane fusion. These novel coiled-coil peptide fusogens showing promising outcomes in terms of membrane fusion studies. Nevertheless, additional experiments need to be executed in order to establish the coiled-coil pep-

tide fusogens as the standard model system in the DIEDERICHSEN group. For example, FCCS measurements can be applied to distinguish between hemi-fusion and full fusion.

In summary, synthesis of artificial model fusogens does not only help to get insight into the biological processes, but also can provide a variety of target structures with respect to medial applications *e.g.* anti-cancer therapeutics.[175] The need in understanding these specific role of SNARE proteins in cellular trafficking, membrane fusion and synaptic vesicle release can be generated with the help of artificial model fusogens. By employing these model peptides in synaptic vesicles , it is possible to get better understanding in the field of natural membrane behavior and their fusogenicity. The approaches with various artificial model systems have been introduced but further experiments need to be executed in order to get more insight about zippering or between hemi- and full fusion.

8 Experimental Section

8.1 Solvents and Reagents

Solvents. Organic solvents (DCM, DMF and NMP) for solid-phase peptide synthesis were purchased from *Merck KGaA* (Darmstadt, Germany), *Fisher Scientific* (Hampton, USA) or *Carl Roth* (Karlsruhe, Germany). Methanol and acetonitrile were obtained from *Fisher Scientific*. All used solvents were at least laboratory grade (≥99.8 %). For spectroscopic measurements and purification applications solvents of HPLC grade (≥99.9 %) were used. Demineralized water was filtered using a water purification system by *arium mini lab* water system by *Sartorius* (Göttingen, Germany) prior to use.

Reagents. Amino acids were purchased from *GL Biochem Ltd.* (Shanghai, China), *Sigma Aldrich* (Munich, Germany) and *Iris Biotech* (Marktredwitz, Germany). PNA monomers were purchased from *ASM Research Chemicals* (Hanover, Germany). For solid-phase peptide synthesis, resins were obtained from *Novabiochem* (Darmstadt, Germany), *Iris Biotech* and *Sigma Aldrich*. Phospholipids were obtained from *Avanti Polar Lipids, Inc.* (Alabaster, USA). Labeled lipids were purchased from *Fluorochem* (Hadfield, UK) and *molecular probes* (Eugene, USA).

8.2 General Methods

Lyophilization. Water was removed from aqueous samples by lyophilization. The samples were frozen with liquid nitrogen and subsequently put under reduced pressure using *Alpha-2-4-LD* freeze-dryer from *Christ* (Osterode am Harz, Germany). Small amounts of raw peptide were solved in HFIP or TFE, diluted with ultrapure water and vortexed for a few seconds prior to freezing. Small quantities of peptides were lyophilized using a *RVC 2-18* centrifuge from *Christ*.

Storage. Freeze-dried peptides were stable at room temperature for days to few weeks. For long-term storage, purified peptides were stored at −20 °C. On-resin peptides were stored under reduced pressure at room temperature. Phospholipids as well as labeled phospholipids were stored under argon atmosphere at −20 °C. PBS buffer stock solution (10x) as well as HEPES buffer stock solution (10x) were stored at 8 °C. Photo-sensitive compounds were protected with aluminum foil and were stored at room temperature.

Mass Spectrometry. Electrospray ionization (ESI) mass spectra were recorded on a *maXis* spectrometer by *Bruker Daltonik GmbH* (Bremen, Germany). For sample preparation, peptides were dissolved in MeOH. Transmembrane based peptides (*e.g.* PNA/peptide hybrids and coiled-coil peptide fusogens) were dissolved in TFE/MeOH (1:1). Addtionally, 10 % formic acid was added to each transmembrane based peptide sample before every measurement. High-resolution mass spectra (HR-MS) are indicated for calculated (cal.) as well as for the experimentally found peaks. The mass-to-charge (m/z) ratio as well as the relative intensity in percentage (%) are indicated.

Statistical Error Calculations. For repeated measurements the statistical error was calculated and displayed in the plots. The standard deviation of the mean value multiplied by the respective t-value (student's t-distribution) was applied to obtain the statistical errors. The statistical error calculation f was provided by the following equation:

$$f = t_{95\%} \cdot \sqrt{\frac{1}{(n-1)} \sum_{i=0}^{n} (x_i - \tilde{x})^2} \tag{8.1}$$

Here, n is the number of measurements, x_i is the acquired data point of i measurement and $\tilde{x}$ is the mean value of total measurements. In terms of uncertainty, the t-values of 95 % confidence interval were included. Obtained data were plotted as $\tilde{x} \pm f$.

8.3 Chromatographic Methods

Flash Chromatography. Silica gel type 60 (grain size of 40–63 µm) purchased from *Merck KGaA* (Darmstadt, Germany) was used as column material. Column preparation was performed as follows, the crude products were suspended with a small amount of silica gel and a solvent of choice. The solvent was removed on a rotary evaporator to obtain a dry powder. The sample was loaded as a dry powder on the prepacked silica column and diluted with eluent. The purification was performed at a low overpressure of 0.5-1 bar. The column size was chosen depending on the product quantity.

High Performance Liquid Chromatography (HPLC). For HPLC analysis and purification procedures, HPLC systems from *JASCO* (Tokyo, Japan) or *Thermo Fisher* (Massachusetts, USA) were used. Reversed phase high performance liquid chromatography (RP-HPLC) were applied for all peptide purification procedures. Prior to bulk purification, all peptides were run on a UPLC system to determine the correct conditions. Peptides could be detected at wavelenghts of 215 nm, 260 nm and 280 nm. If labeled peptides were used, wavelenght specifications could differ. The used HPLC systems with their specifications are listed in Table 8.1.

Table 8.1: The HPLC systems used to analyze and purify crude peptides. The specific data of the used HPLC systems are listed.

Systems	Specification
UPLC	*Thermo Fisher* (Waltham, USA) Ultimate 3000: detector DAD-3000; pumps LPG-3400SD; column oven TCC-3000SD; autosampler WPS-3000SL.
HPLC Prep	*JASCO* (Tokyo, Japan): detector UV-4075; pumps PU-4086; column oven CO-4060; interface LC-NetII/ADC fraction collector interface; collector CHF122SC (Advantec).
HPLC Semi-Prep	*JASCO* (Tokyo, Japan): Detector UV-2075 Plus/UV-975; pumps PU-2080 Plus; column oven; CO-4060; interface LC-NetII/ADC; degasser DG-2080-53; fraction collector interface.
HPLC Prep-DAD	*JASCO* (Tokyo, Japan): detector MD-2010 Plus; pumps PU-2080 Plus; interface LC-NetII/ADC; degasser DG-2080-53; collector interface FC-2088-30; collector CHF122SC (Advantec).

HPLC bulk purification procedures were performed using a standard solvent system. The standard solvent system with 0.1 % TFA was adjusted for transmembrane peptides

by adding 0.1 % HFIP. The detailed solvent systems are listed Table 8.2.

Table 8.2: Solvent systems used to analyze and purify crude peptides. The solvent system was adjusted with HFIP to realize better separation.

Solvents	Peptides	Transmembrane peptides
Solvent A	H_2O + 0.1 % TFA	H_2O + 0.1 % TFA + 0.1 % HFIP
Solvent B	MeCN + 0.1 % TFA	MeCN + 0.1 % TFA + 0.1 % HFIP
Solvent C	MeOH + 0.1 % TFA	MeOH + 0.1 % TFA + 0.1 % HFIP

For each purification run the applied HPLC columns may differ. In case of transmembrane peptide purification, ACE Excel C18 columns showed good results. Large-scale peptides were purified using semi-preparative or preparative columns. The HPLC columns are listed in Table 8.3.

Table 8.3: HPLC columns used to analyze and purify crude peptides.

Column	Specification	Flow rate
ACE Excel 2 C18	C18, 100 x 2.10 mm, 100 Å, 2 µm	0.3 mL/min
ACE Excel 5 C18	C18, 150 x 10.0 mm, 100 Å, 5 µm	0.3 mL/min
ACE Excel 5 C18	C18, 150 x 21.2 mm, 100 Å, 5 µm	0.3 mL/min

Peptides were generally prepared by solving the sample in ultrapure water. Transmembrane based peptides were solved in HFIP in a ratio of 1 to 10, HFIP to ultrapure water. Before adding the ultrapure water, the peptide was dissolved in HFIP first and sonicated until a homogeneous solution was obtained. For every purification each sample was filtered using a *Phenex-RC* syringe filter (0.45 µm pore size) from *Phenomenex* (Aschaffenburg, Germany).

Thin Layer Chromatography (TLC). Silica gel 60 F254 aluminum coated plates from *Merck KGaA* (Darmstadt, Germany) were employed. The progression of reaction was distinguished by fluorescence deletion at 254 nm or 365 nm.

8.4 Spectroscopic Methods

NMR. ^{1}H-NMR spectra were recorded on a *Varian* (Palo Alto, USA) 300 MHz-instrument from Mercury-VX 300 or VNMRS-300. ^{13}C-NMR spectra were recorded on a *Varian* 126 MHz-instrument from INOVA-500. For each measurement the employed solvent and recorded frequency are indicated. Chemical shifts δ are presented in parts per million (ppm), coupling constants are calculated and presented in Hertz (Hz). Multiplicities abbreviations are listed as: s (singlet), d (doublet), t (triplet), q (quartet) or m (multiplet).

UV Absorption Spectroscopy. All concentration measurements with peptides containing tryptophan were recorded at 280 nm. The PNA/peptide hybrids concentration measurements had to be performed at 260 nm. The spectra were obtained using the *JASCO* UV-Vis spectrophotometer (Model V-650) equipped with the ETCS-761 temperature controller. The temperature was set to 25 °C and the measuring chamber was continuously flushed with nitrogen. The absorption of each peptide was recorded for three measurements. Then, mean absorption was used for the calculation. The molar extinction coefficient for coiled coil peptide fusogens were estimated by sum of the extinction coefficents of amino acids (tryptophan (Trp), tyrosine (Tyr) and cysteine (Cys)). For PNA/peptide hybrids the molar extinction coefficient were calculated by the summation of the molar extinction coefficients of aeg-PNA monomers (guanine (g), adenine (a), cytosine (c) and thymine (t)) and amino acids (tryptophan (Trp), tyrosine (Tyr) and cysteine (Cys)).[127,176] The molar extinction coefficients of amino acids and nucleobases at 260 nm and 280 nm are listed in Table 8.4.

Table 8.4: The molar extinction coefficient of amino acids and nucleobases for 260 nm and 280 nm.

ϵ_{260nm} (Trp)	3300 $cm^{-1} \cdot M^{-1}$	ϵ_{280nm} (Trp)	5700 $cm^{-1} \cdot M^{-1}$
ϵ_{260nm} (Tyr)	600 $cm^{-1} \cdot M^{-1}$	ϵ_{280nm} (Tyr)	1300 $cm^{-1} \cdot M^{-1}$
ϵ_{260nm} (Cys)	400 $cm^{-1} \cdot M^{-1}$	ϵ_{280nm} (Cys)	120 $cm^{-1} \cdot M^{-1}$
ϵ_{260nm} (g)	11700 $cm^{-1} \cdot M^{-1}$	ϵ_{260nm} (a)	13700 $cm^{-1} \cdot M^{-1}$
ϵ_{260nm} (c)	6600 $cm^{-1} \cdot M^{-1}$	ϵ_{260nm} (t)	8600 $cm^{-1} \cdot M^{-1}$

The peptide concentration was obtained according to the Beer-Lambert law. The concentration was calculated with the following equation:

$$c = \frac{A_{260\text{nm}}}{d \cdot \epsilon} \tag{8.2}$$

With the measured absorption A at 260 nm or 280 nm, the sum of extinction coefficients ϵ (cm^{-1} M^{-1}) and the thickness of the cuvette d (mm).
The measurements were carried out by an absorption of 280 nm, except for the PNA/hybrid peptides, which were carried out by an absorption of 260 nm. The extinction values at 260 nm were taken from literature.[127]

CD spectroscopy. All CD-spectra measurements were recorded in a wavelength range from 190 nm to 260 nm. *JASCO* CD Spectrometer (J-1500) with a PTC510 temperature-measuring unit have been used to obtain the spectra measurements. Therefore, the temperature was set at 25 °C and the measuring chamber was flushed with nitrogen in order avoid temperature fluctuations. The applied parameters for each CD-measurements are listed in Table 8.5.

Table 8.5: CD-spectra measurements specifications.

Parameter	spectrum measurement
wavelength	190-260 nm
bandwidth	1 nm
digital integration time (DIT)	2 s
continuous scanning mode	2000 mdeg/1.0 doD
scanning speed	100 nm $\cdot$ min^{-1}

For every measurement, 10 runs were recorded at 20 °C. Moreover, thermal denaturation curves in order to determine melting temperature were recorded at 222 nm at a temperature gradient from 5 °C to 95 °C at 1 °C/min in 0.5 °C intervals. The measurements were carried out in PBS buffer with a sample volume of 250 µL. Peptide concentration was set to 40 µM. Among every, washing steps were performed using aqueous solution of Hellmanex III, ultrapure water and ethanol. Blank signals were recorded using PBS buffer for all data. Subsequently, the measured blank signals were subtracted and the molar mean residue ellipticity θ_{MR} was calculated as follows:

$$\theta_{MR}(\lambda) = \frac{100 \cdot \theta(\lambda)}{l \cdot c \cdot n} \tag{8.3}$$

With the ellipticity θ (mdeg), optical pathway l (cm), peptide concentration c (mmol

· L^{-1}) and number of amino acid residues n (res).

8.5 Standard Operating Procedures (SOPs)

8.5.1 SOP1: Automated Microwave Solid Phase Peptid Synthesis

To obtain long or complicated peptides, the automated microwave solid-phase peptide synthesizer either the model *Liberty Blue* or *Liberty Prime* from *CEM* (Kamp-Lintfort, Germany) was used. Both peptide synthesizer were attachted to a Discover^{TM}-microwave unit from *CEM*. For standard peptide synthesis the following amino acids building blocks are illustrated in Table 8.6.

Table 8.6: Fmoc-protected amino acids for solid phase peptid synthesis.

Fmoc-Glu-(O^{t}Bu)-OH	Fmoc-Ala-OH	Fmoc-Ile-OH	Fmoc-Tyr-(^{t}Bu)-OH
Fmoc-Arg(Pbf)-OH	Fmoc-Gly-OH	Fmoc-Met-OH	Fmoc-Trp(Boc)-OH
Fmoc-Asn(Trt)-OH	Fmoc-Val-OH	Fmoc-Leu-OH	Fmoc-Ser(^{t}Bu)-OH
Fmoc-Cys(Trt)-OH	Fmoc-Phe-OH	Fmoc-Lys(Boc)-OH	

The automated microwave peptide synthesizer is able to prepare peptides in a scale range of 0.01 - 0.50 mmol. For large scale synthesis, a adapted reaction vessel has to be applied. In general, the common peptide synthesis scale varied between 0.05 - 0.10 mmol. For the synthesis of coiled coil recognition units non-preloaded Rink amide ChemMatrix resin was used. Transmembrane based peptides were synthesized on a preloaded NovaPEG-resin and additionally modified manually if required.

The preloaded Fmoc-Gly-Wang resin has a loading of 0.37 mmol/g while the preloaded resin Fmoc-Thr(^{t}Bu) has a loading of 0.32 mmol/g as lowloading (LL) has turned out to be excellent for the synthesis of large peptide sequences.[20] For shorter peptides, especially for the coiled coil recognition units, the preloaded Rink amide ChemMatrix resin with a loading of 0.4 -0.7 mmol/g was used. For the synthesis, the value of 0.5 mmol/g was assumed. Before each synthesis the resin was transferred into a Becton Dickinson (BD) Discardit syringes with polyethylene-frithas and has to swell in DMF for 1 h. Since, the resin swelling increases the size of the beads, larger peptides can

be loaded more easily. The amino acid concentration is set to 0.2 M irrespective of the scale size. In terms of the 0.1 mmol scale, the following amounts have been added to the reaction vessel. First, the *N*-terminal protecting group was removed by adding of a solution of piperidine (20 % in DMF). After successful cleavage the coupling reaction was initated by adding 1.5 mL of respective amino acid (0.2 M), 0.6 mL (1 M) and 0.3 mL Oxyma (1 M). The coupling procedures were applied following the listed specification of Table 8.6. If synthesis was performed on the Liberty Prime synthesizer the synthesis setup may differ in amino acid and activator concentration. Especially, the couple time can be reduced immensively. The amino acid coupling conditions had to be adapted for cysteine and arginine coupling. To prevent racemisation of the cysteine side chains and due to the bulky side chains of arginine specific microwave conditions have to be applied which are listed in Table 8.7. Especially, in case of the hydrophobic transmembrane peptides, the quality of peptides was improved when double coupling was applied.

Table 8.7: Automated microwace peptide synthesizer specifications. For Arg and Cys different settings had to applied.

Standard 90 °C	1. 75 °C, 170 W, 17 s; 2. 90 °C, 30 W, 225 s. 5 eq. aa, 5 eq. DIC, 5 eq. OxymaPure, 0.5 eq. DIPEA.
Carbomax 105 °C	1. 85 °C, 280 W, 20 s; 2. 105 °C, 90 W, 75 s. 5 eq. aa, 10 eq. DIC, 5 eq. OxymaPure, 0.5 eq. DIPEA.
Arginine	1.coupl.: 1. 25 °C, 0 W, 1500 s; 2. 75 °C, 30 W, 120 s. 2.coupl: 75 °C, 30 W, 300 s.
Cysteine	1. 25 °C, 0 W, 120 s; 2. 50 °C, 30 W, 480 s.

8.5.2 SOP2: Manual Solid-Phase PNA Synthesis

The PNA-oligomer synthesis was applied following Fmoc/Bhoc-strategy after successful synthesis of the transmembrane peptide sequence. Each stock solution of needed reagents were prepared daily. The respective on-resin peptide was prepared in a (BD) Discardit syringes with polyethylenefrit. NMP was transferred into a syringe and the resin was swollen for 2 h. Peptide chain elongation was carried out after Fmoc-protecting group removal. Therefore, 2 mL of piperidine solution (20% in NMP) was added to the resin and repeated twice. Before starting the coupling step, wash steps (5 x NMP, 5 x DCM, 5 x NMP) were performed. PNA building blocks (4.0 eq.) and

activator pair of HOAt/HATU (4.0/3.9 eq.) were dissolved in NMP. Due to solubility issues sonication was necessary. Solid phase PNA synthesis achieved the highest success when PNA building block and activator solution were sonicated for 15 min until complete dissolution. Then, 2,6-lutidine and DIPEA mixed with the PNA/activator solution was drawn up into the syringe. This coupling procedure was repeated twice. Unfinished PNA/peptide hybrids sequences were stored over night at −20 °C and reused the day after without reswelling. After successful synthesis of the target compound, the final step was washing the resin with a polar solvent and store the resin under *in vacuo*.

8.5.3 SOP3: Microwave-assisted Solid-Phase PNA Synthesis

Microwave-assisted solid phase PNA synthesis was performed following the Fmoc/Bhoc-strategy. Therefore, the procedure was carried out similar to manual coupling method. The respective on-resin peptide was prepared in BD Discardit^{TM}II syringes with polyethylenefrit. Microwave irradiation was applied using a Discover microwave unit (CEM, Matthews, USA). The resin was swollen in NMP for 2 h. The coupling of PNA monomers was followed by a cycle of three essential steps, starting with the deprotection of the Fmoc-protecting group by treating the resin with piperidine (20 % in NMP). This procedure performed twice. Among every deprotection or coupling step, wash steps (5 x NMP, 5 x DCM, 5 x NMP) was performed to remove nonreactive reagents. After the second deprotection step, the coupling was prepared by adding HATU/HOAt (4.9 /5.0 eq.) in NMP to the PNA monomer (5 eq.). When DIPEA (10.0 eq.) and 2,6-lutidine (10.0 eq.) were added to the PNA and activator solution the coupling process starts and the solution have been drawn up into the syringe immediately. The process was performed twice. To prevent nonreactive sequences to be part in further synthesis, the resin was capped with a mixture of Ac_2O/DIPEA/DMF (1:1:18, *v/v/v*, 10 min), followed by an additional washing step (5 x 5 % DIPEA, 5 x DCM, 5 x NMP). Finally, the resin was washed with a polar solvent and dried *in vacuo*. The specific microwave conditions used for this specific procedure are listed in Table 8.8.

Table 8.8: Microwave settings for the Solid-Phase PNA synthesis.

Deprotection	1. 20 W,40 °C, 60 s 2. 25 W, 50 °C , 300 s
Coupling	25 W, 50 °C, 20min

8.5.4 SOP4: Resin Cleavage

The resin was transferred into a 2 mL Discardit^{TM}II- syringe BD with polyethylene-frit. Peptide sequences were cleaved using a mixture of TFA/EDT/Milli-Q/TIS (94.0/2.5/ 2.5/1.0, $v/v/v/v$). For PNA/peptide hybrids, cleavage cocktail of TFA/Thioanisol/*m*-cresol/ EDT/TIS (63.0/15.0/14.5/5.0/2.5, $v/v/v/v/v$) was used. The addition of *m*-cresol was needed to prevent reactive side reactions caused by the bhoc-protecting group. The peptide cleavage from the resin took 2 h. PNA/peptide hybrids were cleaved up to 3 h. Afterwards the cleavage solution was removed under nitrogen stream. The residue was precipitated in cold Et_2O. After separating the peptide through centrifugation the remaining solution was removed and resolved with Et_2O again. The washing process was repeated 5 times. The final product was then dried *in vacuo* to obtain the crude peptide.

8.6 Fusion Assays

8.6.1 Lipid Film Preparation

Lipsomes were prepared with different molar ratio and fluorophores according to Table 8.9. Depending on which fusion was applied liposomes containing one or two fluorophores were prepared. Lipid stock solutions were prepared by solving lipid powder in chlorofom. The liposome composition consisted of 1,2-dioleoyl-*sn*-glycero-3-phosphocholine (DOPC), 1,2- dioleoyl-*sn*-glycero-3-phosphoethanolamine (DOPE) and cholesterol. The concentration of each lipid stock solution was set to 20 mg mL^{-1} and after usage the stock solutions were stored at -20 °C. The concentration of labeled lipid stock solution of 1,2-dioleoyl-*sn*-glycero-3-phosphoethanolamine-N-(7-nitro-2-1,3-benzoxadiazol-4-yl) (NBD-DOPE), 1,2-dioleoyl-*sn*-glycero-3-phosphoethanolamine-N-(lissamine rhodamine B sulfonyl) (Rh-DOPE), 1,2-dihexadecanoyl-*sn*-glycero-3-phosphoethanolamine (Oregon green 488-DHPE) and 1,2-dihexadecanoyl-*sn*-glycero-3-phosphoethanolamine (Texas red-DHPE) was set to 1 mg mL^{-1}. Transmebrane peptides were dissolved in TFE and their concentration was determined using UV-Vis spectroscopy at 280 nm. Thin lipid films could be prepared by starting to fill chloroform into small test tubes. To prevent evaporation of organic solvent the test

tubes were cooled in an ice bath. Additionally, labeled lipids were protected by aluminum foil. The total lipid concentration was 625 nmol and the peptide to lipid ratio was 1:200. For reference measurements, lipid films without peptides were prepared. Therefore, only TFE was added to the test tube. After adding all components into the test tube, the solution was vortexted for 5 s and was then evaporated under a nitrogen stream at 50 °C. Finally, the test tubes were stored at 50 °C overnight in the vacuum oven to obtain a thin lipid film.

Table 8.9: Lipid composition of labeled and unlabeled vesicles.

Lipids	specfic Lipid composition (molar ratio)
Unlabeled	DOPC/DOPE/Chol 50:25:25
Labeled TR	DOPC/DOPE/TR-DHPE/Chol 50:23.5:1.5:25
Labeled OG	DOPC/DOPE/TR-DHPE/Chol 50:23.5:1.5:25
Labeled OG+TR	DOPC/DOPE/OG-DHPE/TR-DHPE/Chol 50:22:1.5:1.5:25
Labeled Rh	DOPC/DOPE/TR-DHPE/Chol 50:23.5:1.5:25
Labeled NBD	DOPC/DOPE/TR-DHPE/Chol 50:23.5:1.5:25
Labeled Rh+NBD	DOPC/DOPE/OG-DHPE/TR-DHPE/Chol 50:22:1.5:1.5:25

8.6.2 Vesicle Preparation

Proteoliposomes preparation was performed according to the standard procedure via direct mixing.[20,177] The 10-fold HEPES buffer stock solution was diluted with ultrapure water. Buffer preparation was complete after adding 1 mM DTT and adjusting the pH-value to 7.4 by adding 1 M KOH. Rehydration of the lipid films was achieved by adding 500 µL HEPES buffer (20 mM HEPES, 100 mM KCl, 1 mM EDTA, 1 mM DTT, pH = 7.4) and four glass beads into the test tubes. The test tubes were sealed with Parafilm® and placed on an Unimax 1010 platform thermoshaker by *Heidolph* (Schwabach, Germany) equipped with the heating unit incubator at 40 °C for at least 2 h. The shaking speed was set to the minimum of 190 rpm. After 2 h, the test tubes were placed into a water bath of 40 °C prior to extrusion.

To obtain 100 nm LUVs, a *LipoFast-Basic* extruder from *Avestin* (Ottawa, Canada) was used. Prior to use, the extruder was washed thoroughly with ethanol, ultrapure water and HEPES buffer. Then, the extruder was assembled using a polycarbonate membrane with a pore diameter of 100 nm from *Avestin* and *Whatman* polyester drain discs

by *GE Healthcare* (Little Chalfont, UK) placed onto the internal membrane support capsule. The syringe was filled initially with buffer to check if the extruder assembly was successful. The incubated lipid suspensions were vortexed for 5 s, sonicated for 10 s and subsequently vortexed again for another 5 s before starting extruding. The homogenous suspension of MLVs was drawn up into the syringe and were extruded through the 100 nm polycarbonate membrane. The liposomes sizes were determined via DLS.

8.6.3 FRET Quenching Assay

FRET quenching assays were applied to monitor membrane fusion of labeled liposomes containing model peptides. All measurements were performed using the *JASCO* fluorospectrometer (Model J-1500) with an ETC-272T temperature-measuring unit. The measurements were performed in a quartz glass cuvette with a path length of 10 mm and a magnetic stirrer. The measuring chamber was prepared by flusing nitrogen, stirring speed of 600 rpm and the temperature was set to 25 °C. The FRET quenching assay was applied with the FRET pair of Oregon Green and Texas Red as fluorophores. Therefore, the excitation wavelength was set to 495 nm and emission wavelength was 615 nm for monitoring the fusion measurements. Further settings for the measurements are illustrated in Table 8.10.

Table 8.10: Specific parameter settings for the quenching assay.

Parameter	spectrum measurement	time course measurement
excitation wavelength	550-650 nm	615 nm
response	fast	1 s
data pitch	1 nm	1 s
sensitivity	medium	medium
bandwidth	5 nm (em.)/5 nm (ex.)	5 nm (em.)/5 nm (ex.)
scanning speed	125 nm/min	-
measurement time	-	1200 s

All measurements were performed according to the following procedure. First, a fluorescence spectrum of the labeled liposomes were recorded. Therefore, LUV samples of either donor or acceptor containing liposomes were compared with corresponding MLVs samples to verify the lipid loss caused during extrusion (detailed description 9.6.8). After determining final concentration, 1300 µL HEPES buffer was added into

the cuvette. Then, 40 µL of donor labeled liposome were added to cuvette. After that, the time course measurement was launched and 40 µL of acceptor labeled liposome was added after 60 s. The actual loss of lipids were calculated and adjusted by correcting the sample volume. The total lipid concentration was valued to be between 90 and 160 µM, leading to a 1:1 ratio. Before and after each measurement, liposome sizes were determined via DLS. The measurement data was calculated according following equation 8.4.

$$F = \frac{F_T}{F_0} \tag{8.4}$$

Here, F as fusion efficiency, F_T as the recorded fluorescence F at the time t and F_0 as time after addition of the second labeled liposome. The calculated data F is plotted as the function of the time t.

8.6.4 FRET Dequenching Assay

In addition to the FRET quenching assay, the FRET dequenching assay was applied for various experiments to detect membrane fusion. Therefore, the setting for these measurements were similar as previously described. In comparison to FRET quenching assay, the application procedures differs only in the location of the both fluorophores. The fusion measurements were performed using *JASCO* fluorospectrometer (Model J-1500) with an ETC-272T temperature-measuring unit. The measurements were performed in a quartz glass cuvette with a path length of 10 mm and a magnetic stirrer. The measuring chamber was continuously flushed with nitrogen, stirring speed of 600 rpm and the temperature was set to 25 °C. For these measurements different set of FRET pair were used. Depending of used fluorophores the exciation and emission wavelenght may differ. Settings and necessary parameters for the measurements are illustrated in Table 8.11.

All measurements were performed according to the following procedure. The amount of lipids before and after extrusion was determined using the phosphate assay (Section 8.6.7). The HEPES buffer of 1300 µL was added into the cuvette. The time course measurement (TCM) was launched and 40 µL unlabeled liposome was also already added into the cuvette. After 60 s, 10 µL labeled liposome solution was added

Table 8.11: Specific parameter settings for the dequenching assay.

Parameter	TCM NBD + Rh	TCM OG + TR
ex. wavelength	460 nm	495 nm
em. wavelength	530 nm	615 nm
response	1 s	1 s
data pitch	1 s	1 s
sensitivity	fast	medium
bandwidth	5 nm (em.)/5 nm (ex.)	5 nm (em.)/5 nm (ex.)
measurement time	1200s	1200 s

to the cuvette to initiate the membrane fusion process. The lipid loss during extrusion was adapted according to the calculation obtained from the phosphate assay. At the end, to normalize the fusion measurement the highest possible fluorescence intensity has to be determined. Therefore, 30 µL of a TritonX-100 (TX-100) solution (2.5 % in buffer *v/v*) was added. Before and after each measurement, liposome sizes were determined via DLS. The measurement data was calculated according following equation 8.5.

$$F = \frac{F_{\mathrm{T}} - F_0}{F_{\mathrm{Total}} - F_0} \tag{8.5}$$

Here, F_T as recorded fluorescence F at the time t, F_{Total} as the total fluorescence value after adding of TX-100. F_0 was calculated by averaging of the last 10 data points before the addition. F_{Total} was calculated by averaging the 50 data points after adding TX-100. The calculated data F is plotted as the function of the time t.

8.6.5 Uncaging of PNA/Peptide Hybrids

FRET dequenching assays with caged PNA/peptide hybrids were performed according to standard procedures described in Section 8.6.4. For uncaging of the photolabile protecting group some adjustments had to be made. The fusion measurements were prepared by mixing both liposome species into the cuvette. Then, the time course measurement was launched and the fluorescence measurement was recorded for 60 s. After that, the cuvette was irradiated with a laser from above. Therefore, a customized spectrometer lid was constructed in order to irradiate the sample with a 365 nm laser from above. The 365 nm UV-laser was distributed from *Thorlabs Inc.* (New Jersey, United States). The sample was irradiated for 15 min and the measurement was

continued after irradiation.

8.6.6 Dynamic Light Scattering

Size distrubtion of prepared liposomes and fused liposomes were determined using DLS Zetasizer Nano S by *Malvern Panalytical* (Kassel, Germany). The DLS instrument was equipped with a 633 nm laser with a backscattering angle of 173°. Each sample was measured at room temperature using disposable semi-micro cuvette from *Brand GmbH* (Wertheim, Germany). Each measurements were performed according to following procedure. 950 µL buffer and 50 µL of the sample was added into the semi-micro cuvette. The measurements were recorded and averaged according to three measurements. Before every measurement buffer solution was filtered through RC Chromafil. The required information about size and quality was obtained using Zeta sizer software.

8.6.7 Phosphate Test

The determination of lipid loss during extrusion was determined using the standard phosphate test. This test allows to determine the right amount of lipids before and after extrusion. Therefore, 10 µL of liposome suspension was diluted to a defined volume of 200 µL using ultrapure water. Additionally, 200 µL of perchloric acid (70 % aqueous solution) was added and the sample was digested at 200 °C for 60 minutes. The calibration curve was needed to determine the amount of lipids. In order to do that, samples of ultrapure water and aqueous solution of sodium dihydrogenphosphate monohydrate (c = 0.089 g/L) were prepared according to Table 8.12.

The total amount of phosphorus was set from 0 µg to 2 µg and was filled up with ultrapure water to a total volume of 100µL. Each sample was prepared as duplicates. Next, 700 µL of reagents A (0.45 % ammonium molybdate and 12.6 % perchloric acid) and reagent B (1.7 % *(w/v)* sodium ascorbate) were added to each sample and mixed thoroughly. After that, the samples were heated at 80 °C in a water bath for 7 min. The samples had to cool down to room temperature, before transferring 300 µL of the samples to a disposable macro-cuvette from *Brand GmbH* (Wertheim, Germany) and the absorption of phosphomolybdate complexes was determined at 820 nm using the UV-Vis spectrometer by *JASCO* (Model V-650). As result of these measurements, the absorption was plotted against the mass of phosphorus. Based on the calibration curve, the mass of phosphorus determination of each sample could be established.

Table 8.12: sample preparation of different mixtures of ultrapure water and phosphate for calibration curves.

V (H_2O)	V ($NaH_2PO_4 \cdot H_2O$)	m(P)
100.0	0.00	0.00
62.5	37.5	0.75
50.0	50.0	1.00
37.5	62.5	1.25
25.0	75.0	1.50
0.00	100.0	2.00

8.6.8 Fluorescence Spectra Measurement

Beside the standard procedure using the phosphate test to determine the amount of lost lipids, an alternative more time-efficient procedure was established by detecting the fluorescence of used donor or acceptor fluorophore. Therefore, 2 µL of liposome suspension before extrusion and 2 µL of liposome suspension after extrusion was collected. To estimate the amount of lost lipids, the fluorescence spectra of both samples were recorded. Therefore, 1300 µL HEPES buffer and 10 µL sample was added to the cuvette. Then the fluorescence measurement in the range of 575-610 nm was recorded. The change in intensity could be used to estimate the percentage loss of lipids after extrusion.

8.6.9 Atto488 Labeling

Peptides were synthesized by means of solid-phase peptide synthesis. For further modification, such as labeling, the final deprotection step was not performed. Before starting the labeling, the on-resin peptide was swollen for 2 h. Subsequently, the final Fmoc-deprotection was performed by adding 20 % piperdine in DMF into the syringe. This procedure was repeated once (5 min). *N*-terminal Attotec-labeling was achieved by dissolving the Atto643-NHS ester (0.81 eq.) in 400 µL dry DMSO. After that, the mixture of NHS-ester and DIPEA (4.00 eq.) was transferred to the resin. For efficient labeling was performed via CEM microwave unit (10 W, 37 °C) for 2 h followed by shaking at 37 °C overnight. Afterwards, the resin was thoroughly washed (5 x DMF, 5 x MeOH, 5 x DCM and 5 x Et_2O) and was dried under reduced pressure. The peptide was cleaved by adding solution of TFA/H_2O/EDT/TIS/ (94:2.5:2.5,1.0 *v/v/v/v*) into the syringe. The cleavage cocktail was left for 2 h on the shaker at room temperature.

After removing the solvent under nitrogen stream, the precipitation was obtained by washing with cold Et_2O. The obtained crude peptide was stored at -20 °C

8.7 Detailed Synthesis Procedure

Toluene-4-sulfonic acid-2-(2-nitrophenyl)propylester (1)

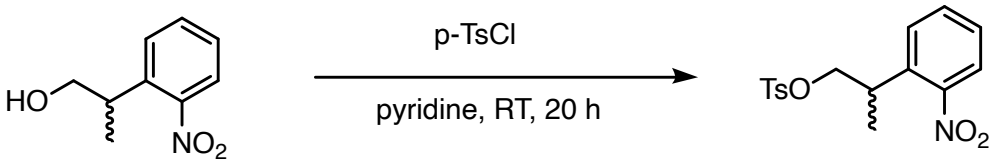

$C_9H_{11}NO_3$
181.19 g/mol

$C_{16}H_{17}NO_5S$
335.37 g/mol

2-(2-Nitrophenyl)propan-1-ol (2.0 g, 11.0 mmol, 1.0 eq.) was dissolved in pyridine (4 ml). *p*-TsCl (2.3 g, 12 mmol, 1.1 eq.) was added to the solution. The reaction mixture was stirred at room temperature over night. The suspension was diluted with DCM and washed with 1 M HCl and brine. Subsequently, combined organic phases were dried over $MgSO_4$, followed by evaporation of the organic solvent. The crude product was filtrated through silica gel with DCM. The solvent was evaporated giving the product **1** (2.87 g, 8.55 mmol, 78 %).

TLC (dichloromethane): $R_f = 0.74$.
^{1}**H-NMR** (300 MHz, $CDCl_3$): δ (ppm) = 1.33 (d, J = 7.0 Hz, 3H, CH_3), 2.42 (s, 3H, CH_3), 3.64 (m, 1H, CH), 4.18 (m, 2H, CH_2), 7.27-7.40 (m, 4H, CH_{ar}), 7.49-7.55 (m, 1H, CH_{ar}), 7.66-7.68 (m, 2H, CH_{ar}), 7.73-7.76 (m, 1H, CH_{ar})
^{13}**C-NMR** (126 MHz, $CDCl_3$): δ (ppm) = 17.8, 21.9 33.9, 73.6, 128.1, 128.1, 128.9, 130.2, 133.0, 133.2, 136.3, 145.2, 150.2
MS (ESI): m/z = 358.1 $[M+Na]^+$, 381.3 $[M+2Na]^+$, 693.2 $[2M+Na]^+$
HR-MS (ESI): calc. for $C_{16}H_{17}NO_5S$ $[M+Na]^+$: 358.0720, found: 358.0723
calc. for $C_{16}H_{17}NO_5S$ $[M+NH_4]^+$ 353.1166, found: 353.1165

1-Azido-2-(2-nitrophenyl)propane (2)

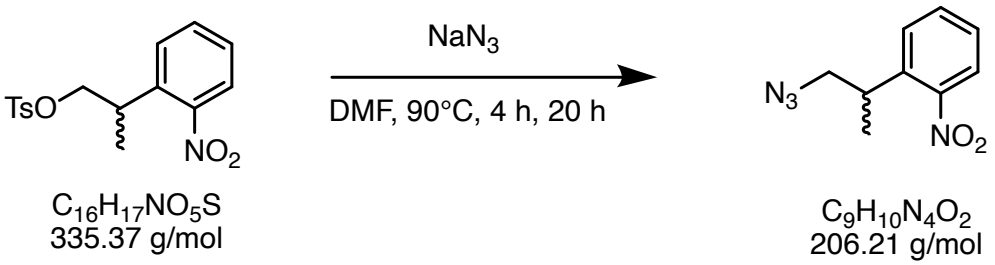

$C_{16}H_{17}NO_5S$
335.37 g/mol

$C_9H_{10}N_4O_2$
206.21 g/mol

Sodium azide (2.22 g, 34.2 mmol, 4.00 eq.) was dissolved in DMF (10 mL). After the addition of **1** (2.87 g, 8.55 mmol, 1.00 eq.), the reaction mixture was heated to 90 °C for 4 h and stirred over night at room temperature. The reaction mixture was quenched with water and the organic phase was extracted with Et_2O (3x20 mL). After drying over $MgSO_4$, the solvent was removed under reduced pressure, resulting in the crude product **2**. Purification using flash chromatography gave product **2** (1.42 g, 6.88 mmol, 80 %) as oil.

TLC (n-hexane/DCM 2:1): $R_f = 0.48$
^{1}**H-NMR** (300 MHz, $CDCl_3$): δ (ppm) = 1.37 (d, J = 6.7 Hz, 3H, CH_3), 3.41-3.63 (m, 3H, CH, CH_2), 7.35-7.62 (m, 3H, CH_{ar}), 7.78 (dd, J = 6.7 Hz, J = 1.3 Hz, 1H, CH_{ar})
^{13}**C-NMR** (126 MHz, $CDCl_3$): δ (ppm) = 18.6, 34.1, 57.2 124.4, 127.7, 128.3, 132.9, 137.4, 150.2

2-(2-Nitrophenyl)propylamine (3)

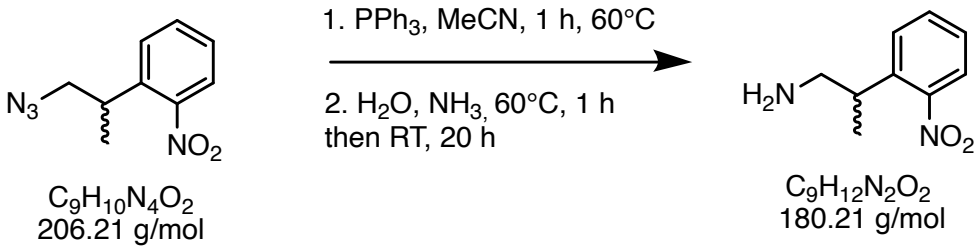

PPh_3 (3.61 g, 13.8 mmol, 2.00 eq.) was dissolved in MeCN (8 mL). Product **2** (1.42 g, 6.88 mmol, 1.00 eq.) dissolved in MeCN (4 mL) was added to the reaction mixture and the solution was heated to 60 °C for 1 h. At room temperature, water (8 mL) and conc. NH_3 (12 mL) were added and the reaction mixture was heated to 60 °C for 45min cooled down to room temperature over night. The solution was extracted with EtOAc (3x20 mL), followed by evaporation of the organic solvent. The residue was dissolved in Et_2O (20 mL) and treated with 1 M aqueous HCl. The aqueous phase was extracted and neutralized with 1 M NaOH. The organic phase was extracted with EtOAc (3x20 mL) and dried over $MgSO_4$. The solvent was evaporated to afford product **3** (1.03 g, 5.72 mmol, 83 %) as orange oil.

^{1}**H-NMR** (300 MHz, MeOH-d_4): δ (ppm) = 1.30 (d, J = 6.9 Hz, 3H, CH_3), 2.87 (m, 2H, CH_2), 3.23 (m, 1H, CH), 4.72 (s, 2H, NH_2), 7.36-7.43 (m, 1H, CH_{ar}), 7.52-7.69 (m, 2H, CH_{ar}), 7.72 (dd, J = 8.1 Hz, J = 1.2 Hz, 1H, CH_{ar})
^{13}**C-NMR** (126 MHz, MeOH-d_4): δ (ppm) = 19.7, 38.4, 49.1, 124.9, 128.4, 129.2, 133.9, 140.0, 152.3
MS (ESI): m/z = 164.1 $[M\text{-}NH_2]^+$, 181.1 $[M]^+$
HR-MS (ESI): calc. for $C_9H_{13}N_2O_2$ $[M]^+$: 181.09718, found: 181.09718,
calc. for $C_9H_{12}N_2O_2$ $[M+Na]^+$: 203.0791, found: 203.0787

tert-Butyl-2-(6-chloro-9H-purin-9-yl)acetate (4)

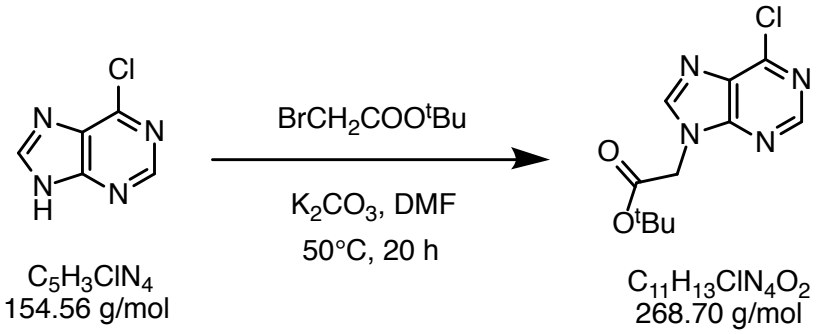

6-Chloropurine (1.20 g, 7.76 mmol, 1.08 eq.) and anhydrous K_2CO_3 (1.08 g, 7.76 mmol, 1.08 eq.) were dissolved in DMF (24 mL). *tert*-Butyl bromoacetate (1.40 g, 7.18 mmol, 1.00 eq.) was added to the solution and heated to 50 °C for 20 h. The solid was removed by filtration and the solvent was evaporated. Then, the remaining residue was treated with 0.5 N HCl (20 mL) and stirred for an additional 20 min. At last, the solid was filtered off and the residue was washed thoroughly with H_2O. Product **4** (1.52 g, 5.6 mmol, 72 %) was afforded as yellow solid.

^{1}**H-NMR** (300 MHz, DMSO-d_6): δ (ppm) = 1.41 (s, 9H, $C(CH_3)_3$), 5.14 (s, 2H, CH_2), 8.66 (s, 1H, CH_{ar}), 8.78 (s, 1H, CH_{ar})
^{13}**C-NMR** (126 MHz, DMSO-d_6): δ (ppm) = 27.5, 45.2, 82.5, 130.4, 147.8, 149.0, 151.7, 152.0, 166.1
MS (ESI): m/z = 268.1 $[M]^+$, 134.5 $[M]^{2+}$
HR-MS (ESI): calc. for $C_{11}H_{13}ClN_2O_2$ $[M]^+$: 269.0800, found: 269.0797

tert-Butyl-2(6-((2-(2-nitrophenyl)propyl)amino)-9H-purin-9-yl) acetate (5)

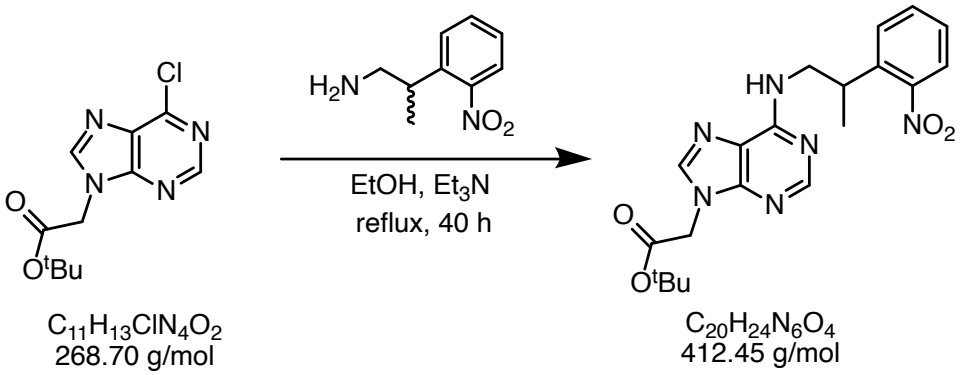

$C_{11}H_{13}ClN_4O_2$
268.70 g/mol

$C_{20}H_{24}N_6O_4$
412.45 g/mol

Product **4** (660 mg, 2.61 mmol, 1.00 eq.) was suspended in EtOH (7.30 ml). Product**3** (0.94 g, 5.22 mmol, 2.06 eq.) and Et_3N (0.70 ml) were added to the solution and heated to 75 °C for 40 h. The reaction mixture was evaporated under reduced pressure. Purification using flash chromatography (pentane/acetone 2:1) gave product **5** (0.73 g, 1.77 mmol, 72 %) as white solid.

^{1}**H-NMR** (300 MHz, DMSO-d_6): δ (ppm) = 1.30 (d, J = 6.0 Hz, 3H, CH_3) 1.41 (s, 9H, $C(CH_3)_3$), 3.65-3.75 (m, 3H, CH, CH_2), 4.92 (s, 2H, CH_2-COOtBu), 7.40-8.06 (m, 6H, CH_{ar}), 8.16 (s, 1 H, NH)
^{13}**C-NMR** (126 MHz, DMSO-d_6): δ (ppm) = 27.5, 45.2, 82.5, 130.4, 147.8, 149.0, 151.7, 152.0, 166.1

2-(6-((2-(2-Nitrophenyl)propyl)amino)-9H-purin-9-yl)acetic acid (6)

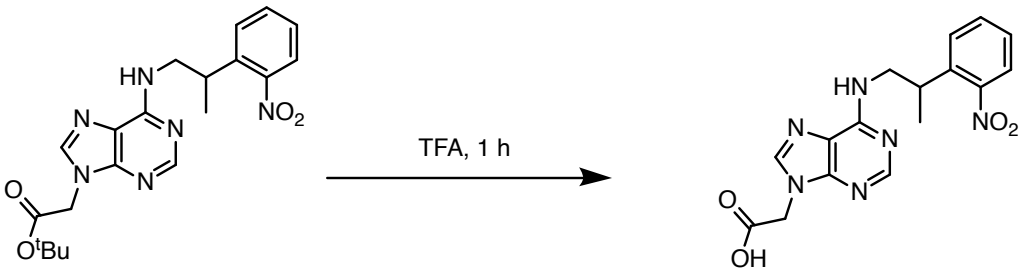

$C_{20}H_{24}N_6O_4$
412.45 g/mol

$C_{16}H_{16}N_6O_4$
356.34 g/mol

Product **5** (600 mg, 1.45 mmol, 1.00 eq.) was suspended in TFA (6 ml) and stirred at room temperature for 1 h. The solvent reduced under nitrogen stream. Then, the remaining residue was poured into with Et_2O at 0 °C. The white precipitate was thoroughly washed with cold Et_2O and dried *in vacuo*. Product **6** (0.41 g, 1.16 mmol, 90 %) was obtained as white solid.

^{1}**H-NMR** (300 MHz, DMSO-d_6): δ (ppm) = 1.32 (d, J = 6.9 Hz, 3H, CH_3), 3.63-3.78 (m, 3H, CH, CH_2), 5.01 (s, 2H, CH_2-COOH), 7.41-8.31 (m, 6H, CH_{ar}), 8.48 (s, 1H, NH), 13.00 (s, 1H, COOH)
^{13}**C-NMR** (126 MHz, DMSO-d_6): δ (ppm) = 19.4, 33.1, 44.3, 64.8, 118.2, 123.6, 127.5, 128.4, 132.8, 137.8, 142.1, 148.2, 150.2, 158.7, 168.9
MS (ESI): m/z = 279.1 $[M]^+$, 381.3 $[M+Na]^+$
HR-MS (ESI): calc. for $C_{16}H_{16}N_6O_4$ $[M]^+$: 357.1306, found: 357.1310
calc. for $C_{16}H_{16}N_6O_4Na$ $[M+Na]^+$: 379.1125, found: 379.1138

Fmoc-a^{NPP}-aeg-O^{t}Bu (7)

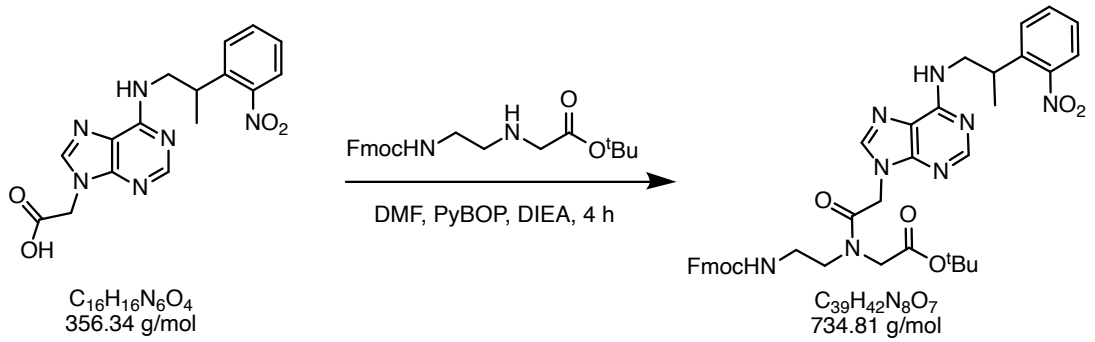

$C_{16}H_{16}N_6O_4$
356.34 g/mol

$C_{39}H_{42}N_8O_7$
734.81 g/mol

Product **6** (0.31 g, 0.86 mmol, 1.25 eq.) was suspended in DMF (3 ml) under cooling. PyBOP (0.44 g, 0.86 mmol, 1.25 eq.) and Fmoc-aeg-O^{t}Bu (0.31 g, 0.69 mmol, 1.00 eq.) were added to the reaction mixture, followed by stirring at 0 °C for additional 10 min. The reaction mixture was cooled to room temperature and stirred for 4 h. The solvent was removed under reduced pressure and the remaining residue was dissolved in EtOAc (20 mL). The organic layer was extracted with 10% NH_4Cl-solution (3x20 mL), 6% $NaHCO_3$-solution (3x20 mL) and brine (3x20 mL). The solvent was dried over Na_2SO_4, followed by solvent evaporation. Product **7** (0.27 g, 0.36 mmol, 42 %) was obtained as yellow solid.

^{1}**H-NMR** (300 MHz, DMSO-d_6): δ (ppm) = 1.29 (d, J= 6.0 Hz, 3H, CH_3) 1.40 (s, 9H, $C(CH_3)_3$), 3.45-3.44 (m, 1H, CH), 3.54-3.54 (m, 2H, CH_2), 3.78-3.65 (m, 4H, 2x CH_2), 3.94 (m, 2H, CH_2), 4.40-4.20 (m, 5H, CH_2, OCH_2, CH), 5.18 (s, 1H, NH), 7.88-7.30 (m, 14H, CH_{ar}), 8.13 (s, 1H, NH)
^{13}**C-NMR** (126 MHz, DMSO-d_6): δ (ppm) = 168.4, 167.9, 166.8, 156.3, 152.1, 150.3, 143.8, 141.4, 140.6, 138.2, 132.6, 128.4, 127.5, 127.2, 126.9, 125.0, 123.4, 120.0, 82.0, 80.9, 65.4, 50.0, 48.7, 47.0, 46.7, 43.6, 43.3, 37.9, 33.3, 27.6, 19.5
HR-MS (ESI): calc. for $C_{39}H_{42}N_8O_7$ $[M+Na]^+$: 757.3069, found: 757.3065

Fmoc-a^{NPP}-aeg-OH (8)

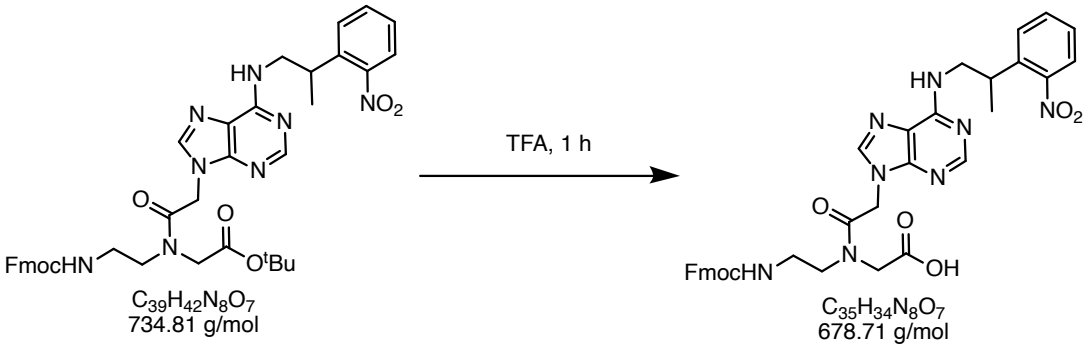

Product **7** (0.27 g, 0.36 mmol, 1.00 eq.) was suspended in TFA (3 ml) and stirred at room temperature for 1 h. The solvent was evaporated under reduced pressure and the remaining residue was treated with cold Et_2O. The resulting precipitate was washed with cold Et_2O and dried *in vacuo*. Product **8** (0.14 g, 0.21 mmol, 52 %) was obtained as white solid.

^{1}**H-NMR** (300 MHz, DMSO-d_6): δ (ppm) = 1.32 (d, J= 6.0 Hz, 3H, CH_3), 3.34-3.39 (m, 3H, CH, CH_2), 3.53-3.68 (m, 4H, 2 x CH_2), 4.01 (s, 2H, CH_2), 4.19-4.37 (m, 5H, CH_2, OCH_2, CH), 5.27 (s, 1H, NH), 7.29-8.30 (m, 14H, CH_{ar}), 8.66 (s, 1H, NH), 12.50 (s, 1H, NH)
HR-MS (ESI): calc. for $C_{35}H_{34}N_8O_7$ $[M+H]^+$: 679.2478, found: 679.2480

tert-Butyl-uracil-1-yl-actetate (9)

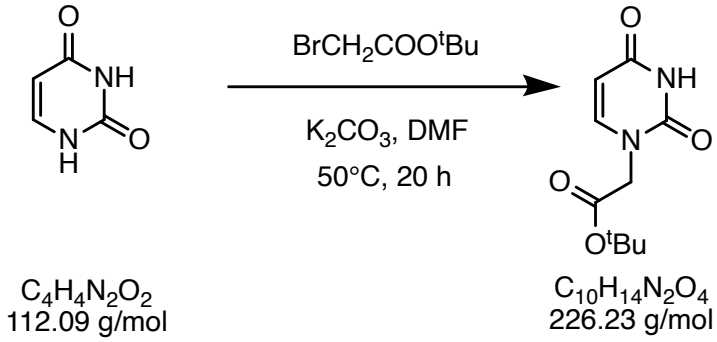

Uracil (2.20 g, 19.8 mmol, 1.10 eq.) and K_2CO_3 (2.74 g, 19.8 mmol, 1.10 eq.) were dissolved in DMF (60 ml). *tert*-Butyl bromoacetate (3.51 g, 18.0 mmol, 1.00 eq.) was added to the reaction mixture was stirred at room temperature for 20 h. After filtration, the organic phase was evaporated under reduced pressure. The remaining residue was treated with 0.5 N HCl (50 ml) and stirred for 20 min. The solid was filtered and the residue was washed with H_2O. Product **9** (2.74 g, 12.1 mmol, 62 %) was afforded as a white solid.

^{1}**H-NMR** (300 MHz, $CDCl_3$): δ (ppm) = 1.49 (s, 9H, $C(CH_3)_3$), 4.37 (s, 2H, CH_2), 5.74 (d, J= 7.9 Hz, 1H, CHCH), 7.11 (d, J= 7.9 Hz, 1H, CHCH), 9.62 (s, 1H, NH)
^{13}**C-NMR** (126 MHz, $CDCl_3$): δ (ppm) = 27.7, 49.8, 83.8, 102.5, 144.6, 150.7, 163.9, 166.5
HR-MS (ESI): calc. for $C_{10}H_{14}N_2O_4$ $[M+Na]^+$: 227.1026, found: 227.1025
calc. for $C_{10}H_{14}N_2O_4$ $[M+Na]^+$: 249.0846, found: 249.0841

***tert*-Butyl-2-(4-((2-(2-nitrophenyl)propyl)amino)-2-oxopyrimidin-1-(2H)-yl-acetate (10)**

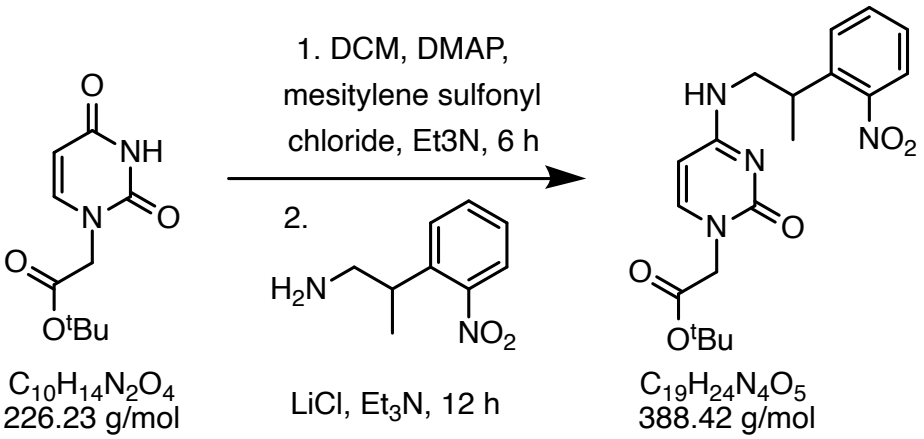

DMAP (380 mg, 3.10 mmol, 1.00 eq.), mesitylene-2-sulfonyl chloride (1.74 g, 7.96 mmol, 2.57 eq.), and Et_3N (3.07 ml) were added to a solution of product **9** (1.00 g, 4.42 mmol, 1.43 eq.) in DCM (50 ml). Then, the reaction mixture was stirred at room temperature for 6 h. The solvent was evaporated under reduced pressure, followed by resolving in DCM (20 mL) and adding of product **3** (1.59 g, 8.84 mmol, 2.63 eq.). Afterwards, LiCl (1.05 g, 24.8 mmol, 7.92 eq.) and Et_3N (5.24 mL) was added dropwise and the solution was stirred at room temperature for 20 h. The organic solvent was evaporated under reduced pressure. Product **10** (1.13 g, 2.92 mmol, 62 %) was obtained as a white solid.

^{1}**H-NMR** (300 MHz, DMSO-d_6): δ (ppm) =1.27 (d, J= 6.5 Hz, 3H, CH_3), 1.40 (s, 9H, $C(CH_3)_3$), 3.29 (s, 1H, NH), 3.36-3.52 (m, 2H, CH_2),3.55-3.67 (m, 1H, CH), 4.30 (s, 2H, CH_2), 5.62 (d, J= 7.5 Hz, 1H, CH), 7.42-7.70 (m, 4H, CH_{ar}), 7.79 (d, J= 7.5 Hz, 1H, CH)
HR-MS (ESI): calc. for $C_{15}H_{16}N_4O_5$ $[M+Na]^+$: 389.1819, found: 389.1815
HR-MS (ESI): calc. for $C_{15}H_{16}N_4O_5$ $[M+Na]^+$: 411.1639, found: 411.1629

2-(4-((2-(2-Nitrophenyl)propyl)amino)-2-oxopyrimidin-1(2H)-yl)-acetic acid (11)

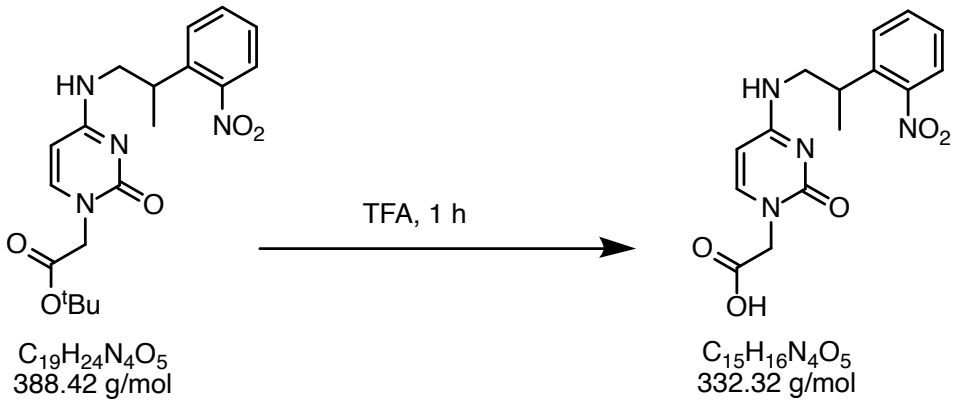

$C_{19}H_{24}N_4O_5$
388.42 g/mol

$C_{15}H_{16}N_4O_5$
332.32 g/mol

Product **10** (330 mg, 0.85 mmol, 1.00 eq.) was suspended in TFA (3 ml) and stirred at room temperature for 1 h. The solvent was removed under reduced pressure and the precipitate was treated with cold Et_2O. The solid was washed again with cold Et_2O and dried *in vacuo*. Product **11** (0.33 g, 0.99 mmol, 77 %) was obtained as a white solid.

^{1}**H-NMR** (300 MHz,DMSO-d_6): δ (ppm) = 1.30 (d, J = 6.7 Hz, 3H, CH_3), 3.34-3.52 (m, 1H, CH), 3.54-3.84 (m, 2H, CH_2), 4.49 (s, 2H, CH_2), 4.5 (s, 1H, NH), 5.93 (d, J= 7.6 Hz, 1H, CHCH), 7.46-7.86 (m, 5H, CH_{ar}, CHCH) 12.4 (s, 1H, COOH)
^{13}**C-NMR** (126 MHz, DMSO-d_6): δ (ppm) = 19.3, 32.9, 46.6, 49.8, 94.0, 123.5, 127.6, 127.9, 132.9, 137.2, 137.2, 146.9, 149.7, 150.5, 159.6, 168.9
HR-MS (ESI): calc. for $C_{15}H_{16}N_4O_5$ $[M+Na]^+$: 355.1013, found 355.1015.

Fmoc-c^{NPP}-aeg-OtBu (12)

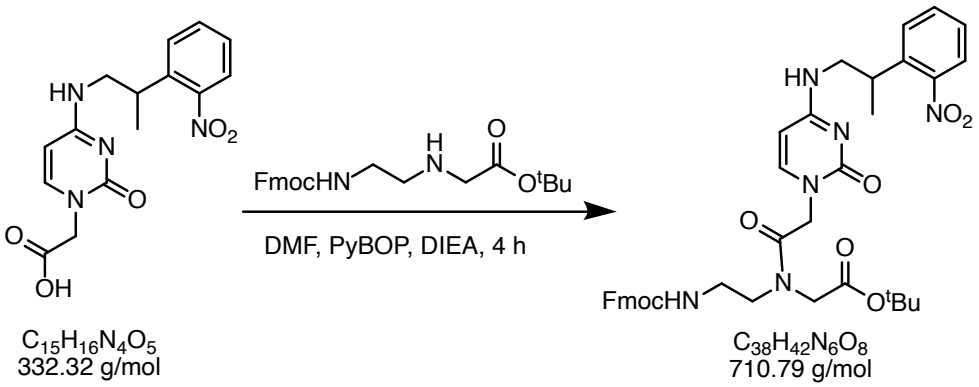

$C_{15}H_{16}N_4O_5$
332.32 g/mol

$C_{38}H_{42}N_6O_8$
710.79 g/mol

Product **11** (0.33 g, 0.99 mmol, 1.00 eq.) was suspended in DMF (3 ml) and cooled down to 0 °C. PyBOP (0.44 g, 0.86 mmol) and Fmoc-aeg-O^{t}Bu HCl (0.30 g, 0.70 mmol) were mixed and stirred at 0 °C for 10 min. DIPEA (0.52 mL) was added at 0 °C, followed by stirring at room temperature for 4 h. The solvent was evaporated under reduced pressure. The remaining residue was suspended in EtOAc. The organic phase was extracted with 10 % NH_4Cl solution, 6 % $NaHCO_3$ solution and brine. The organic phase was dried over Na_2SO_4 and the solvent was evaporated under reduced pressure. Product **12** (0.29 g, 0.41 mmol, 41 %) was afforded as yellow solid.

^{1}**H-NMR** (300 MHz, DMSO-d_6): δ (ppm) = 1.27 (d, J= 6.5 Hz, 3H, CH_3), 1.40 (s, 9H, $C(CH_3)_3$) 2.98-3.66 (m, 7H, CH, CH_2, CH_2CH_2) 3.93 (s, 2H, CH_2), 4.19-4.68 (m, 5H, CH_2, OCH_2, CH), 5.62 (d, J= 7.2 Hz, 1H, CHCH), 5.74 (s, 1H, NH), 7.25-7.87 (m, 14 H, CH_{ar}, NH, CHCH)
HR-MS (ESI): calc. for $C_{15}H_{16}N_4O_5$ $[M+H]^+$: calc. 711.3137, found 711.3146.

Fmoc-c^{NPP}-aeg-OH (13)

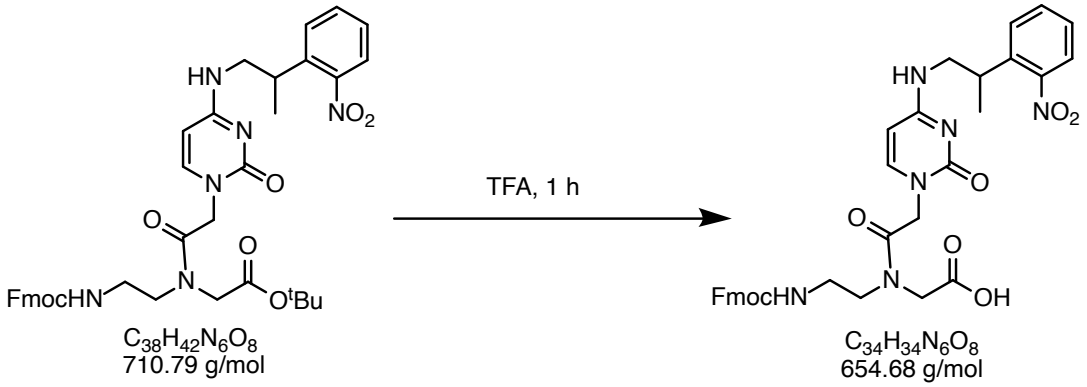

Product **12** (0.29 g, 0.41 mmol, 1.00 eq.) was suspended in TFA (3 ml) and stirred at room temperature for 1 h. The solvent was evaporated under reduced pressure and the precipitate was treated with cold Et_2O. The solid was washed with cold Et_2O and dried *in vacuo*. Product **13** (0.16 g, 0.24 mmol, 57 %) was afforded as white solid.

^{1}**H-NMR** (300 MHz, DMSO-d_6): δ (ppm) = 1.30 (d, J= 6.6 Hz, 3H, CH_3) 3.10-3.49 (m, 4H, CH_2), 3.57-3.81 (m, 3H, CH_2, CH), 4.00 (s, 2 H, CH_2), 4.23-4.35 (m, 4H, CH, OCH_2, NH), 4.62-4.83 (m, 2H, CH_2), 5.92 (d, J = 7.6 Hz, 1H, CHCH) 7.27-7.96 (m, 14H, CH_{ar}, NH, CHCH), 12.30 (s, 1H, COOH)
HR-MS (ESI): calc. for $C_{15}H_{16}N_4O_5$ $[M+H]^+$: calc. 655.2511, found 655.2510

7-(diethylamino)-4-ethanalcoumarin

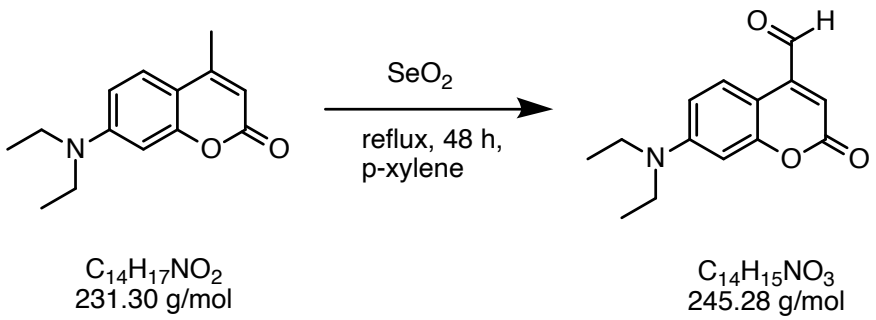

A solution of 7-dimethylamino-4-methylcoumarin (2.50 g, 10.81 mmol, 1.00 eq..) and selenium dioxide (1.39 g, 12.53 mmol, 1.16 eq.) in *p*-xylene (250 mL) was heated to 140 °C for 48 h. Then, the solution was cooled to room temperature, filtered, and the solvent was evaporated under reduced pressure.

7-diethylamino-4-(hydroxymethyl)coumarin

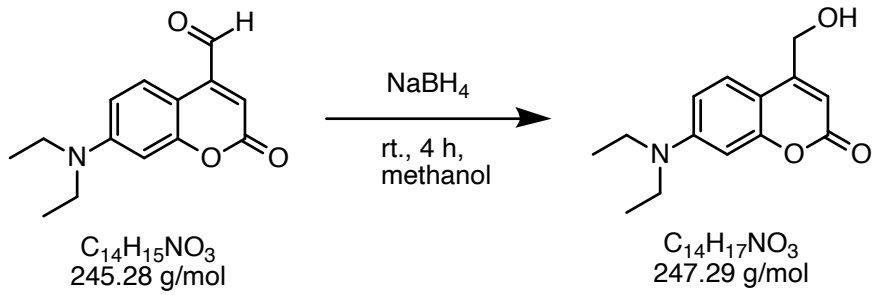

MeOH (2.5 mL) and sodium borohydride (0.40 mg, 10.8 mmol, 1.00 eq.) were added to 7-(diethylamino)-4-ethanalcoumarin and stirred at room temperature for 4 h. After that, the reaction mixture was neutralized with 1 N HCl and the solvent was removed under reduced pressure. The solution was extracted with DCM, followed by drying over Na_2SO4. After purification by flash chromatography (n-hexane/EtOAc 1:1), product **14** was obtained (0.82 g, 3.31 mmol, 38 %) as orange solid.

^{1}**H-NMR** (300 MHz,DMSO-d_6): δ (ppm) = 1.11 (t, J= 7.0 Hz, 6 H, 2 x CH_3), 3.41 (q, J= 7.0 Hz, 4 H, 2 x CH2), 4.66 (dd, J = 5.50 Hz, J= 1.40 Hz, 2 H, CH_2-OH), 5.50 (t, J= 5.60 Hz, 1 H, OH), 6.06 (d, J= 2.50 Hz, 1 H, CHArom), 6.51 (d, J= 2.50 Hz, 1 H, CH_{ar}), 6.65 (dd, J = 9.0 Hz, J= 2.50 Hz, 1 H, CH_{ar}), 7.42 (d, J= 9.0 Hz, 1 H, CH_{ar})

MS (ESI): m/z = 248.1 [M+H]$^+$, 270.1 [M+Na]$^+$

HR-MS (ESI): calc. for $C_{14}H_{18}NO_3$ [M+H]$^+$: 248.1281, found: 248.1279;
calc. for $C_{14}H_17NO_3Na$ [M+Na]$^+$: 270.1101, found: 270.1103.

8.8 Peptide Synthesis

The synthesis was performed via automated SPPS according to SOP1. For SxTMD, Wang-resin preloaded with Fmoc-Gly-OH was used. For SybTMD, Wang-resin preloaded with Fmoc-Thr(tBu)-OH was used. In order to obtain *C*-terminal NH_2 modification, ChemMatrix rink amide resin was used. Resin cleavage was performed according to SOP4.

SxTMD-OH

H-K Y Q S K A R R K K I M I I I C C V I L G I I I A S T I G G I F G -OH
$C_{165}H_{288}N_{44}O_{39}S_3$
3608.57 g/mol

MS (ESI): *m/z* (%) = 722.6 $[M+5H]^{+5}$, 903.0 $[M+4H]^{+4}$, 1203.7 $[M+3H]^{+3}$
HR-MS (ESI): calc. for $C_{165}H_{293}N_{44}O_{39}S_3$ ($[M+5H]^{+5}$): 722.6299, found: 722.6296;
calc. for $C_{165}H_{292}N_{44}O_{39}$ ($[M+4H]^{+4}$): 903.0355, found: 903.0359;
calc. for $C_{111}H_{291}N_{44}O_{39}$ ($[M+3H]^{+3}$): 1203.7116, found: 1203.7111.

Fmoc-SxTMD-NH_2

Fmoc-K Y Q S K A R R K K I M I I I C C V I L G I I I A S T I G G I F G -NH_2
$C_{180}H_{299}N_{45}O_{40}S_3$
3629.83 g/mol

MS (ESI): *m/z* (%) = 958.6 $[M+4H]^{+4}$, 1277.4 $[M+3H]^{+3}$
HR-MS (ESI): calc. for $C_{180}H_{303}N_{45}O_{40}S_3$ ($[M+4H]^{+4}$): 958.3063, found: 958.3059;
calc. for $C_{180}H_{302}N_{45}O_{40}S_3$ ($[M+3H]^{+3}$): 1277.4059, found: 1277.4053.

SybTMD-OH

H-K R K Y W W K N L K M M I I L G V I C A I I L I I I I V Y F S T -OH
$C_{190}H_{308}N_{42}O_{38}S_3$
3884.99 g/mol

MS (ESI): *m/z* (%) = 777.9 $[M+5H]^{+5}$, 972.0 $[M+4H]^{+4}$, 1295.7 $[M+3H]^{+3}$
HR-MS (ESI): calc. for $C_{190}H_{313}N_{42}O_{38}S_3$ ($[M+5H]^{+5}$): 777.8608, found: 777.8601;
calc. for $C_{190}H_{312}N_{42}O_{38}S_3$ ($[M+4H]^{+4}$): 972.0742, found: 972.0742;
calc. for $C_{190}H_{311}N_{42}O_{38}S_3$ ($[M+3H]^{+3}$): 1295.7631, found: 1295.7624.

SybTMD-NH_2

Fmoc- K R K Y W W K N L K M M I I L G V I C A I I L I I I I V Y F S T -NH_2
$C_{205}H_{323}N_{43}O_{39}S_3$
4106.25 g/mol

MS (ESI): *m/z* (%) = 1027.3 $[M+4H]^{+4}$, 1369.8 $[M+3H]^{+3}$
HR-MS (ESI): calc. für $C_{205}H_{327}N_{43}O_{39}S_3$ ($[M+4H]^{+4}$): 1027.3452, found: 1027.3443;
calc. für $C_{205}H_{326}N_{43}O_{39}S_3$ ($[M+3H]^{+3}$): 1369.7919, found: 1369.7907.

8.8.1 PNA/Peptid Hybrids

PNA1s-SybTMD (14)

t c a c t -**SybTMD**
$C_{243}H_{375}N_{67}O_{54}S_3$
5195.27 g/mol

The synthesis was performed via manual SPPS according to SOP3. The resin was preloaded with SybTMD. Resin cleavage was performed according to SOP4.

MS (ESI): *m/z* (%) = 743.1 $[M+7H]^{+7}$, 867.0 $[M+6H]^{+6}$ 1040.0 $[M+5H]^{+5}$
HR-MS (ESI): calc. for $C_{243}H_{382}N_{67}O_{54}S_3$ ($[M+7H]^{+7}$): 743.1204, found: 743.1192;
calc. for $C_{243}H_{381}N_{67}O_{54}S_3$ ($[M+6H]^{+6}$): 867.0212, found: 867.0220;
calc. for $C_{243}H_{380}N_{67}O_{54}S_3$ ($[M+5H]^{+5}$): 1039.9656, found: 1039.9660.

PNA2s-SxTMD (15)

a g t g a -**SxTMD**
$C_{220}H_{354}N_{76}O_{53}S_3$
5007.91 g/mol

The synthesis was performed via manual SPPS according to SOP3. The resin was preloaded with SxTMD. Resin cleavage was performed according to SOP4.

MS: *m/z* (%) = 835.8 $[M+6H]^{+6}$, 1002.5 $[M+5H]^{+5}$, 1252.9$[M+4H]^{+4}$
HR-MS (ESI): calc. for $C_{220}H_{361}N_{76}O_{53}S_3$ ($[M+6H]^{+6}$): 835.4499, found: 835.4520;
calc. for $C_{220}H_{360}N_{76}O_{53}S_3$ ($[M+5H]^{+5}$): 1002.5392, found: 1002.5404
calc. for $C_{220}H_{359}N_{76}O_{53}S_3$ ($[M+4H]^{+4}$): 1252.9222, found: 1252.9231

PNA1-SybTMD (16)

g t a g a t c a c t -**SybTMD**
$C_{298}H_{441}N_{99}O_{68}S_3$
6591.61 g/mol

The synthesis was performed via manual SPPS according to SOP3. The resin was preloaded with SybTMD. Resin cleavage was performed according to SOP4.

MS (ESI): *m/z* (%) = 943.1 $[M+7H]^{+7}$, 1100.1 $[M+6H]^{+6}$ 1319.7 $[M+5H]^{+5}$
HR-MS (ESI): calc. for $C_{298}H_{448}N_{99}O_{68}S_3$ ($[M+7H]^{+7}$): 943.0552, found: 943.0557;
calc. for $C_{298}H_{447}N_{99}O_{68}S_3$ ($[M+6H]^{+6}$): 1100.0632, found: 1100.0645;
calc. for $C_{298}H_{446}N_{99}O_{68}S_3$ ($[M+5H]^{+5}$): 1319.8744, found: 1319.8763.

PNA2-SxTMD (17)

c a t c t a g t g a -**SxTMD**
$C_{273}H_{421}N_{101}O_{69}S_3$
6318.19 g/mol

The synthesis was performed via manual SPPS according to SOP3. The resin was preloaded with SxTMD. Resin cleavage was performed according to SOP4.

MS: *m/z* (%) = 790.7 $[M+8H]^{+8}$, 903.5 $[M+7H]^{+7}$, 1053.9 $[M+6H]^{+6}$, 1264.4 $[M+5H]^{+5}$
HR-MS (ESI): calc. for $C_{273}H_{429}N_{101}O_{69}S_3$ ($[M+8H]^{+8}$): 790.6545, found: 790.6562;
calc. for $C_{273}H_{428}N_{101}O_{69}S_3$ ($[M+7H]^{+7}$): 903.4612, found: 903.4629
calc. for $C_{273}H_{427}N_{101}O_{69}S_3$ ($[M+6H]^{+6}$): 1053.4177, found: 1053.4146
calc. for $C_{273}H_{426}N_{101}O_{69}S_3$ ($[M+5H]^{+5}$): 1264.4197, found: 1264.4165

NPP-PNA1-SyTMD (18)

g t a^{NPP} g a^{NPP} t c a c t -**SybTMD**
$C_{316}H_{459}N_{101}O_{72}S_3$
6916.45 g/mol

The synthesis was performed via manual SPPS according to SOP3. The resin was preloaded with SybTMD. Resin cleavage was performed according to SOP4.

MS: *m/z* (%) = 866.1 $[M+8H]^{+8}$, 989.6 $[M+7H]^{+7}$, 1154.4 $[M+6H]^{+6}$, 1385.1 $[M+5H]^{+5}$
HR-MS (ESI): calc. for $C_{316}H_{467}N_{101}O_{72}S_3$ ($[M+8H]^{+8}$): 866.0651, found: 866.0636;
calc. for $C_{316}H_{466}N_{101}O_{72}S_3$ ($[M+7H]^{+7}$): 989.6406, found: 989.6447
calc. for $C_{316}H_{465}N_{101}O_{72}S_3$ ($[M+6H]^{+6}$): 1154.4177, found: 1154.4146
calc. for $C_{316}H_{464}N_{101}O_{72}S_3$ ($[M+5H]^{+5}$): 1385.0997, found: 1385.0965

NPP-PNA2-SxTMD (19)

c^{NPP} a t c^{NPP} t a g t g a -**SxTMD**

$C_{291}H_{439}N_{103}O_{73}S_3$
6644.35 g/mol

The synthesis was performed via manual SPPS according to SOP3. The resin was preloaded with SxTMD. Resin cleavage was performed according to SOP4.

MS: *m/z* (%) = 948.2 $[M+7H]^{+7}$, 1106.3 $[M+6H]^{+6}$, 1385.1 $[M+5H]^{+5}$

HR-MS (ESI): calc. for $C_{291}H_{446}N_{103}O_{73}S_3$ ($[M+7H]^{+7}$): 951.6406, found: 951.6447
calc. for $C_{291}H_{445}N_{103}O_{73}S_3$ ($[M+6H]^{+6}$): 1109.3177, found: 1109.3186
calc. for $C_{291}H_{444}N_{103}O_{73}S_3$ ($[M+5H]^{+5}$): 1330.8197, found: 1330.8165

8.8.2 Coiled Coil Peptide Synthesis

E3 (20)

E I A A L E K E I A A L E K E I A A L E K-NH_2
$C_{111}H_{181}N_{27}O_{27}$
2453.82 g/mol

The synthesis was performed via manual SPPS according to SOP1. ChemMatrix Rink amide resin was used. Resin cleavage was performed according to SOP4.
MS: *m/z* (%) = 818.8 $[M+3H]^{+3}$, 1227.7 $[M+2H]^{+2}$.
HR-MS (ESI): calc. for $C_{111}H_{184}N_{27}O_{35}$ ($[M+3H]^{+3}$): 818.7820, found: 818.7828;
calc. for $C_{111}H_{185}N_{27}O_{35}$ ($[M+2H]^{+2}$): 1227.6694, found: 1227.6696.

K3 (21)

K I A A L K E K I A A L K E K I A A L K E-NH_2
$C_{115}H_{201}N_{31}O_{27}$
2450.06 g/mol

The synthesis was performed via manual SPPS according to SOP1. ChemMatrix Rink amide resin was used. Resin cleavage was performed according to SOP4.

MS: *m/z* (%) = 490.9 $[M+5H]^{+5}$, 613.4 $[M+4H]^{+4}$, 817.5 $[M+3H]^{+3}$
HR-MS (ESI): calc. for $C_{115}H_{206}N_{31}O_{27}$ ($[M+5H]^{+5}$): 490.9140, found: 490.9150;
calc. for $C_{115}H_{205}N_{31}O_{27}$ ($[M+4H]^{+4}$): 613.3923, found: 613.3907;
calc. for $C_{115}H_{204}N_{31}O_{27}$ ($[M+3H]^{+3}$): 817.5185, found: 817.5208.

EKE-V1 (22)

G E I A A L E K K N A A L K W E I A A L E K G -NH_2
$C_{111}H_{186}N_{30}O_{32}$
2452.89 g/mol

The synthesis was performed via manual SPPS according to SOP1. ChemMatrix Rink amide resin was used. Resin cleavage was performed according to SOP4.

MS: *m/z* (%) = 613.5 $[M+4H]^{+4}$, 817.2 $[M+3H]^{+3}$

KEK-V1 (23)

G K I A A L K W E N A A L E K K I A A L K E G -NH_2
$C_{112}H_{191}N_{31}O_{30}$
2451.95 g/mol

The synthesis was performed via manual SPPS according to SOP1. ChemMatrix Rink amide resin was used. Resin cleavage was performed according to SOP4.

MS: *m/z* (%) = 613.4 $[M+4H]^{+4}$, 817.5 $[M+3H]^{+3}$
HR-MS (ESI): calc. for $C_{112}H_{194}N_{31}O_{30}$ ($[M+4H]^{+4}$): 613.3923, found: 613.3907;
calc. for $C_{115}H_{193}N_{31}O_{30}$ ($[M+3H]^{+3}$): 817.5185, found: 817.5208.

EKE-V2 (24)

G E I A A L E K K I A A L K W E I A A L E K G -NH_2
$C_{113}H_{191}N_{29}O_{31}$
2451.94 g/mol

The synthesis was performed via manual SPPS according to SOP1. ChemMatrix Rink amide resin was used. Resin cleavage was performed according to SOP4.

MS: *m/z* (%) = 817.5 $[M+3H]^{+3}$, 1227.2 $[M+2H]^{+2}$
HR-MS (ESI): calc. for $C_{113}H_{194}N_{31}O_{27}$ ($[M+3H]^{+3}$): 817.7885, found: 817.7908.

KEK-V2 (25)

G K I A A L K W E I A A L E K K I A A L K E G -NH_2
$C_{114}H_{196}N_{30}O_{29}$
2451.89 g/mol

The synthesis was performed via manual SPPS according to SOP1. ChemMatrix Rink amide resin was used. Resin cleavage was performed according to SOP4.

MS: *m/z* (%) = 613.4 $[M+4H]^{+4}$, 817.5 $[M+3H]^{+3}$
HR-MS (ESI): calc. for $C_{114}H_{200}N_{31}O_{27}$ ($[M+4H]^{+4}$): 613.3923, found: 613.3932;

ber. for $C_{114}H_{199}N_{31}O_{27}$ ($[M+3H]^{+3}$): 817.5185, found: 817.5232.

EKE-V3 (26)

G E I A A L E Q K I A A L K W E I A A L E K G -NH_2
$C_{112}H_{186}N_{28}O_{33}$
2452.88 g/mol

The synthesis was performed via manual SPPS according to SOP1. ChemMatrix Rink amide resin was used. Resin cleavage was performed according to SOP4.

MS: *m/z* (%) = 490.9 $[M+5H]^{+5}$, 613.4 $[M+4H]^{+4}$, 817.5 $[M+3H]^{+3}$
HR-MS (ESI): calc. for $C_{112}H_{191}N_{28}O_{33}$ ($[M+5H]^{+5}$): 490.9140, found: 490.9150;
calc. for $C_{112}H_{190}N_{28}O_{33}$ ($[M+4H]^{+4}$): 613.3923, found: 613.3907;
calc. for $C_{112}H_{189}N_{28}O_{33}$ ($[M+3H]^{+3}$): 817.5185, found: 817.5208.

KEK-V3 (27)

G K I A A L K W E I A A L E Q K I A A L K E G -NH_2
$C_{113}H_{191}N_{29}O_{31}$
2451.94 g/mol

The synthesis was performed via manual SPPS according to SOP1. ChemMatrix Rink amide resin was used. Resin cleavage was performed according to SOP4.

MS: *m/z* (%) = 490.9 $[M+5H]^{+5}$, 613.4 $[M+4H]^{+4}$, 817.5 $[M+3H]^{+3}$
HR-MS (ESI): calc. for $C_{115}H_{196}N_{31}O_{27}$ ($[M+5H]^{+5}$): 490.8240, found: 490.8250;
calc. for $C_{115}H_{197}N_{31}O_{27}$ ($[M+4H]^{+4}$): 613.3223, found: 613.3207;
calc. for $C_{115}H_{198}N_{31}O_{27}$ ($[M+3H]^{+3}$): 817.1185, found: 817.1198.

EKE-V4 (28)

G E I A A L E W K I A A L K E E I A A L E K G -NH_2
$C_{113}H_{191}N_{29}O_{31}$
2451.94 g/mol

The synthesis was performed via manual SPPS according to SOP1. ChemMatrix Rink

amide resin was used. Resin cleavage was performed according to SOP4.

MS: *m/z* (%) = 818.5 $[M+3H]^{+3}$
HR-MS (ESI): calc. for $C_{115}H_{194}N_{31}O_{27}$ ($[M+3H]^{+3}$): 818.4685, found: 818.4668.

KEK-V4 (29)

G K I A A L K W E I A A L E K K I A A L K E G -NH_2
$C_{114}H_{196}N_{30}O_{29}$
2451.89 g/mol

The synthesis was performed via manual SPPS according to SOP1. ChemMatrix Rink amide resin was used. Resin cleavage was performed according to SOP4.

MS: *m/z* (%) = 613.4 $[M+4H]^{+4}$, 817.5 $[M+3H]^{+3}$
HR-MS (ESI): calc. for $C_{115}H_{201}N_{31}O_{27}$ ($[M+4H]^{+4}$): 613.6260, found: 613.6278;
calc. for $C_{115}H_{200}N_{31}O_{27}$ ($[M+3H]^{+3}$): 817.8312, found: 817.8333.

E3T1 (35)

G E L A A I K W E L A A I E K E L A A I E K G -NH_2
$C_{111}H_{181}N_{27}O_{35}$
2453.82 g/mol

The synthesis was performed via manual SPPS according to SOP1. ChemMatrix Rink amide resin was used. Resin cleavage was performed according to SOP4.

MS: *m/z* (%) = 818.8 $[M+3H]^{+3}$, 1227.7 $[M+2H]^{+2}$
HR-MS (ESI): calc. for $C_{111}H_{184}N_{31}O_{27}$ ($[M+3H]^{+3}$): 818.7819, found: 818.7820;
calc. for $C_{111}H_{183}N_{31}O_{27}$ ($[M+2H]^{+2}$): 1227.6694, found: 1227.6694.

K3T1 (39)

G K L A A I E W K L A A I K E K L A A I K E G -NH_2
$C_{115}H_{201}N_{31}O_{27}$
2450.90 g/mol

The synthesis was performed via manual SPPS according to SOP1. ChemMatrix Rink amide resin was used. Resin cleavage was performed according to SOP4.

MS: *m/z* (%) = 613.4 $[M+4H]^{+4}$, 817.8 $[M+3H]^{+3}$, 1225.8 $[M+2H]^{+2}$
HR-MS (ESI): calc. for $C_{115}H_{205}N_{31}O_{27}$ ($[M+4H]^{+4}$): 613.3927, found: 613.3940;
calc. for $C_{115}H_{204}N_{31}O_{27}$ ($[M+3H]^{+3}$): 817.8465, found: 817.8469;
calc. for $C_{115}H_{203}N_{31}O_{27}$ ($[M+2H]^{+2}$): 1225.7711, found: 1225.7757.

E3T2 (36)

G E L A A I K W E L A A I E K E L A A I E K G -NH_2
$C_{111}H_{181}N_{27}O_{35}$
2453.82 g/mol

The synthesis was performed via manual SPPS according to SOP1. ChemMatrix Rink amide resin was used. Resin cleavage was performed according to SOP4.

MS: *m/z* (%) = 818.8 $[M+3H]^{+3}$, 1227.7 $[M+2H]^{+2}$.
HR-MS (ESI): calc. for $C_{111}H_{178}N_{27}O_{35}$ ($[M+3H]^{+3}$): 818.7820, found: 818.7820;
calc. for $C_{111}H_{179}N_{27}O_{35}$ ($[M+2H]^{+2}$): 1227.6694, found: 1227.6691.

K3T2 (40)

G K L A A I E W K L A A I K E K L A A I K E G -NH_2
$C_{115}H_{201}N_{31}O_{27}$
2450.06 g/mol

The synthesis was performed via manual SPPS according to SOP1. ChemMatrix Rink amide resin was used. Resin cleavage was performed according to SOP4.

MS: *m/z* (%) = 613.4 $[M+4H]^{+4}$, 817.8 $[M+3H]^{+3}$, 1225.8 $[M+2H]^{+2}$
HR-MS (ESI): calc. for $C_{115}H_{197}N_{31}O_{27}$ ($[M+4H]^{+4}$): 613.3907, found: 613.3909;
calc. for $C_{115}H_{198}N_{31}O_{27}$ ($[M+3H]^{+3}$): 817.8465, found: 817.8468;
calc. for $C_{115}H_{199}N_{31}O_{27}$ ($[M+2H]^{+2}$): 1225.7741, found: 1225.7733.

E3T3 (37)

G E L A A I K W E L A A I E K E L A A I E K G -NH_2
$C_{111}H_{181}N_{27}O_{35}$
2453.82 g/mol

The synthesis was performed via manual SPPS according to SOP1. ChemMatrix Rink amide resin was used. Resin cleavage was performed according to SOP4.

MS: *m/z* (%) = 819.0 (100) $[M+3H]^{+3}$, 1228.0 (11) $[M+2H]^{+2}$.
HR-MS (ESI): calc. for $C_{111}H_{178}N_{27}O_{35}$ ($[M+3H]^{+3}$): 818.9820, found: 818.9821;
calc. for $C_{111}H_{179}N_{27}O_{35}$ ($[M+2H]^{+2}$): 1227.6694, found: 1227.6673.

K3T3 (41)

G K L A A I E W K L A A I K E K L A A I K E G -NH_2
$C_{115}H_{201}N_{31}O_{27}$
2450.06 g/mol

The synthesis was performed via manual SPPS according to SOP1. ChemMatrix Rink amide resin was used. Resin cleavage was performed according to SOP4.

MS: *m/z* (%) = 613.5 (100) $[M+4H]^{+4}$, 817.7 (96) $[M+3H]^{+3}$, 1226.1 (13) $[M+2H]^{+2}$
HR-MS (ESI): calc. for $C_{115}H_{205}N_{31}O_{27}$ ($[M+4H]^{+4}$): 613.3907, found: 613.3917;
calc. for $C_{115}H_{204}N_{31}O_{27}$ ($[M+3H]^{+3}$): 817.5685, found: 817.5686;
calc. for $C_{115}H_{203}N_{31}O_{27}$ ($[M+2H]^{+2}$): 1225.7741, found: 1225.7731.

8.8.3 Synthesized Model Peptides

EKE V3-SybTMD (30)

G E L A A I K W E L A A I E K E L A A I E K-**SybTMD**

$C_{301}H_{493}N_{69}O_{68}S_3$

6258.64 g/mol

The synthesis was performed via manual SPPS according to SOP1. The resin was preloaded with SybTMD. Resin cleavage was performed according to SOP4.

MS: *m/z* (%) = 1044.8 $[M+6H]^{+6}$, 1252.1 (72) $[M+5H]^{+5}$,
HR-MS (ESI): calc. for $C_{299}H_{489}N_{67}O_{72}S_3$ ($[M+6H]^{+6}$): 1044.6153, found: 1044.6163;
calc. for $C_{299}H_{488}N_{67}O_{72}S_3$ ($[M+5H]^{+5}$): 1253.3410, found: 1253.3422;

KEK V3-SxTMD (31)

G K L A A I E W K L A A I K E K L A A I K E G -**SxTMD**

$C_{277}H_{478}N_{72}O_{67}S_3$

5988.59 g/mol

The synthesis was performed via manual SPPS according to SOP1. The resin was preloaded with SxTMD. Resin cleavage was performed according to SOP4.

MS: *m/z* (%) = 998.6 $[M+6H]^{+6}$, 1198.1 $[M+5H]^{+5}$, 1497.6 $[M+4H]^{+4}$
HR-MS (ESI): calc. for $C_{278}H_{489}N_{73}O_{65}S_3$ ($[M+6H]^{+6}$): 998.4315, found: 998.4314;
calc. for $C_{278}H_{488}N_{73}O_{65}S_3$ ($[M+5H]^{+5}$): 1197.9184, found: 1197.9173;
calc. for $C_{278}H_{487}N_{73}O_{65}S_3$ ($[M+4H]^{+4}$): 1497.5430, found: 1497.5436;

EKE V4-SybTMD (32)

G E L A A I K W E L A A I E K E L A A I E K G -**SybTMD**

$C_{299}H_{483}N_{67}O_{72}S_3$

6264.73 g/mol

The synthesis was performed via manual SPPS according to SOP1. The resin was preloaded with SybTMD. Resin cleavage was performed according to SOP4.

MS: *m/z* (%) = 895.4 $[M+7H]^{+7}$, 1044.7 $[M+6H]^{+6}$, 1253.4 $[M+5H]^{+5}$
HR-MS (ESI): calc. for $C_{115}H_{196}N_{31}O_{27}$ ($[M+7H]^{+7}$): 895.6758, found: 895.6753;

calc. for $C_{115}H_{197}N_{31}O_{27}$ ($[M+6H]^{+6}$): 1044.7824, found: 1044.7818;
calc. for $C_{115}H_{198}N_{31}O_{27}$ ($[M+3H]^{+5}$): 1253.5374, found: 1253.5363.

KEK V4-SxTMD (33)

G K L A A I E W K L A A I K E K L A A I K E G -**SxTMD**
$C_{278}H_{483}N_{73}O_{65}S_3$
5984.55 g/mol

The synthesis was performed via manual SPPS according to SOP1. The resin was preloaded with SxTMD. Resin cleavage was performed according to SOP4.

MS: *m/z* (%) = 853.8 $[M+7H]^{+7}$, 996.7 $[M+6H]^{+6}$
HR-MS (ESI): calc. for $C_{278}H_{483}N_{73}O_{65}S_3$ ($[M+7H]^{+7}$): 853.8168, found: 853.8176;
calc. for $C_{278}H_{483}N_{73}O_{65}S_3$ ($[M+6H]^{+7}$): 996.7172, found: 996.7176.

E3T1-SybTMD (42)

G E L A A I K W E L A A I E K E L A A I E K G -**SybTMD**
$C_{299}H_{483}N_{67}O_{72}S_3$
6264.73 g/mol

The synthesis was performed via manual SPPS according to SOP1. The resin was preloaded with SybTMD. Resin cleavage was performed according to SOP4.

MS: *m/z* (%) = 894.3 (40) $[M+7H]^{+7}$, 1044.9 (100) $[M+6H]^{+6}$, 1252.1 (72) $[M+5H]^{+5}$, 1566.1 (12) $[M+4H]^{+4}$
HR-MS (ESI): calc. für $C_{299}H_{490}N_{67}O_{72}S_3$ ($[M+7H]^{+7}$): 894.3932, found: 894.3927;
calc. for $C_{299}H_{489}N_{67}O_{72}S_3$ ($[M+6H]^{+6}$): 1044.9239, found: 1044.9226;
calc. for $C_{299}H_{488}N_{67}O_{72}S_3$ ($[M+5H]^{+5}$): 1252.1131, found: 1252.1129;
calc. for $C_{299}H_{487}N_{67}O_{72}S_3$ ($[M+4H]^{+4}$): 1566.4540, found: 1566.4531;

E3T1-SxTMD (43)

G K L A A I E W K L A A I K E K L A A I K E G -**SybTMD**
$C_{278}H_{483}N_{73}O_{65}S_3$
5984.55 g/mol

The synthesis was performed via manual SPPS according to SOP1. The resin was preloaded with SxTMD. Resin cleavage was performed according to SOP4.

MS: *m/z* (%) = 853.5 (45) $[M+7H]^{+7}$, 996.4 (100) $[M+6H]^{+6}$, 1195.1 (79) $[M+5H]^{+5}$, 1495.1 (17) $[M+4H]^{+4}$

HR-MS (ESI): calc. für $C_{278}H_{490}N_{73}O_{65}S_3$ ($[M+7H]^{+7}$): 853.5613, found: 853.5617;
calc. for $C_{278}H_{489}N_{73}O_{65}S_3$ ($[M+6H]^{+6}$): 996.6339, found: 996.6333;
calc. for $C_{278}H_{488}N_{73}O_{65}S_3$ ($[M+5H]^{+5}$): 1195.1139, found: 1195.1136;
calc. for $C_{278}H_{487}N_{73}O_{65}S_3$ ($[M+4H]^{+4}$): 1495.1330, found: 1495.1331;

E3T1s-SybTMD (44)

G E L A A I K W E L A A I E K E L A A I E K - W W K N L K M M I I L G V I C A I I L I I I I V Y F S T

$C_{262}H_{439}N_{65}O_{67}S_3$

5668.02 g/mol

The synthesis was performed via manual SPPS according to SOP1. The resin was preloaded with SybTMD. Resin cleavage was performed according to SOP4.

MS: *m/z* (%) = 810.8 $[M+7H]^{+7}$, 949.9 $[M+6H]^{+6}$, 1139.7 $[M+5H]^{+5}$,

HR-MS (ESI): calc. for $C_{262}H_{439}N_{65}O_{67}S_3$ ($[M+7H]^{+7}$): 810.7529, found: 810.7523;
calc. for $C_{262}H_{439}N_{65}O_{67}S_3$ ($[M+6H]^{+6}$): 945.5437, found: 945.5434;
calc. for $C_{262}H_{439}N_{65}O_{67}S_3$ ($[M+5H]^{+5}$): 1134.4510, found: 1134.4500;

E3T1s-SxTMD (45)

G E L A A I K W E L A A I E K E L A A I E K - K A R R K K I M I I I C C V I L G I I I A S T I G G I F G

$C_{251}H_{429}N_{63}O_{66}S_3$

5481.75 g/mol

The synthesis was performed via manual SPPS according to SOP1. The resin was preloaded with SxTMD. Resin cleavage was performed according to SOP4.

MS: *m/z* (%) = 784.1 $[M+7H]^{+7}$, 914.8 $[M+6H]^{+6}$, 1096.3 $[M+5H]^{+5}$,

HR-MS (ESI): calc. for $C_{251}H_{436}N_{63}O_{66}S_3$ ($[M+7H]^{+7}$): 784.1088, found: 784.1078;
calc. for $C_{251}H_{435}N_{63}O_{66}S_3$ ($[M+6H]^{+6}$): 914.8339, found: 914.8333;

calc. for $C_{251}H_{434}N_{63}O_{66}S_3$ ($[M+5H]^{+5}$): 1096.3539, found: 1096.3540;

Appendix

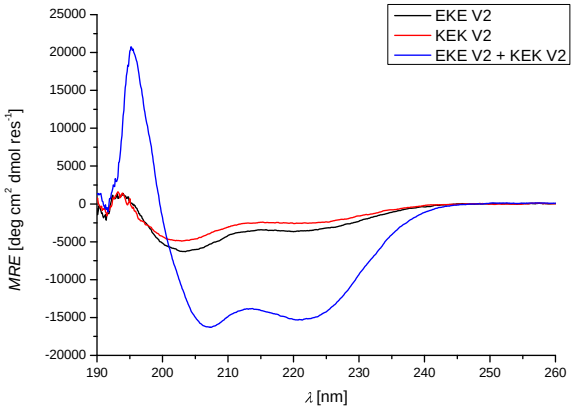

Figure 8.1: CD-spectra of alternating recognition units of each monomer of EKE V2 and KEK V2 was tested. Additionally the combination of both coils with each other. Peptide concentration was set to 40 µM.

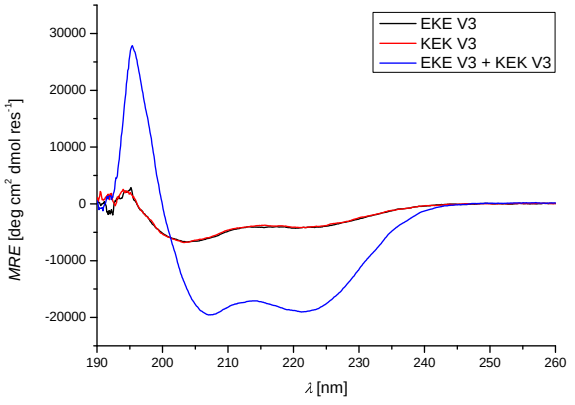

Figure 8.2: CD-spectra of alternating recognition units of each monomer of EKE V3 and KEK V3 was tested. Additionally the combination of both coils with each other. Peptide concentration was set to 40 µM.

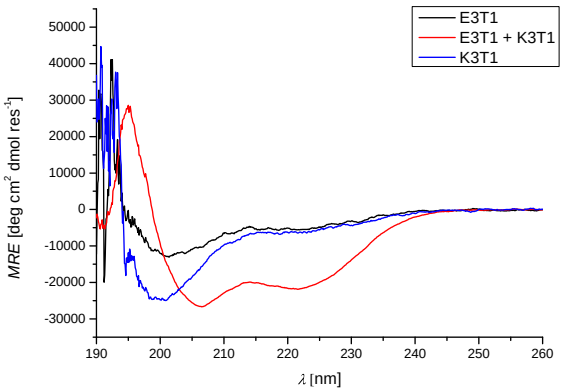

Figure 8.3: CD-spectra of alternating recognition units of each monomer of E3T1 and K3T1 was tested. Additionally the combination of both coils with each other. Peptide concentration was set to 40 µM.

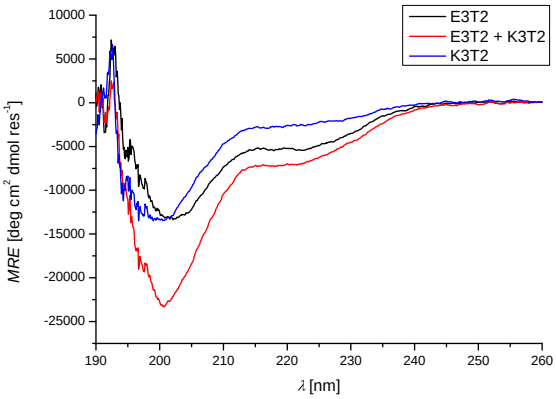

Figure 8.4: CD-spectra of alternating recognition units of each monomer of E3T2 and K3T2 was tested. Additionally the combination of both coils with each other. Peptide concentration was set to 40 µM.

List of Abbreviations

General. Abbreviations for amino acids has been related to one-to-three code.

A	absorption intensity
AA	amino acid
aeg-PNA	*N*-(2-aminoethyl)glycine-PNA
aq.	aqueous
ATP	adenosine triphosphate
BD syringe	syringe by *Becton Dickinson*
Bhoc	benzhydryloxycarbonyl protection group
Boc	*tert*-butoxycarbonyl protection group
calc.	calculated
Cbz	benzyloxycarbonyl
chol	cholesterol
cm	centimeter
d	doublet
DCM	dichloromethane
DIC	*N,N*-diisopropylcarbodiimide
DIPEA	*N,N*-diisopropylethylamine
DLS	dynamic light scattering
DMF	Dimethylformamide
DNA	deoxyribonucleic acid
DOPC	1,2-Dioleoyl-*sn*-glycero-3-phosphocholine
DOPE	1,2-Dioleoyl-*sn*-glycero-3-phosphocholine
EDT	1,2-ethanedithiole
EDTA	ethylenediaminetetraacetic acid
eq	Equivalent
ESI-MS	electrospray ionisation mass spectrometry
F	normalized fluorescence intensity
FA	formic acid

Fmoc	9-fluorenylmethyloxycarbonyl protection group
FRET	Förster resonance energy transfer
GUV	Giant unilamellar vesicle
HATU	*O*-(7-Azabenzotriazole-1-yl)-*N,N,N,N*-tetramethyluroniumhexafluorophosphate
HEPES	4-(2-hydroxyethyl)-1-piperazineethanesulfonic acid
HFIP	1,1,1,3,3,3-hexafluoro-2-propanol
HOAt	1-hydroxy-7-azabenzotriazole
HPLC	high-performance liquid chromatography
HR-MS	high resolution mass spectrometry
J	coupling constant
LUV	large unilamellar vesicle
MeCN	acetonitrile
MeOH	acetonitrile
MS	Mass spectrometry
m/z	mass-to-charge ratio
NBD	7-nitro-2-1,3-benzoxadiazole
NMP	*N*-methyl-2-pyrrolidon
NMR	nuclear magnetic resonance
NPP	2-(*o*-nitrophenyl)-propyl protection group
NSF	*N*-ethylmaleide-sensitive factor
OG	Oregon Green 488
Oxyma	ethyl cyanohydroxyiminoacetate
p.a.	Pro analysi
Pbf	2,2,4,6,7-pentamethyldihydrobenzofuran-5-sulfonyl protection group
PC	phosphatidylcholine
PE	phosphatidylethanolamine
PEG	polyethylene glycol
P/L ratio	peptide-to-lipid ratio
PNA	peptide nucleic acid
POPC	1-palmitoyl-2-oleoyl-*sn*-glycero-3-phosphocholine
ppm	parts per million
PyBOP	benzotriazol-1-yl-oxytripyrrolidinophosphonium hexafluorophosphate
Rh	Lissamine Rhodamine B

rpm	rotations per minute
rt	room temperature
SNAP	soluble NSF attachment protein
SNAP-25	25-kDa synaptosome-associated protein
SNARE	soluble *N*-ethylmaleimide-sensitive factor attachment protein receptor
SOP	standard operating procedure
SPPS	solid phase peptide synthesis
SUV	small unilamellar vesicle
Sx	Syntaxin-1A
SxTMD	Syntaxin-1A (256-288)
Syb	Synaptobrevin-2
SybTMD	Synaptobrevin-2 (85-116)
tBu	*tert*-butyl protection group
TFA	trifluoroacetic acid
TFE	2,2,2-trifluoroethanol
TIS	triisopropylsilane
THF	tetrahydrofuran
TMD	transmembrane domain
TR	Texas Red
Trt	trityl protection group
TX-100	Triton X-100
UV	ultraviolett
v/v	volume/volume ratio
Z	carboxybenzyl protection group

Bibliography

[1] D. Wicher, R. Schäfer, R. Bauernfeind, M. C. Stensmyr, R. Heller, S. H. Heinemann, B. S. Hansson, *Nature* **2008**, *452*, 1007–1011.

[2] K. Sato, M. Pellegrino, T. Nakagawa, T. Nakagawa, L. B. Vosshall, K. Touhara, *Nature* **2008**, *452*, 1002–1006.

[3] J. P. Overington, B. Al-Lazikani, A. L. Hopkins, *Nature Reviews Drug Discovery* **2006**, *5*, 993–996.

[4] R. Santos, O. Ursu, A. Gaulton, A. P. Bento, R. S. Donadi, C. G. Bologa, A. Karlsson, B. Al-Lazikani, A. Hersey, T. I. Oprea, J. P. Overington, *Nature Reviews Drug Discovery* **2016**, *16*, 19–34.

[5] Cournia, T. W. Allen, I. Andricioaei, B. Antonny, D. Baum, G. Brannigan, N.-V. Buchete, J. T. Deckman, L. Delemotte, C. del Val, R. Friedman, P. Gkeka, H.-C. Hege, J. Hénin, M. A. Kasimova, A. Kolocouris, M. L. Klein, S. Khalid, M. J. Lemieux, N. Lindow, M. Roy, J. Selent, M. Tarek, F. Tofoleanu, S. Vanni, S. Urban, D. J. Wales, J. C. Smith, A.-N. Bondar, *The Journal of Membrane Biology* **2015**, *248*, 611–640.

[6] J.-L. Rigaud, B. Pitard, D. Levy, *Biochimica et Biophysica Acta (BBA) - Bioenergetics* **1995**, *1231*, 223–246.

[7] J. Knol, K. Sjollema, B. Poolman, *Biochemistry* **1998**, *37*, 16410–16415.

[8] T. M. Weiss, P. C. van der Wel, J. A. Killian, R. E. Koeppe, H. W. Huang, *Biophysical Journal* **2003**, *84*, 379–385.

[9] R. P. Richter, A. R. Brisson, *Biophysical Journal* **2005**, *88*, 3422–3433.

[10] Y.-H. M. Chan, S. G. Boxer, *Current Opinion in Chemical Biology* **2007**, *11*, 581–587.

[11] D. Sames, M. Dunn, R. J. Karpowicz, D. Sulzer, *ACS Chemical Neuroscience* **2013**, *4*, 648–651.

[12] R. Jahn, R. H. Scheller, *Nature Reviews Molecular Cell Biology* **2006**, *7*, 631–643.

[13] M. A. Poirier, W. Xiao, J. C. Macosko, C. Chan, Y.-K. Shin, M. K. Bennett, *Nature Structural Biology* **1998**, *5*, 765–769.

[14] T. H. Kloepper, C. N. Kienle, D. Fasshauer, *Molecular Biology of the Cell* **2007**, *18*, 3463–3471.

[15] N. Furukawa, J. Mima, *Scientific Reports* **2014**, *4*, DOI `DOI:10.1038/srep04277`.

[16] J. R. Litowski, R. S. Hodges, *Journal of Biological Chemistry* **2002**, *277*, 37272–37279.

[17] K. Meyenberg, A. S. Lygina, G. van den Bogaart, R. Jahn, U. Diederichsen, *Chemical Communications* **2011**, *47*, 9405.

[18] J.-D. Wehland, PhD thesis, Georg-August-Universität, **2017**.

[19] M. C. Groth, PhD thesis, Georg-August-Universität, **2021**.

[20] B. E. Hubrich, PhD thesis, Georg-August-Universität, **2017**.

[21] G. A. Daudey, H. R. Zope, J. Voskuhl, A. Kros, A. L. Boyle, *Langmuir* **2017**, *33*, 12443–12452.

[22] G. A. Daudey, C. Schwieger, M. Rabe, A. Kros, *Langmuir* **2019**, *35*, 5501–5508.

[23] A. Stein, G. Weber, M. C. Wahl, R. Jahn, *Nature* **2009**, *460*, 525–528.

[24] P. Kumar, S. Guha, U. Diederichsen, *Journal of Peptide Science* **2015**, *21*, 621–629.

[25] S. Guha, J. Graf, B. Göricke, U. Diederichsen, *Journal of Peptide Science* **2013**, *19*, 415–422.

[26] S. J. Singer, G. L. Nicolson, *Science* **1972**, *175*, 720–731.

[27] D. Lopes, S. Jakobtorweihen, Nunes, B. Sarmento, S. Reis, *Progress in Lipid Research* **2017**, *65*, 24–44.

[28] F. Cohen, G. Melikyan, *Journal of Membrane Biology* **2004**, *199*, 1–14.

[29] G. L. Nicolson, *Biochimica et Biophysica Acta (BBA) - Biomembranes* **2014**, *1838*, 1451–1466.

[30] L. Fagerberg, K. Jonasson, G. von Heijne, L. Berglund, *PROTEOMICS* **2010**, *10*, 1141–1149.

[31] C. Klose, M. A. Surma, K. Simons, *Current Opinion in Cell Biology* **2013**, *25*, 406–413.

[32] M. F. Brown, *Annual Review of Biophysics* **2017**, *46*, 379–410.

[33] S. Higgins, *Biochemical Education* **1978**, *6*, 22.

[34] S. Nagar, K. Korzekwa, *Pharmaceutical Research* **2016**, *34*, 535–543.

[35] X. Liu, B. Testa, A. Fahr, *Pharmaceutical Research* **2010**, *28*, 962–977.

[36] A. Dahan, J. M. Miller, *The AAPS Journal* **2012**, *14*, 244–251.

[37] L. Lautner, K. Pluhackova, N. K. Barth, T. Seydel, W. Lohstroh, R. A. Böckmann, T. Unruh, *Chemistry and Physics of Lipids* **2017**, *206*, 28–42.

[38] L. Bagatolli, P. B. S. Kumar, *Soft Matter* **2009**, *5*, 3234.

[39] J. E. Rothman, *Angew. Chem.* **2014**, *126*, 12886–12905.

[40] J. S. Bonifacino, B. S. Glick, *Cell* **2004**, *116*, 153–166.

[41] M. B. Sankaram, D. Marsh, **1993**, 127–162.

[42] S. J. Singer, *Annual Review of Cell Biology* **1990**, *6*, 247–296.

[43] L. E. Hedin, A. Elofsson, *Journal of Proteome Research* **2011**, *10*, 3324–3331.

[44] J. W. Fairman, N. Noinaj, S. K. Buchanan, *Current Opinion in Structural Biology* **2011**, *21*, 523–531.

[45] R. Winter, *Chemie in unserer Zeit* **1990**, *24*, 71–81.

[46] G. van Meer, D. R. Voelker, G. W. Feigenson, *Nature Reviews Molecular Cell Biology* **2008**, *9*, 112–124.

[47] C. Peetla, A. Stine, V. Labhasetwar, *Molecular Pharmaceutics* **2009**, *6*, 1264–1276.

[48] P. R. Cullis, M. J. Hope, C. P. Tilcock, *Chemistry and Physics of Lipids* **1986**, *40*, 127–144.

[49] C. Tanford, *Science* **1978**, *200*, 1012–1018.

[50] T. Skotland, K. Sagini, K. Sandvig, A. Llorente, *Advanced Drug Delivery Reviews* **2020**, *159*, 308–321.

[51] L. Chernomordik, M. Kozlov, J. Zimmerberg, *The Journal of Membrane Biology* **1995**, *146*, DOI `https://doi.org/10.1007/BF00232676`.

[52] T. Harayama, H. Riezman, *Nature Reviews Molecular Cell Biology* **2018**, *19*, 281–296.

[53] O. G. Mouritsen, *Biochimica et Biophysica Acta (BBA) - Biomembranes* **2010**, *1798*, 1286–1288.

[54] M. Cebecauer, M. Amaro, P. Jurkiewicz, L. Cwiklik, M. Hof, *Chemical Reviews* **2018**, *118*, 11259–11297.

[55] R. Jahn, R. Scheller, *Nat. Rev. Mol. Cell Biol.* **2006**, *7*, 631–643.

[56] W. S. Trimble, D. M. Cowan, R. H. Scheller, *Proc. Natl. Acad. Sci. U. S. A.* **1988**, *85*, 4538–4542.

[57] R. Jahn, T. Lang, T. C. Südhof, *Cell* **2003**, *112*, 519–533.

[58] A. Inoue, K. Obata, K. Akagawa, *J. Biol. Chem.* **1992**, *267*, 10613–10619.

[59] M. Bennet, N. Calakos, R. H. Scheller, *Science* **1992**, *257*, 255–259.

[60] G. A. Oyler, G. A. Higgins, R. A. Hart, *J. Cell Biol.* **1989**, *109*, 3039–3052.

[61] T. Galli, E. Garcia, O. Mundigl, T. Chilcote, P. D. Camilli, *Neuropharmacology* **1995**, *34*, 1351–1360.

[62] D. Fasshauer, *Biochem. Biophys. Acta* **2003**, *1641*, 87–97.

[63] J. C. Lerman, J. Robblee, R. Fairman, F. M. Hughson, *Biochemistry* **2000**, *39*, 8470–8479.

[64] D.Fasshauer, H.Otto, W.K.Eliason, R.Jahn, A. Brünger, *J. Biol. Chem.* **1997**, *272*, 28036–41.

[65] X. Lu, F. Zhang, J. A. McNew, Y. K. Shin, *J. Biol. Chem.* **2005**, *280*, 30538–30541.

[66] A. Bracher, J. Kadlec, H. Betz, W. Weissenhorn, *J. Biol. Chem.* **2002**, *277*, 26517–26523.

[67] A. Stein, G. Weber, M. C. Wahl, R. Jahn, *Nature* **2009**, *460*.

[68] Y. Chen, S. J. Scales, R. Scheller, *Neuron* **2001**, *30*, 161–170.

[69] P. I. Hanson, R. Roth, H. Morisaki, R. Jahn, J. E. Heuser, *Cell* **1997**, *90*, 523–535.

[70] R. C. Lin, R. H. Scheller, *Neuron* **1997**, *19*, 1087–1094.

[71] K. M. Fiebig, L. M. Rice, E. Pollock, A. T. Brunger, *Nat. Struct. Mol. Biol.* **1999**, *6*, 117–123.

[72] A. V. Pobbati, A. Stein, D. Fasshauer, *Science* **2006**, *13*, 673–676.

[73] W. Liu, R. F. Stout, V. Papura, *Cell Calcium* **2012**, *52*, 241–249.

[74] M. A. Poirer, W. Xiao, J. C. Macosko, C. Chan, Y. K. Shin, M. K. Bennet, *Nat. Struct. Biol.* **1998**, *5*, 765–769.

[75] Y. Hua, R. H. Scheller, *Proceedings of the National Academy of Sciences* **2001**, *98*, 8065–8070.

[76] T. Hayashi, H. McMahon, S. Yamasaki, T. Binz, Y. Hata, T. C. Südhof, H. Niemann, *EMBO J.* **1994**, *13*, 5051–5061.

[77] L. Chernomordik, M. Kozlov, *Cell* **2005**, *123*, 375–382.

[78] P. Kasson, N. Kelley, N. Singhal, A. T. Brunger, *Proc. Natl. Acad. Sci.* **2006**, *110*, 11916–11921.

[79] P. Kuzmin, J. Zimmerberg, Y. A. Chizmadzhev, F. S. Cohen, *Proc. Natl. Acad. Sci.* **2001**, *98*, 7235–7240.

[80] J. A. McNew, T. Weber, F. Parlati, *J. Cell Biol.* **2000**, *150*, 105–117.

[81] L. V. Chernomordik, M. M. Kozlov, *Nat. Struct. Mol. Biol.* **2008**, *15*, 675–683.

[82] L. Yang, H. W. Huang, *Science* **2002**, *297*, 1877–1897.

[83] Y. Xu, F. Zhang, Z. Su, J. A. McNew, Y. K. Shin, *Nat. Struct. Mol. Biol.* **2005**, *12*, 417–422.

[84] T. Y. Yoon, B. Okumus, T. Ha, Y. K. Y. Shin, F. Zhang, *Proc. Natl. Acad. Sci.* **2006**, *103*, 19731–19736.

[85] K. Stiasny, F. X. Heinz, *Journal of Virology* **2004**, *78*, 8536–8542.

[86] I. K. Jarsch, F. Daste, J. L. Gallop, *Journal of Cell Biology* **2016**, *214*, 375–387.

[87] L. Chernomordik, M. Kozlov, *Annu. Rev. Biochem.* **2003**, *72*, 175–207.

[88] R. Jahn, J. H. Hernandez, A. Stein, A. Cypionka, *Science* **2012**, *336*, 1581–1584.

[89] Y. Gao, Z. Xi, G. Sirinakis, *Science* **2012**, *337*, 1340–1342.

[90] S. P. Sansom, O. Beckstein, A. Chetwynd, M. Lindau, *Biophys. J.* **2012**, *103*, 959–969.

[91] F. Pincet, F. Li, D. Kümmel, J. Coleman, *J. Am. Chem. Soc.* **2014**.

[92] D. K. Struck, D. Hoekstra, R. E. Pagano, *Biochemistry* **1981**, *20*, 4093–4099.

[93] J. Wilschut, N. Duzgunes, R. Fraley, D. Papahadjopoulos, *Biochemistry* **1980**, *19*, 6011–6021.

[94] C. Ma, L. Su, A. B. Seven, Y. Xu, J. Rizo, *Science* **2012**, *339*, 421–425.

[95] P. Mühlenbrock, K. Herwig, L. Vuong, I. Mey, C. Steinem, **2020**, DOI `https://doi.org/10.1101/2020.01.16.909044`.

[96] G. Stengel, R. Zahn, F. Höök, *Journal of the American Chemical Society* **2007**, *129*, 9584–9585.

[97] G. Stengel, L. Simonsson, R. A. Campbell, F. Höök, *The Journal of Physical Chemistry B* **2008**, *112*, 8264–8274.

[98] Y.-H. M. Chan, B. van Lengerich, S. G. Boxer, *Proceedings of the National Academy of Sciences* **2009**, *106*, 979–984.

[99] Y.-H. M. Chan, B. van Lengerich, S. G. Boxer, *Biointerphases* **2008**, *3*, FA17–FA21.

[100] M. Pieren, Y. Desfougères, L. Michaillat, A. Schmidt, A. Mayer, *Journal of Biological Chemistry* **2015**, *290*, 12821–12832.

[101] P. Wittung, P. E. Nielsen, O. Buchardt, M. Egholm, B. Nordén, *Nature* **1994**, *368*, 561–563.

[102] A. S. Lygina, K. Meyenberg, R. Jahn, U. Diederichsen, *Angewandte Chemie International Edition* **2011**, *50*, 8597–8601.

[103] J.-D. Wehland, A. S. Lygina, P. Kumar, S. Guha, B. E. Hubrich, R. Jahn, U. Diederichsen, *Molecular BioSystems* **2016**, *12*, 2770–2776.

[104] B. E. Hubrich, P. Kumar, H. Neitz, M. Grunwald, T. Grothe, P. J. Walla, R. Jahn, U. Diederichsen, *Angewandte Chemie International Edition* **2018**, *57*, 14932–14936.

[105] H. R. Mardsen, I. Tomatsu, A. Kros, *Chem. Soc. Rev* **2011**, *40*, 1572–1585.

[106] D. Papahadjopoulos, A. D. Bangham, *Biochimica et Biophysica Acta (BBA) - Biophysics including Photosynthesis* **1966**, *126*, 185–188.

[107] H. Robson Marsden, N. Elbers, P. Bomans, N. Sommerdijk, A. Kros, *Angewandte Chemie International Edition* **2009**, *48*, 2330–2333.

[108] L. Kong, S. H. C. Askes, S. Bonnet, A. Kros, F. Campbell, *Angewandte Chemie International Edition* **2015**, *55*, 1396–1400.

[109] D. A. Lindhout, J. R. Litowski, P. Mercier, R. S. Hodges, B. D. Sykes, *Biopolymers* **2004**, *75*, 367–375.

[110] B. Hochreiter, A. Pardo-Garcia, J. Schmid, *Sensors* **2015**, *15*, 26281–26314.

[111] J. A. Broussard, K. J. Green, *Journal of Investigative Dermatology* **2017**, *137*, e185–e191.

[112] T. Chen, B. He, J. Tao, Y. He, H. Deng, X. Wang, Y. Zheng, *Advanced Drug Delivery Reviews* **2019**, *143*, 177–205.

[113] I. Medintz, N. Hildebrandt, *FRET - Förster Resonance Energy Transfer*, Wiley VCH Verlag GmbH, **2013**.

[114] J. F. Lovell, J. Chen, M. T. Jarvi, W.-G. Cao, A. D. Allen, Y. Liu, T. T. Tidwell, B. C. Wilson, G. Zheng, *The Journal of Physical Chemistry B* **2009**, *113*, 3203–3211.

[115] N. Moskowitz, S. Puszkin, W. Schook, *Journal of Neurochemistry* **1983**, *41*, 1576–1586.

[116] V. Trivedi, C. Yu, B. Veeramuthu, S. Francis, D. Chang, *Chemistry and Physics of Lipids* **2000**, *107*, 99–106.

[117] S. Castorph, S. S. Henriques, M. Holt, D. Riedel, R. Jahn, T. Salditt, *The European Physical Journal E* **2011**, *34*, DOI `https://doi.org/10.1140/epje/i2011-11063-2`.

[118] J. Stetefeld, S. A. McKenna, T. R. Patel, *Biophysical Reviews* **2016**, *8*, 409–427.

[119] F. R. Hallett, *Food Research International* **1994**, *27*, 195–198.

[120] M. Sadek, D. Berndt, D. Milovanovic, R. Jahn, U. Diederichsen, *ChemBioChem* **2016**, *17*, 479–485.

[121] J. R. Lakowicz, *Principles of Fluorescence Spectroscopy*, Springer-Verlag GmbH, **2007**, 954 pp.

[122] H. Yu, S. S. Rathore, J. Shen, *Journal of Biological Chemistry* **2013**, *288*, 18885–18893.

[123] R. B. Merrifield, *J. Am. Chem. Soc.* **1963**, *85*, 2149–2154.

[124] Y. Nishiuchi, M. Nakao, M. Nakata, T. Kimura, S. Sakakibara, *International Journal of Peptide and Protein Research* **2009**, *42*, 533–538.

[125] I. Coin, M. Beyermann, M. Bienert, *Nature Protocols* **2007**, *2*, 3247–3256.

[126] L. K. Mueller, A. C. Baumruck, H. Zhdanova, A. A. Tietze, *Frontiers in Bioengineering and Biotechnology* **2020**, *8*, DOI `https://doi.org/10.3389/fbioe.2020.00162`.

[127] *Peptide Nucleic Acids*, (Ed.: P. E. Nielsen), Springer US, **2020**.

[128] G. S. Vanier, **2013**, 235–249.

[129] R. Casale, I. S. Jensen, M. Egholm, *ChemInform* **2005**, *36*, DOI `http://dx.doi.org/10.1002/chin.200514268`.

[130] D. Fasshauer, R. B. Sutton, A. T. Brunger, R. Jahn, *Proceedings of the National Academy of Sciences* **1998**, *95*, 15781–15786.

[131] G. L. Igloi, *Proceedings of the National Academy of Sciences* **1998**, *95*, 8562–8567.

[132] A. Kiliszek, K. Banaszak, Z. Dauter, W. Rypniewski, *Nucleic Acids Research* **2015**, *44*, 1937–1943.

[133] M. Egholm, O. Buchardt, P. E. Nielsen, R. H. Berg, *Journal of the American Chemical Society* **1992**, *114*, 1895–1897.

[134] M. Egholm, O. Buchardt, L. Christensen, C. Behrens, S. M. Freier, D. A. Driver, R. H. Berg, S. K. Kim, B. Norden, P. E. Nielsen, *Nature* **1993**, *365*, 566–568.

[135] A. Banerjee, S. Bagmare, M. Varada, V. A. Kumar, *Bioconjugate Chemistry* **2015**, *26*, 1737–1742.

[136] H. Margus, P. Arukuusk, Ü. Langel, M. Pooga, *Molecular Pharmaceutics* **2015**, *13*, 172–179.

[137] D.-F. K. Toh, G. Devi, K. M. Patil, Q. Qu, M. Maraswami, Y. Xiao, T. P. Loh, Y. Zhao, G. Chen, *Nucleic Acids Research* **2016**, gkw778.

[138] P. Nielsen, M. Egholm, R. Berg, O. Buchardt, *Science* **1991**, *254*, 1497–1500.

[139] T. Ratilainen, B. Nordén, 59–88.

[140] L. Betts, J. A. Josey, J. M. Veal, S. R. Jordan, *Science* **1995**, *270*, 1838–1841.

[141] P. E. Nielsen, *Current Opinion in Biotechnology* **2001**, *12*, 16–20.

[142] L. Christensen, R. Fitzpatrick, B. Gildea, K. H. Petersen, H. F. Hansen, T. Koch, M. Egholm, O. Buchardt, P. E. Nielsen, J. Coull, R. H. Berg, *Journal of Peptide Science* **1995**, *1*, 175–183.

[143] T. Kofoed, H. F. Hansen, H. Ørum, T. Koch, *Journal of Peptide Science* **2001**, *7*, 402–412.

[144] D. W. Will, G. Breipohl, D. Langner, J. Knolle, E. Uhlmann, *Tetrahedron* **1995**, *51*, 12069–12082.

[145] P. Klán, T. Šolomek, C. G. Bochet, A. Blanc, R. Givens, M. Rubina, V. Popik, A. Kostikov, J. Wirz, *Chemical Reviews* **2012**, *113*, 119–191.

[146] G. Dormán, G. Prestwich, *Trends in Biotechnology* **2000**, *18*, 64–77.

[147] V. Gatterdam, T. Stoess, C. Menge, A. Heckel, R. Tampé, *Angewandte Chemie International Edition* **2012**, *51*, 3960–3963.

[148] B. Ghosn, F. R. Haselton, K. R. Gee, W. T. Monroe, *Photochemistry and Photobiology* **2005**, DOI `https://doi.org/10.1562/2004-11-15-ra-373`.

[149] P. K. Jain, S. Shah, S. H. Friedman, *Journal of the American Chemical Society* **2010**, *133*, 440–446.

[150] O. Srinivas, N. Mitra, A. Surolia, N. Jayaraman, *Glycobiology* **2005**, *15*, 861–873.

[151] R. H. Scott, J. Pollock, A. Ayar, N. M. Thatcher, U. Zehavi, **2000**, 387–400.

[152] C. G. Bochet, A. Blanc, 417–447.

[153] A. Rodrigues-Correia, X. M. M. Weyel, A. Heckel, *Organic Letters* **2013**, *15*, 5500–5503.

[154] W. Zhao, Y. Zhao, Q. Wang, T. Liu, J. Sun, R. Zhang, *Small* **2019**, *15*, 1903060.

[155] S. Walbert, W. Pfleiderer, U. Steiner, *Helvetica Chimica Acta* **2001**, *84*, 1601–1611.

[156] J. E. T. Corrie, A. Barth, V. R. N. Munasinghe, D. R. Trentham, M. C. Hutter, *Journal of the American Chemical Society* **2003**, *125*, 8546–8554.

[157] V. N. R. Pillai, *Synthesis* **1980**, *1980*, 1–26.

[158] A. P. Pelliccioli, J. Wirz, *Photochemical & Photobiological Sciences* **2002**, *1*, 441–458.

[159] L. Kröck, A. Heckel, *Angewandte Chemie International Edition* **2004**, *44*, 471–473.

[160] G. Mayer, L. Kröck, V. Mikat, M. Engeser, A. Heckel, *ChemBioChem* **2005**, *6*, 1966–1970.

[161] F. Schäfer, K. B. Joshi, M. A. H. Fichte, T. Mack, J. Wachtveitl, A. Heckel, *Organic Letters* **2011**, *13*, 1450–1453.

[162] A. V. Pobbati, *Science* **2006**, *313*, 673–676.

[163] K. Meyenberg, PhD thesis, Georg-August-Universität, **2011**.

[164] A. Lupas, *Trends Biochem. Sci.* **1996**, *21*, 375.

[165] K. M. Müller, K. M. Arndt, T. Alber, *Elsevier* **2000**, 261–282.

[166] D. N. Woolfson, **2005**, 79–112.

[167] C. Aronsson, S. Dånmark, F. Zhou, P. Öberg, K. Enander, H. Su, D. Aili, *Scientific Reports* **2015**, *5*, DOI `https://doi.org/10.1038/srep14063`.

[168] F. Thomas, A. Niitsu, A. Oregioni, G. J. Bartlett, D. N. Woolfson, *Biochemistry* **2017**, *56*, 6544–6554.

[169] A. J. de Jesus, T. W. Allen, *Biochimica et Biophysica Acta (BBA) - Biomembranes* **2013**, *1828*, 864–876.

[170] J. Kypr, I. Kejnovska, D. Renciuk, M. Vorlickova, *Nucleic Acids Research* **2009**, *37*, 1713–1725.

[171] S. M. Kelly, T. J. Jess, N. C. Price, *Biochimica et Biophysica Acta (BBA) - Proteins and Proteomics* **2005**, *1751*, 119–139.

[172] B. Apostolovic, H.-A. Klok, *Biomacromolecules* **2008**, *9*, 3173–3180.

[173] E. E. O. Blenke, J. van den Dikkenberg, B. van Kolck, A. Kros, E. Mastrobattista, *Nanoscale* **2016**, *8*, 8955–8965.

[174] J. Yang, A. Bahreman, G. Daudey, J. Bussmann, R. C. L. Olsthoorn, A. Kros, *ACS Central Science* **2016**, *2*, 621–630.

[175] J. Meng, J. Wang, *Biochimica et Biophysica Acta (BBA) - Reviews on Cancer* **2015**, *1856*, 1–12.

[176] H. Edelhoch, *Biochemistry* **1967**, *6*, 1948–1954.

[177] M. Hope, M. Bally, G. Webb, P. Cullis, *Biochimica et Biophysica Acta (BBA) - Biomembranes* **1985**, *812*, 55–65.

Acknowledgements

Zunächst möchte ich mich bei Herrn Prof. Dr. Ulf Diederichsen für die interessanten Themenstellungen und die mir gewährte wissenschaftliche Freiheit bedanken. Insbesondere möchte ich mich bei Prof. Dr. Claudia Steinem für die freundliche Übernahme des Korreferates bedanken.

Darüber hinaus danke ich den weiteren Mitgliedern meiner Prüfungskommission Prof. Dr. Kai Tittmann, Prof. Dr. Jörg Enderlein, Dr. Michael John und Dr. Holm Frauendorf.

Ich bedanke mich außerdem bei Dr. Michael John und dem Team der NMR-Abteilung für die Aufnahme von NMR-Spektren und auch bei Dr. Holm Frauendorf und seinen Mitarbeitern für das Messen meiner zahlreichen Proben.

Von ganzem Herzen bedanke ich mich bei meinen aktuellen Laborkollegen und allen Mitgliedern der Arbeitsgruppe für die schöne Zeit. Martin Kloos, Nils Hesselbarth, Silan Toy und Maria Orenes für die angenehme Atmosphäre im Labor 108.

Ich danke meiner Bachelorstudentin Patricia Ruhl für ihre Unterstützung in der Endphase dieser Arbeit.

Für das Korrekturlesen dieser Arbeit danke ich Martin Kloos, Tobias Schmidt und Elena Cotroneo, Fehmke Reichardt und Clara Bosbach.

Außerdem möchte ich meiner Familie und meinen Freunden danken für ihre Unterstützung.